EMPIRICAL EVALUATION OF STORAGE MATERIALS AND CONDITIONS FOR PROPELLANT GRADE WHITE FUMING NITRIC ACID

A THESIS SUBMITTED TO
THE GRADUATE SCHOOL OF NATURAL AND APPLIED SCIENCES
OF
MIDDLE EAST TECHNICAL UNIVERSITY

BY

KAAN SAÇ

IN PARTIAL FULFILLMENT OF THE REQUIREMENTS
FOR
THE DEGREE OF MASTER OF SCIENCE
IN
CHEMICAL ENGINEERING

DECEMBER 2022

Approval of the thesis:

EMPIRICAL EVALUATION OF STORAGE MATERIALS AND CONDITIONS FOR PROPELLANT GRADE WHITE FUMING NITRIC ACID

submitted by **KAAN SAÇ** in partial fulfillment of the requirements for the degree of **Master of Science** i**n Chemical Engineering, Middle East Technical University** by,

Prof. Dr. Halil Kalıpçılar
Dean, Graduate School of **Natural and Applied Sciences** _____

Prof. Dr. Pınar Çalık
Head of the Department, **Chemical Engineering** _____

Prof. Dr. Deniz Üner
Supervisor, **Chemical Engineering** _____

Dr. Hacı Eşiyok
Co-Supervisor, **Roketsan Missiles INC.** _____

Examining Committee Members:

Assoc. Prof. Dr. Harun Koku
Chemical Engineering, METU _____

Prof. Dr. Deniz Üner
Chemical Engineering, METU _____

Assoc. Prof. Dr. Emre Büküşoğlu
Chemical Engineering, METU _____

Assoc. Prof. Dr. Bahar İpek Torun
Chemical Engineering, METU _____

Assoc. Prof. Dr. Selis Önel
Chemical Engineering, Hacettepe University _____

Date: 02.12.2022

I hereby declare that all information in this document has been obtained and presented in accordance with academic rules and ethical conduct. I also declare that, as required by these rules and conduct, I have fully cited and referenced all material and results that are not original to this work.

Name, Last name: Kaan Saç

Signature:

ABSTRACT

EMPIRICAL EVALUATION OF STORAGE MATERIALS AND CONDITIONS FOR PROPELLANT GRADE WHITE FUMING NITRIC ACID

Saç, Kaan
Master of Science, Chemical Engineering
Supervisor: Prof. Dr. Deniz Üner
Co-Supervisor: Dr. Hacı Eşiyok

December 2022, 145 pages

The stability of propellant grade white fuming nitric acid (WFNA) during storage was investigated experimentally. A custom method was developed to monitor the propellant storage up to 600 hours at elevated temperatures. Two sets of test matrices were designed: a control test matrix was conducted for safety and test system qualification, and the master test matrix was carried out to assess the WFNA storage. The test parameters were selected as follows: two different ullage space values – 13.0% & 19% –, five different storage container material types – PTFE, AISI316L, AISI904L, Al5083-H111 & Al6061-T6 –, three different pressurizing gases – helium, nitrogen & air. Furthermore, whether the surface of the container is passivated by citric acid surface treatment was also an experimental parameter. The temperature was kept at 50 °C for all tests. To carry out the tests, a pressure vessel body and a test tube were designed, qualified and manufactured. Commercial connections, measurement and safety equipment were combined with the manufactured parts to assemble the MPV (Mini Pressure Vessel) fixture. The effect of each of the four variables were analyzed individually, by keeping the others at a fixed value. Time-dependent pressure data was collected and recorded at 1 Hertz.

This time-dependent pressure data was used to monitor the effects of control variables on pressure. Moreover, samples of stored white fuming nitric acid were analyzed for their elemental and chemical compositions by inductively coupled plasma optical emission spectroscopy, and ultraviolet-visible spectroscopy. The effect of dissolved metals and composition shifts were further analyzed by performing ignition delay tests with a fresh amine based fuel. In addition, mass losses of test tubes after storage was measured and the corrosion rate of each tube was determined based upon ASTM G31 – 72 standard.

The experiments and subsequent analyses revealed that stainless steel containers were not suitable for WFNA storage: stainless steel containers deteriorated very rapidly while corroding the container tubes. This was independent of the storage conditions and whether the tube was passivated with citric acid. In contrast, Aluminum based containers performed better compared to stainless steel in terms of the WFNA deterioration, but they corroded by forming $Al(NO_3)_2$, $Mg(NO_3)_2$ and $Mn(NO_3)_2$ which precipitated extensively. Furthermore, Al6061 provided the best performance in terms of corrosion rate with an average of 0.11 mm per year. According to the ignition delay results, which are specific to the test conditions, the shortest times were generally obtained from the acid in the Al6061 material, at the order of 10 ms.

Keywords: Storage Conditions of White Fuming Nitric Acid • Corrosion Rate • Ignition Delay • Pressure Rise Rate • Elemental Analysis

ÖZ

YAKIT SINIFINDAKİ BEYAZ DUMANLI NİTRİK ASİT İÇİN DEPOLAMA MALZEMELERİ VE KOŞULLARININ DENEYSEL DEĞERLENDİRMESİ

Saç, Kaan
Yüksek Lisans, Kimya Mühendisliği
Tez Danışmanı: Prof. Dr. Deniz Üner
Ortak Tez Danışmanı: Dr. Hacı Eşiyok

Aralık 2022, 145 sayfa

Roket yakıtı sınıfındaki beyaz dumanlı nitrik asidin depolama sırasındaki kararlılığı deneysel olarak araştırılmıştır. Yüksek sıcaklıklarda 600 saate kadar yakıt depolama sürecini izlemek için özel bir yöntem geliştirildi. İki set test matrisi tasarlandı: güvenlik ve test sistemi kalifikasyonu için kontrol test matrisi uygulandı ve beyaz dumanlı nitrik asidin depolanmasını değerlendirmek için asil test matrisi uygulandı. Test parametreleri şu şekilde seçilmiştir: iki farklı tepe boşluk değeri – %13.0 & %19.0 –, beş farklı depolama tankı malzeme tipi – PTFE, AISI316L, AISI904L, Al5083-H111 & Al6061-T6 –, üç farklı basınçlandırma gazı – helyum, nitrojen & hava. Ayrıca, depolama tankının yüzeyinin sitrik asit yüzey işlemi ile pasifleştirip pasifleştirilmediği deneysel bir parametreydi. Tüm testler için sıcaklık 50°C'de tutulmuştur. Testleri gerçekleştirmek için bir adet basınçlı kap gövdesi ve bir adet test tüpü tasarlanmış, kalifiye edilmiş ve üretilmiştir. Ticari bağlantılar, ölçü ve güvenlik ekipmanları imal edilen parçalar ile birleştirilerek MPV armatürü montajı yapılmıştır. Dört değişkenin her birinin etkisi, diğerleri sabit bir değerde tutularak ayrı ayrı analiz edildi. Zamana bağlı basınç verileri 1 Hertz ile toplantı ve kaydedildi. Bu zamana bağlı basınç verileri, kontrol değişkenlerinin basınç üzerindeki etkilerini

gözlemlemek için kullanıldı. Ayrıca, depolanan beyaz dumanlı nitrik asit numuneleri, endüktif olarak eşleştirilmiş plazma optik emisyon spektroskopisi, ultraviyole görünür spektroskopi ile elementsel ve kimyasal bileşimleri açısından analiz edildi. Çözünmüş metallerin ve bileşim değişimlerinin etkisi, kabul limitlerine uygun saflıkta amin bazlı yakıtla tutuşma gecikmesi testleri yapılarak ayrıca analiz edildi. Ek olarak, test tüplerinin depolama sonrası kütle kayıpları ölçülmüş ve her bir tüpteki korozyon hızı ASTM G31 – 72 standardına göre hesaplanmıştır.

Deneyler ve sonraki analizler paslanmaz çelik kapların WFNA depolamaya uygun olmadığını ortaya çıkardı: Paslanmaz çelik kaplarda depolanan WFNA, tüpleri aşındırırken çok hızlı bozuldu. Bu depolama koşullarından ve tüpün sitrik asit ile pasivasyon işleminin olup olmadığından bağımsızdı. Buna karşılık, alüminyum esaslı kaplar, WFNA bozulması açısından paslanmaz çeliğe kıyasla daha iyi performans gösterdi ancak tüplerin aşınması esnasında oluşan $Al(NO_3)_2$, $Mg(NO_3)_2$ ve $Mn(NO_3)_2$ bileşikleri yoğun bir şekilde çökeldi. Ayrıca, Al6061, yılda ortalama 0.11 mm korozyon oranı ile en iyi performansı sağlamıştır. Test koşullarına özgü olmak kaydıyla tutuşma gecikmesi sonuçlarına göre en kısa süreler genel olarak 10 ms mertebesinde Al6061 malzemesindeki asitten elde edilmiştir.

Anahtar Kelimeler: Beyaz Dumanlı Nitrik Asidin Depolama Koşulları • Korozyon Hızı • Tutuşma Gecikmesi • Basınç Artış Hızı • Elementsel Analiz

Solely

Dedicated

To

My

Beloved

Mom

ACKNOWLEDGEMENTS

First, I would like to express my heartfelt appreciation to my irreplaceable thesis supervisor, Prof. Dr. Deniz Üner, for her immeasurable and unlimited encouragements as well as guidance both in my graduate studies and in my life to endeavor towards not for the better but for the best all the time.

Additionally, I wish to thank my company executive and thesis Co-Supervisor Dr. Hacı Eşiyok, for his encouragements, and my colleagues Ali Erdem Önder, Dr. Ahmet Koç, Melike Özkan, Murat Öztürk, Gizem Avcı, Berfin Bölükemini, Dr. Kerem Emre Ercan, Adil Ekincik, Uğur Şahin, Erdi Aydın, and Erkan İlhan for their assistance and help during my studies at Roketsan Missiles Incorporated.

Furthermore, I would like to thank Roketsan Missiles Incorporated for the financial aid and infrastructural support throughout this comprehensive research.

Most prominently, I want to express my sincerest gratitude to my mother, Huriye, for her unconditional and endless love as well as support throughout all my life; and my brother, Hüseyin, as a big brother he always stand by my side for better or worse and taught me everything I know and made me who I am today.

TABLE OF CONTENTS

LIST OF TABLES

TABLES

LIST OF FIGURES

FIGURES

LIST OF ABBREVIATIONS

ACGIH	American Conference of Governmental and Industrial Hygienists
AISI	American Iron and Steel Institute
BEI	Biological Exposure Indices
EDS	Energy Dispersive Spectroscopy
EPA	Environmental Protection Agency
GC	Gas Chromatograph
HB	Brinell Hardness
HMX	Cyclotetramethylenetetranitramine
LDPE	Low-Density Polyethylene
LOX	Liquid Oxygen
LH_2	Liquid Hydrogen
LPRE	Liquid Propellant Rocket Engine
ICP-OES	Inductively Couples Plasma – Optical Emission Spectroscopy
ISP	Specific Impulse
MMH	Monomethylhydrazine
MPV	Mini Pressure Vessel
ms	Millisecond
NASA	National Aeronautics and Space Administration
NIOSH	National Institute of Occupational Safety and Health
NPs	Nano Powders
NSPV	Non-Stirred Pressure Vessel

NTO	Nitrogen Tetroxide
PEL	Permissible Exposure Limits
PMRS	Pressure Measurement and Relief System
ppm	Parts Per Million
PT	Pressure Transducer (Transmitter)
PTFE	Polytetrafluoroethylene
RCS	Reaction Control System
RDX	Cyclotrimethylenetrinitramine
REL	Recommended Exposure Limits
RFNA	Red Fuming Nitric Acid
RP-1	Rocket Propellant 1
OSHA	Occupational Safety and Health Administration
SCC	Standard Cubic Centimeters
SEM	Scanning Electron Microscopy
SS	Stainless Steel
TYS	Tensile Yield Stress
UDMH	Unsymmetrical Dimethyl Hydrazine
UNS	Unified Numbering System
USSR	Union of Soviet Socialist Republics
UTS	Ultimate Tensile Stress
UV	Ultraviolet
WFNA	White Fuming Nitric Acid

LIST OF SYMBOLS

$Al(NO_3)_2$	Aluminum Nitrate
ρ	Density
N_2O_4	Nitrogen Tetroxide
$Mg(NO_3)_2$	Magnesium Nitrate
$Mn(NO_3)_2$	Manganese Nitrate
H_3PO_4	Phosphoric acid
$KF \cdot 2H_2O$	Potassium fluoride dihydrate
P	Pressure
T	Temperature

CHAPTER 1

INTRODUCTION

Success in space demands perfection. This moving sentence was once said by Wernher von Braun, who was a World War II-era rocket scientist and pioneer in rocket technology in Nazi Germany (Musgrave, Larsen, & Sgobba, 2009). He and many other German Rocket scientists were exfiltrated via an operation called Paperclip by the United States of America from defeated Germany in the summer of 1945 (Clark, 1972). They paved the way for Apollo Program and extensively contributed to the moon landing of Apollo 11 on 20 July 1969. Since that time, mankind has excelled in space technology and propelled itself in the development of novel types of rocket engines as well as propellants. In this chapter, the fundamental essence of liquid propellant rocket engines, propellant types, and the objective of this research is given in detail.

1.1 The History of Liquid Propellant Rocket Engines

The history of liquid propellant rocket engines (LPREs) is relatively recent when compared to the solid propellant-powered boosters. The United States of America, the United Socialist Soviet Republic, or U.S.S.R., and Germany before being defeated at the end of World War II were the pioneering countries. Robert H. Goddard started working on LPREs at the beginning of 1920 and achieved the first test flight of a LPRE in the USA in 1926. However, comprehensive studies did not initiate until after WWII in the United States. The work done by the Soviet Union and Germany was performed under the government roof and all the operation was kept secret at that time. Soviet Union initiated LPRE development projects around 1930 and was capable of producing effective products at the beginning of 1950. On the other hand, critical studies were performed by Germany throughout the 1930s

and at the beginning of the 1940s, they managed to successfully fly the very first large-scale LPRE called V-2 (Vergeltungswaffen 2 in German roughly translated as Vengeance Weapon 2). At the time, Wernher von Braun, who worked for the United States after World War II, led the V-2 design team (Sutton G. , History of Liquid Propellant Rocket Engines, 2006).

LPRE domain was primarily established and formed by three counties as stated above, however, there are at least ten plus counties that are highly capable of designing and producing their own advanced LPREs today. Additionally, multiple countries initiate and proceed with the development of particular models of LPREs. As of 2006, since the emergence of LPREs, roughly thirteen hundred distinct rockets have been produced and tested. There is no simple rule when it comes to LPRE design, which is why the differences are more pronounced than the similarities of these LPREs. In terms of differences, they could be high-thrust or low thrust, also the liquid propellant that they use might be storable, non-storable (cryogenic), bipropellant or monopropellant and so on (Sutton G. , History of Liquid Propellant Rocket Engines, 2006).

Starting from their first successful tests, between the 1940s and 1970s LPREs were primarily utilized for sounding rockets, jet-assisted takeoff systems, and ballistic as well as tactical missiles since they could provide operational functionality and superiority over solid propellant boosters. For instance, LPREs provide higher performance, they could be uniquely pulsed and restarted to control velocity, attitude, and thrust. Today, a significant percentage of space launch vehicles, spacecraft propulsion systems, and reaction control systems continue to utilize LPREs as the main propulsion medium (Sutton G. , History of Liquid Propellant Rocket Engines, 2006).

1.2 Classification of Rocket Propellants

Rocket propellants consist of an oxidizer and a fuel; they are usually the combination of several chemical compounds that are mixed in precisely determined specific ratios. Propellants are atomized via tiny holes on the injector plate and then mixed in the combustion chambers. After burning out, they generate propulsion gas that is utilized to produce thrust in rocket nozzles. The efficiency of rocket propellants is measured by the specific impulse, which is simply defined as the change in momentum per unit propellant consumed in one second. Propellants are consumed more efficiently when the specific impulse of the propulsion system is higher (Braeunig, 2014).

Simply, propellants are classified as solid, liquid, and gelled. Each propellant type has exclusive chemical ingredients, different specific impulses, and distinct physical properties. Solid propellants are a mixture of a fuel and an oxidizer that is usually enclosed in a steel casing where it burns from inside out when ignited. Most cured solid propellants do not pose a toxicity threat and only a few special ingredients like burning rate modifiers and binding agents are toxic until the propellant mix is cured. There are several types of solid propellants, but two of the commonly known are called double-base and composite. Double-base propellants are homogeneous and consist of nitrocellulose and nitroglycerine, where solid nitrocellulose absorbs liquid nitroglycerine, along with some performance enhancer additives. When crystalline nitramines like HMX or RDX are added the performance is improved, this form is called cast-modified double-base propellant. Further advancements are the addition of elastomeric binder like crosslinked polybutadiene, which enhances physical properties. The final product is known as an elastomeric-modified cast double-base propellant that has smokeless exhaust and is primarily used for tactical missiles (Sutton & Oscar, Rocket Propulsion Elements, 2001). Generally, since double-base propellants create explosion hazards, in United Nations Recommendations on the Transport of Dangerous Goods (UN 2005) double-base propellants are labeled as Class 1.1 (Musgrave, Larsen, & Sgobba, 2009). On the other hand, composite

propellants are heterogeneous and consist of powdered fuels like aluminum and crystallized oxidizers like ammonium perchlorate that are kept together in a synthetic liquid rubber binder such as hydroxyl-terminated polybutadiene. After mixing, the hardening process of composite propellant is achieved by adding curing agents like methyl aziridinyl phosphine oxide and then curing at elevated temperatures, changing between 20°C to 150°C, in an oven. In short, a solid propellant is generally composed of an oxidizer, a fuel, a binder, a plasticizer, and a curing agent (Sutton & Oscar, Rocket Propulsion Elements, 2001). However, there is a vast number of different solid propellant formulations that have been synthesized by using special chemical ingredients, which are greatly detailed by George Sutton in his book called Rocket Propulsion Elements. Compared to double-base propellants, composite propellants are categorized as Class 1.3 in UN 2005, implying that they only introduce fire or slight blast and projection hazard, i.e., mass explosion is not a concern for composite propellants (Musgrave, Larsen, & Sgobba, 2009).

Liquid propellant term compromises diverse liquid substances that may fall under the category of oxidizer, fuel, or a mixture of an oxidizer and a fuel, which can self-decompose, and any of the previous ones with a gelling additive also known as the gelled propellant. Additionally, they could be either categorized as bipropellants and monopropellants or storable propellants and non-storable (cryogenic) propellants. In a bipropellant rocket engine, there are two distinct propellants, a fuel, and an oxidizer. They are kept inside their isolated tanks until mixed in the combustion chamber. Monopropellants, on the other hand, are composed of a fuel and an oxidizer in such a way that it is stable at standard atmospheric states (1atm, 20°C), however, decompose quickly when catalyzed. Monopropellants might be homogeneous chemicals like hydrazine, or they might be a combination of several substances such as hydroxyl ammonium nitrate (HAN). Apart from bipropellant and monopropellant classification, there are storable (sometimes called earth storable) and non-storable propellant categorizations. At room temperature, storable propellants are liquid and when the optimal storage conditions are satisfied, they could be stored in properly sealed vessels for long periods. Storable propellant class compromises a subcategory

called hypergolic propellants. Hypergolic fuel pairs spontaneously ignite upon contact with one another, i.e., they do not require an external ignition source. However, hypergolic fuels like hydrazine derivatives are carcinogenic and release highly flammable vapors, whereas hypergolic oxidizers like nitrogen tetroxide along with nitric acid derivatives are quite corrosive and release extremely toxic fumes under normal conditions (Sutton & Oscar, Rocket Propulsion Elements, 2001). Historically, numerous manned and unmanned spacecraft that ever served in a commercial or military mission utilized some of the foremost storable propellant combinations (given in Table 1-1) (Boyd & Brasher, 1989).

Table 1-1 Historically Used Storable Liquid Propellant Pairs (Boyd & Brasher, 1989)

Manned Earth Storable Propellant Spacecraft

Spacecraft	Propulsion System	Propellants	Vacuum Thrust (N)
Gemini	Altitude Control	NTO / A-50	100
Gemini	Re-entry Control	NTO / MMH	100
Gemini	Maneuvering	NTO / MMH	420
Gemini / Agena	Target Vehicle	IRFNA / UDMH	71,200
Apollo CM	RCS	NTO / MMH	415
Apollo SM	SPS	NTO / A-50	91,220
Apollo SM	RCS	NTO / MMH	445
Apollo LMD	DPS	NTO / A-50	4,670 – 43,830
Apollo LMA	APS	NTO / A-50	15,570
Apollo LMA	RCS	NTO / A-50	445
Shuttle Orbiter	OMS	NTO / MMH	26,700
Shuttle Orbiter	RCS Primary	NTO / MMH	3,870
Shuttle Orbiter	RCS Vernier	NTO / MMH	110

Unmanned Earth Storable Propellant Spacecraft

Spacecraft	Propulsion System	Propellants	Vacuum Thrust (N)
Titan III	Transtage	NTO / A-50	36,260
Titan II 624A	Transtage RCS	NTO / A-50	110 – 200
Delta	Second Stage	NTO / A-50	44,050
Arabsat, L-Sat	Altitude Control	NTO / MMH	20
Intelsat	Altitude Control	NTO / MMH	4
Agena	Altitude Control	IRFNA / UDMH	400
Galileo	Propulsion Module	NTO / MMH	400
OMV	Propulsion Module	NTO / MMH	2310
Syncom	Apogee Kick System	NTO / MMH	890

In addition to the mentioned storable liquid fuels, another liquid propellant class consists of hydrocarbon fuels. Hydrocarbon fuels are cheap, not carcinogenic and they do not release toxic fumes. The most extensively known and employed types are diesel oil, jet fuel, and kerosene. However, the chemical composition of these fuels varies in quite a wide range of organic ingredients because of the differences in chemical processes and manufacturing exercises implemented in different refineries. Rocket propellant one, abbreviated as RP-1, is a kerosene-based chemical mixture in which its chemical properties such as vapor pressure and density lie in a narrow acceptance range; as a result, it must be precisely refined from crude oil.

Historically, RP-1 was utilized for the Thor, Soyuz, Atlas, Saturn V, Falcon 9, and Delta rocket engines. Conversely, non-storable or cryogenic propellants are simply liquefied gases at significantly low temperatures, for instance, it is ~90K for oxygen and ~20K for hydrogen (Sutton & Oscar, Rocket Propulsion Elements, 2001). Under extremely low liquidation temperatures, it is not feasible to store cryogenic propellants for long periods due to constant boiling. For this reason, cryogenic propellants are not a priority choice for military applications, but they are commonly preferred for non-military space objectives where storability is not the key factor. For instance, the primary engines of the Space Shuttle utilized liquid hydrogen and liquid oxygen pair (Braeunig, 2014). When compared to one another, storable liquid propellants grant some remarkable superiorities over cryogenic and solid propellants (shown in Table 1-2). Exemplarily, while cryogenic systems require complicated refrigeration structures along with continuous chill-down, solid propellants offer inadequate thrust performance in comparison with storable propellants (Boyd & Brasher, 1989).

Table 1-2 Characteristic Comparison amongst Solid, Cryogenic, and Storable Liquid Propellants (Boyd & Brasher, 1989)

			Storables*	
Characteristic	**Solid**	**Cryo**	**Earth**	**Space**
Performance	Poor	Excellent	Good	Very Good
Space Storability	Excellent	Poor	Excellent	Good
Space Length	Good	Poor	Good	Good
• Propellant Density	Very Good	Poor	Very Good	Very Good
• System Mass Fraction	Very Good	Poor	Good	Good
Duty Cycle Flexibility	Poor	Good	Excellent	Very Good
• On-Orbit Demand Start	Yes	No	Yes	No
• On-Orbit Restart	No	Yes	Yes	Yes
Operations Complexity	Low	High	Low	Moderate
• System Complexity	Low	High	Low	Moderate
• On-Orbit Venting Requirement	No	Yes	No	Yes
Toxicity	High	Low	High	High
Corrosivity	High	Low	High	Low

*Earth storable propellants remain liquid under atmospheric conditions, whereas the normal boiling point of space storable propellants is generally higher than -184°C.

The third kind of propellant category is gelled propellants that fall into the thixotropic fluid class. Thixotropic fluids are in viscous form like thick paint when at rest and there is no shear stress, however, they turn into less viscous material and liquefy when agitated, stirred, or shaken. As a result, they could flow right through pipes and other equipment when the shear load is sufficiently exerted. Gelled propellants provide some application advantages as well as disadvantages. In terms of advantages, flow rate control within the system is good and the plugging risk of inline equipment seats is low. They do not readily decompose, deteriorate, or precipitate during storage (Sutton G. , History of Liquid Propellant Rocket Engines, 2006). Additionally, the likelihood of spills, leaks, and sloshing in the vessels is minimized extensively, and when spilled, gelled propellants could be disposed of by simply diluting with excess water. About disadvantages, the specific impulse of gelled propellants decreases due to inefficient atomization on the injector exit compared to their non-gelled counterparts. Additionally, propellant charging and discharging are complicated to execute. Lastly, gelled propellants are more sensitive to changes in surrounding temperatures and storage poses extra issues. For this reason, gelling additives must be selected in such a way that the changes in rheological properties of propellants and gelling agents through a temperature range should bear resemblance with one another to some extent (Sutton & Oscar, Rocket Propulsion Elements, 2001).

1.3 Properties of Liquid Propellants

It is a well-known fact that rocket engines and their liquid propellant propulsion systems are highly complex which is why there is not a single, yet effective design solution accepted by the majority of the field. As a result, in the early years, approximately two thousand different liquid propellants and slightly more bipropellant combinations have been experimented in the laboratory. Later, approximately three hundred combinations were tested with a thrust chamber. In the end, roughly forty liquid propellant combinations have been utilized. During the

elimination period, initially, each propellant's chemical, physical, and combustion properties such as density, vapor pressure, freezing point, ignition delay, specific impulse were determined. Then, propellants with low performance with poor qualities were directly eliminated. Consequently, today some common liquid propellant combinations like LOX/RP-1, LOX/LH_2, NTO/MMH (United States), and NTO/UDMH (Russia) have been proven satisfactory and are still in wide use (Sutton G. , History of Liquid Propellant Rocket Engines, 2006). These liquid propellant pairs provide some characteristic advantages along with disadvantages and there is always an opportunity cost when it comes to performance and ease of use. For instance, the specific impulse of storable propellants is less than that of cryogenic propellants, however, in terms of bulk density, i.e., overall system performance, storable propellants are far superior to cryogenic counterparts (shown in Table 1-3) (Boyd & Brasher, 1989).

Table 1-3 Performance Comparison of Liquid Propellant Combinations (Boyd & Brasher, 1989)

Propellant Type	Propellant Combination	Optimum O/F	ISP (N.s/kg)	Bulk Density (kg/m^3)	Density Impulse ($N.s/m^3$)
Earth Storable	NTO / Hydrazine	1.42	3600	1220.5	4,393,800
	NTO / MMH	2.00	3540	1185.3	4,194,900
Space Storable	LOX / MMH	1.65	3933	1042.8	4,101,120
	LOX / RP-1	2.75	3815	1017.1	3,879,860
	LOX / Ethanol	1.75	3658	988.3	3,614,100
	LOX / Propane	2.80	3835	911.4	3,497,520
	LOX / Ammonia	1.40	3619	893.8	3,235,390
	LOX / Methane	3.45	3923	706.4	2,769,640
Cryogenic	F2 / Hydrogen	9.74	4927	520.6	2,565,000
	LOX / Hydrogen	5.75	4737	352.4	1,661,350

Properties of liquid propellants could be hypothetically divided as desired qualities and not preferred qualities. Desired qualities are high density, low vapor pressure, short ignition delay time, stable storage, and high specific heat. Conversely, not preferred qualities are high vapor pressure, susceptibility to self-decomposition, combustion instability, and releasing fumes that are either toxic, flammable, or

corrosive. Commonly utilized liquid propellants' significant physical properties are shown in Table 1-4. Yet, there is a trade-off between good performance and the number of poor qualities such that liquid propellants with higher performance are usually dangerous, carcinogenic, unstable, incompatible with a great deal of materials, and potentially explosive (Sutton G. , History of Liquid Propellant Rocket Engines, 2006). For example, a theoretical chemical liquid propellant combination utilizes hydrogen with solid suspended particles of toxic beryllium as the fuel and toxic fluorine as the oxidizer. This combination provides one of the highest theoretical specific impulses; however, no one has ever come up with neither a feasible way to store nor an operable rocket engine to utilize these propellants (Sutton & Oscar, Rocket Propulsion Elements, 2001).

Table 1-4 Physical Properties of Liquid Propellants (Sutton & Oscar, Rocket Propulsion Elements, 2001)

Propellants→	**Liquid Fluorine**	**Hydrazine**	**Liquid Hydrogen**	**Methane**	**MMH**
Chemical formula	F_2	N_2H_4	H_2	CH_4	CH_3NHNH_2
Molecular mass	38.0	32.05	2.016	16.03	46.072
Melting or freezing point (K)	53.54	274.69	14.0	90.5	220.7
Boiling point (K)	85.02	386.66	20.4	111.6	360.6
The Heat of vaporization (kJ/kg)	166.26[b]	44.7[b] (298.15K)	446	510[b]	875
Specific heat (kcal/kg.K)	0.368 (85K) 0.357 (69.3K)	0.736 (293K) 0.758 (338K)	1.75[b] (20.4K)	0.835[b]	0.698 (293K) 0.735 (393K)
Specific gravity	1.636 (66K) 1.440 (93K)	1.005 (293K) 0.952 (350K)	0.071 (20.4K) 0.076 (14K)	0.424 (111.5K)	0.8788 (293K) 0.857 (311K)
Viscosity (cP)	0.305 (77.6K) 0.397 (70K)	0.97 (298K) 0.913 (330K)	0.024 (14.3K) 0.013 (20.4K)	0.12 (111.6K) 0.22 (90.5K)	0.855 (293K) 0.40 (344K)
Vapor pressure (MPa)	0.0087 (100K) 0.00012 (66.5K)	0.0014 (293K) 0.016 (340K)	0.2026 (23K) 0.87 (30K)	0.033 (100K) 0.101 (117K)	0.0073 (300K) 0.638 (428K)

Nitric Acid[a] (99%)	**Nitrogen Tetroxide**	**Liquid Oxygen**	**RP-1**	**UDMH**	**Water**
HNO_3	N_2O_4	O_2	Hydrocarbon	$(CH_3)_2NNH_2$	H_2O
63.016	92.016	32.00	~175	60.10	18.02
231.6	261.95	54.4	225	216	273.15
355.7	294.3	90.0	460 – 540	336	373.15
480	413[b]	213	246[b]	542 (298K)	2253[b]
0.042 (311K) 0.163 (373K)	0.374 (290K) 0.447 (360K)	0.4 (65K)	0.45 (298K)	0.672 (298K) 0.71 (340K)	1.008 (273.15K)
1.549 (273.15K)	1.447 (293K)	1.14 (90.4K)	0.58 (422K)	0.856 (228K)	1.002 (373.15K)
1.476 (313.15K)	1.38 (322K)	1.23 (77.6K)	0.807 (289K)	0.784 (244K)	1.00 (293.4K)
1.45 (273K)	0.47 (293K) 0.33 (315K)	0.87 (53.7K) 0.19 (90.4K)	0.75 (289K) 0.21 (366K)	4.4 (220K) 0.48 (300K)	0.284 (373.15K) 1.000 (277K)
0.0027 (273.15K) 0.605 (343K)	0.01014 (293K) 0.2013 (328K)	0.0052 (88.7K)	0.002 (344K) 0.023 (422K)	0.0384 (289K) 0.1093 (339K)	0.00689 (312K) 0.03447 (345K)

[a] Red fuming nitric acid (RFNA) has 5 to 20% dissolved NO_2 with an average molecular weight of about 60, and a density and vapor pressure relatively higher than those of pure nitric acid.
[b] At the boiling point.
[c] Reference for specific gravity ratio: 10^3 kg/m^3 or 62.42 lbm/ft^3.

1.4 Liquid Propellant Storage

Today, almost all the government-based organizations and private space, military, as well as satellite companies heavily depend on the utilization of at least one type of liquid propellant in their unique propulsion stages. Liquid propellants and their propulsion systems on a space vehicle make up approximately ninety percent of the entire gross weight of a rocket engine system. Hence, propellants determine all

operational limits, total useful payload, spacecraft dimensions, and reliability along with cost indirectly. Because of this reason, the utmost importance is required to be given to the selection of liquid propellant combinations. However, due to their characteristic nature, almost all the storable liquid propellants, which satisfy the desired outputs like being hypergolic, providing short ignition delay lags, and staying at a liquid state under atmospheric conditions, are highly reactive and energetic materials (Boyd & Brasher, 1989). As mentioned before, fuels are strong reducing agents that usually decompose exothermically and spontaneously catalyze, whereas concentrated oxidizers continuously attack most organic and inorganic materials of the propellant system in which they are enclosed. Both propellant types could be stored for long periods when suitable conditions are provided (Terlizzi & Streim, 1956). As a result, the chemical and physical properties of the propellant might change drastically. This leads to a decrease in combustion performance along with thrust loss and it may result in leaks and catastrophic failures in the long run. Therefore, to avoid these circumstances once the appropriate propellant combination is settled, the immediate next issue is their preservation requirements in a storage tank, where it is positioned within the spacecraft itself until used. For example, to overcome storage problems of red fuming nitric acid, a highly reactive strong oxidizing agent, inside metal vessels an additive called hydrogen fluoride was introduced at about 0.5 percent by weight. That significantly reduced corrosion of metallic tanks and precluded the composition change, as well as the formation of metallic salts. There on the metal surface, HF induces the formation of an insoluble metal fluoride coating, which is impervious therewithal (Sugur & Manwani, 1983).

1.5 Preservation Complexities of Liquid Propellants

Several problems arise throughout the storage of liquid propellants depending on the propellant characteristics. The most pronounced issues are continuous composition change of propellants, metal weakening through corrosion of metal surfaces, and

pressure build-up due to homogeneous and catalytic decomposition. These could be resolved by implementing convenient practices (Sugur & Manwani, 1983).

1.5.1 Corrosion on Metals and Decomposition of Liquid Propellants

Corrosion of metals and decomposition of the liquid propellants are the most frequently experienced problems during the preservation period. The reactions involve vary from propellant to propellant and they heavily depend on the materials employed. In this section, for simplicity, only hydrazine as fuel and red fuming nitric acid as an oxidizer are discussed. While decomposing, hydrazine generates bulk amounts of ammonia and nitrogen along with a scarce quantity of hydrogen when stored in stainless steel tanks. Accordingly, the overall decomposition reaction of hydrazine is shown by,

$$3N_2H_4 \rightleftharpoons 4NH_3 + N_2 \tag{1.1}$$

Based on the reaction (see (1.1)), the hydrazine decomposition rate is assumed to be implicitly related to the nitrogen formation rate (Sutton D. , 1986). Similarly, RFNA undergoes thermal decomposition (see (1.2)) and forms water, nitrogen dioxide, and oxygen. As a result, extreme pressure rise occurs due to the formation of oxygen, in addition to that continuous change in propellant composition takes place. Ultimately, the propulsion system might not meet the predefined requirements by the time a need for use of propellant arises (Sugur & Manwani, 1983).

$$4HNO_3 \rightleftharpoons 4NO_2 + 2H_2O + O_2 \tag{1.2}$$

1.5.2 Weakening of Storage Container and Corrosion Resistance

Corrosion, extraction, or absorption occurrences on the metal surfaces are an important downside of liquid oxidizers, specifically nitric acid derivatives and nitrogen tetroxide if the composition of the propellant is not coherent with the materials or they are stored inside containers that consist of incompatible material of

constructions. Consequently, in both cases, the structural integrity, as well as physical properties like tensile strength, hardness, and elongation of the materials are usually affected adversely. Independent of the fate of the liquid propellant under investigation, the weakening of metal may lead to substantial changes in material dimensions and decreases in hardware performance. For instance, while experimenting the long-term nitrogen tetroxide storage with 6Al-4V titanium alloy vessels, the stress corrosion cracking phenomenon was experienced. Later, it was determined that the slight presence of nitrogen oxide, around 0.6 percent, eliminated this phenomenon, and nitrogen tetroxide was successfully utilized in Apollo 9 (American Institute of Aeronautics and Astronautics Liquid Propulsion Committee on Standards, 2001). In the following years, well-defined characteristics of stress corrosion cracking events were clearly illustrated, contrary to the common belief at that time that nitrogen tetroxide does not have serious effects on the titanium alloys at all (Tiffany & Masters, 1967).

Regarding the corrosion resistance, it decreases as the amount and variety of impurities in metals increase. It is a fact that pure metals depict extreme corrosion resistance compared to impure ones. For instance, as slight as 0.02 percent iron impurity in aluminum leads to a reduction in corrosion resistance by approximately 100 times. In other words, once impurities are removed from the material, better corrosion resistance is obtained. However, the physical features of super-pure materials are inadequate and there is a trade-off between high purity and better mechanical properties (Sugur & Manwani, 1983).

1.6 Objectives and Methodology

In this specific study, the main interest is given to the characteristics of liquid propellant storage and the primary objective is the determination of optimum preservation conditions for a specific type of liquid oxidizer, namely white fuming nitric acid (WFNA). The selection criteria are thoroughly clarified in the subsequent chapters.

The methods applied here are the reflection of the literature investigations that have been primitively done by primarily using small cylindrical seal tight vessels with safety and measurement instruments on top of it. The studies executed here could be gathered under the umbrella of tensile specimen tests and time-limited storage tests in a temperature-controlled environment. The former is performed to make sure that materials satisfy the physical properties, and their properties lie within the acceptable bands. The purpose of the latter one is to identify the independent effects of parameters in question including but not limited to material of construction, temperature, ullage ratio, blanket gas type, and citric acid passivation presence.

1.7 Hazards of Liquid Propellants on Environment and Human Health

Due to the energetic nature of liquid rocket propellants, a strong understanding is an obligation to implement safety in complete rocket systems along with minimizing the risks involved. In fact, there are countless stages, sections, and trade-offs while maintaining the overall launch system safety.

Simply, toxicity, carcinogenicity, flammability, and explosiveness define the fateful nature of liquid rocket propellants. That is to say, many liquid propellants have at least one of the aforementioned characteristics that could not be easily replaced. Due to those features they possess, disposing of liquid propellants, their wastes, and other contaminated materials to nature is significantly harmful to both the environment and other living organisms in the immediate region. For this reason, strict regulations usually specific to the chemicals have been implemented over the years to protect the environment and animals in the vicinity.

In terms of human health, all the liquid propellants release harmful vapors continuously and their threshold exposure limits are well defined by organizations such as OSHA, EPA, NIOSH, and ACGIH to protect personnel from excess exposure and minimize the serious detrimental effects, which could even result in death if sufficient care not taken. The symptoms of exposure are strongly related to

the type of exposure, the total amount of substance being exposed, frequency of exposure, and amount of time that the exposure takes place. For instance, short periods of exposure to low concentrations of nitrogen tetroxide fumes (less than 0.5 ppm of NO_2 in combination with 5.0 ppm NO) could cause nose and throat irritation. On the other hand, ongoing exposure to these fumes may lead to inflammation of the lungs and eventually death. The exposure limits and other safety regulations stipulated by the former two agencies are obligatory, whereas recommendations provided by the latter two agencies are not. For instance, the toxicity of chemicals is measured by ppm and different classifications such as STEL, BEI, REL, PEL, TLV, TLV-C, TLV-TWA, and so on are employed (American Institute of Aeronautics and Astronautics Liquid Propulsion Committee on Standards, 2001). However, the complete classification of these and other categories is rather lengthy. For more information regarding those classifications and about safety, one could look for Chemical Process Safety Fundamentals with Applications (Crowl & Louvar, 2014).

CHAPTER 2

LITERATURE REVIEW

Every aspect of liquid rocket propellants has been widely investigated throughout the past century by various researchers mostly independent of one another. However, great quantities of those literature documents primarily consisted of formerly confidential sources which were mostly performed by military and commercial organizations under the supervision of the United States government. Currently available literature data were mainly concentrated within the time interval between the end of the second world war and the end of the cold war. Unfortunately, recent studies covering storage tests of liquid propellants were limited, scarce, and largely focused on particular test conditions in a laboratory setting. Most of these studies were discontinued single-phase academic projects that usually served to answer constrained specific questions. In the following subsections of this chapter existing literature sources about the storage of liquid rocket propellants were comprehensively addressed and supported by reliable data.

2.1 Storage Fundamentals of Liquid Propellants

The basic concept of long-term liquid propellant storage in a leak-proof rigid tank primarily depends on the type of propellant. For instance, continuous evaporation takes place during cryogenic propellant storage therefore these kinds of propellants could only be kept for up to several days. For this reason, the storability and storage conditions of these fuels are rather different from the ones belonging earth storable propellant class. Earth storable propellants could be kept sealed inside vehicle tanks for decades without a need for serious maintenance if the proper conditions are met (Sutton & Oscar, Rocket Propulsion Elements, 2001).

The stability of long-term propellant storage can be drastically influenced by diverse external factors including but not limited to ullage space atmosphere, tank material, internal pressure, dissolved impurities, and temperature (Mohammadi & Gorji, 2013). In other words, the propellants might become thermodynamically unstable when one or more of those conditions are not properly met (Uney & Fester, 1972).

Earth storable propellants such as hydrazine slowly undergo continuous decomposition at a finite rate under normal conditions. However, under non-ideal storage conditions, the rate of decomposition reactions accelerates appreciably. This leads to an increase in pressure that in return might greatly exceed the maximum allowable pressure limits of the system (Mellor, Smith, Carr, & Bellis, 1993).

2.2 Adverse Effects Caused by Improper Storage Conditions

Liquid propellants are easily affected by slight negative changes in thermal and environmental storage conditions. The type of adverse effects ranges from minor problems like ignition performance degradation to relatively major problems like explosion during storage or combustion (Mohammadi & Gorji, 2013). In addition to these, after long-term storage formation of flaking, etching, pitting, cracking, and staining could be observed on the material surfaces in contact with propellant due to violent corrosion or catalytic reactions (Moran & Bjorklund, 1982). Additionally, reactions between propellants and materials might create hazardous products. For instance, if nitrogen tetroxide is stored via containers made of organic substances or reducing agents then due to accelerated reactions detonation and explosion might occur. Thermal runaway is another issue that may be encountered. Such that, during storage, monomethylhydrazine releases heat through decomposition and if the retained thermal energy is larger than the dissipated then a thermal runaway reaction (shown in Figure 2.1) takes place which could lead to fire and explosion. Unfortunately, it is extremely difficult to accurately determine the individual impact of poor conditions since a change in each parameter also influences the weight of

other parameters in effect (American Institute of Aeronautics and Astronautics Liquid Propulsion Committee on Standards, 1999).

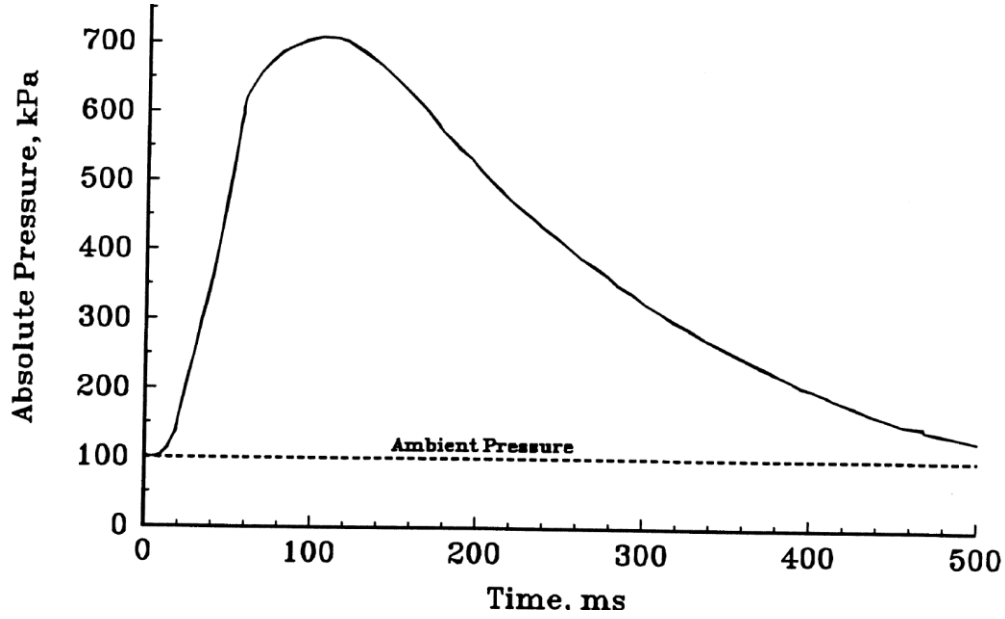

Figure 2.1 Pressure change with respect to time in a confined thermal runaway reaction (American Institute of Aeronautics and Astronautics Liquid Propulsion Committee on Standards, 1999) Reproduced with permission from AIAA

2.2.1 Compatibility of Liquid Propellants with Materials

Material selection for the liquid propellant containment systems requires detailed verification of the compatibility with the proposed conditions. Essentially, compatibility is a reciprocal instance in which both the propellant effect on the material and the material effect on the propellant shall be taken into account (Martin Marietta Corporation, 1977). For instance, nitrogen tetroxide could induce a dimensional disruption in the material, which are strong enough to disrupt its intended features, due to severe chemical and physical interactions (American Institute of Aeronautics and Astronautics Liquid Propulsion Committee on Standards, 2001). In particular, apart from the material and propellant composition, compatibility is mainly determined by temperature and exposure time. In terms of temperature, the mechanical properties of materials are negatively affected as

temperature increases. Similarly, even at normal temperatures prolonged exposure could cause permanent decreases in material strength and lead to extensive propellant deterioration (National Aeronautics and Space Administration, 1974). The risk of explosion is a possible incident if incompatible materials are employed during long-term storage. In fact, when hydrogen peroxide is confined in a vessel manufactured with improper materials it undergoes self-decomposition leading to an explosion (Sutton & Oscar, Rocket Propulsion Elements, 2001).

2.2.2 Pressure Build-Up inside Propellant Storage Systems

Pressure accumulation in a closed rigid system is presumed if the storage system pressure goes beyond the vapor pressure of the chemical at the same temperature. Pressure build-up or rise inside the leak-tight liquid propellant storage systems takes place due to a different number of reasons. Such that, accelerated self-decomposition of the propellant in which gaseous products form, incompatible material utilization that stimulates surface catalytic reactions, elevated temperature that disrupts thermodynamic stability leading to shifting in reaction balance, and presence of impurities that reacts with propellant constituents resulting in co-occurring side reactions (American Institute of Aeronautics and Astronautics Liquid Propulsion Committee on Standards, 1999). In addition to these, a sustained pressure increase is observed during the long-term storage of liquid propellants (shown in Figure 2.2). In some cases, the pressure rise reaches a peak value that remains steady or decreases instead of rising more (Mellor, Smith, Carr, & Bellis, 1993). In other words, the pressure rise phenomenon is caused by the low solubility of the foreign gases in the propellant that is created through one of the reasons explained above. For instance, oxygen solubility in nitric acid reduces steeply while acid concentration is increasing and becomes zero when acid concentration is above 79 percent. Consequently, according to nitric acid decomposition reaction (see (1.2)) relative pressure rise encountered (Ladanyi, Miller, Karo, & Feiler, 1953).

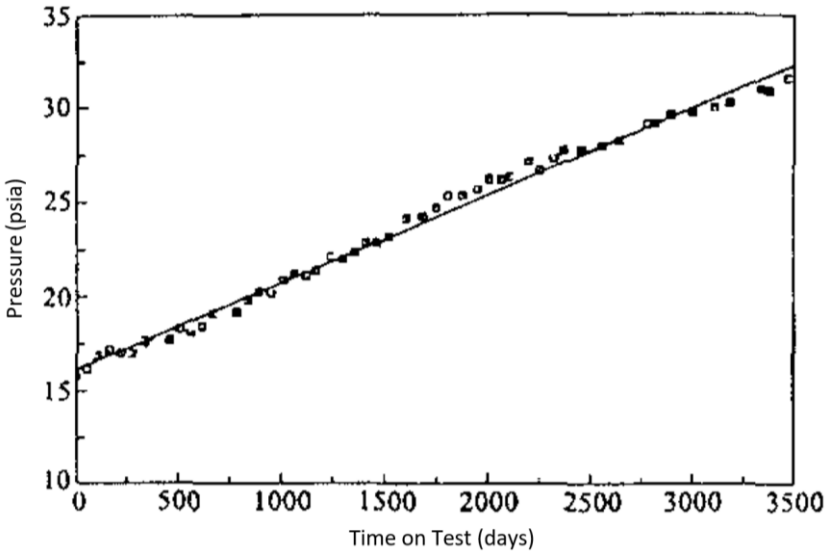

Figure 2.2 Pressure change with respect to time for hydrazine storage (Mellor, Smith, Carr, & Bellis, 1993) Reproduced with permission from AIAA

2.2.3 Intergranular Corrosion of Austenitic Steels and Titanium Alloys

Spontaneous chromium carbide, $Cr_{23}C_6$, precipitation takes place around austenitic grain boundaries specific to austenitic stainless steels if they are exposed to temperatures ranging from 425°C to 900°C for long periods during welding. This leads to depletion of chromium on the exterior surface of the grain domain resulting in sensitization of the processed section (Sugur & Manwani, 1983). Low chromium area has quite a low creep and reduced corrosion resistance, additionally, such processed profiles have the tendency to fail sooner. If these defective materials are employed to store strong oxidizers like nitric acid or nitrogen tetroxide for prolonged periods, then intergranular corrosion initiates to form. Similar to stainless steel, titanium alloys are extremely resistant to strong oxidizing agents below boiling temperatures. However, the extent of corrosion resistance substantially decreases when concentrated hot acids meet titanium alloys then an intergranular attack starts to form. Usage of high purity unalloyed titanium grades, also known as ASTM grade 2, might overcome this issue. Apart from that, the presence of quite scarce amounts

of metals like silicon or metal ions like platinum might help to limit titanium corrosion occurring at high temperatures (Carderelli, 2008).

There are several methods used to combat intergranular corrosion formation that is proved functional to some extent. The first method is annealing at 1050±50°C and fast quenching along with the sensitization interval. The annealing and quenching steps are performed when the dissolution of chromium carbide is induced. The second method is to add a stabilizer that will create carbides, as a result, during welding chromium will not be disturbed. Lastly, utilization of low carbon steels, around 0.05%, like AISI 304L and AISI 316L significantly prevent the chromium carbide precipitation since carbon is required for precipitation to occur (Sugur & Manwani, 1983).

2.2.4 Flow Decay Phenomena

The flow decay phenomenon is a complex issue that is affected by several variables such as temperature, pressure, and material compatibility. However, the influence of these variables is usually not independent from one another or straightforward to interpret (Martin Marietta Corporation, 1977). In other words, each parameter has distinct threshold values toward to amount of flow decay formed (American Institute of Aeronautics and Astronautics Liquid Propulsion Committee on Standards, 2001). By definition, flow decay is a spontaneous flow rate decrease taking place in a constant flow course. During storage, usually insoluble metal adducts, viscous sludge-like gels, and solid corrosion precipitates could be formed because of the propellants affecting the tank material with which they are in contact. In turn, this might lead to serious flow decay issues in propellant flow systems due to the accumulation of these residues on the instruments like filters, orifices, and valve seats. This type of flow blockage problem could cause shifts in the propellant mixture ratio. For instance, a flow decay issue was observed on the Titan III aluminum Transtage injector. Later investigation tests confirmed that an extreme amount of solid crystalline substances were found (Uney & Fester, 1972).

2.3 Pressure Measurement Equipment and Test Set-Up Designs

Numerous different types of test equipment have been designed to conduct storage experiments and used to monitor the pressure change caused by deterioration as well as decomposition of liquid propellants inside sealed containers mostly at elevated temperatures (Bennett, Saw, & Sutton, 1979).

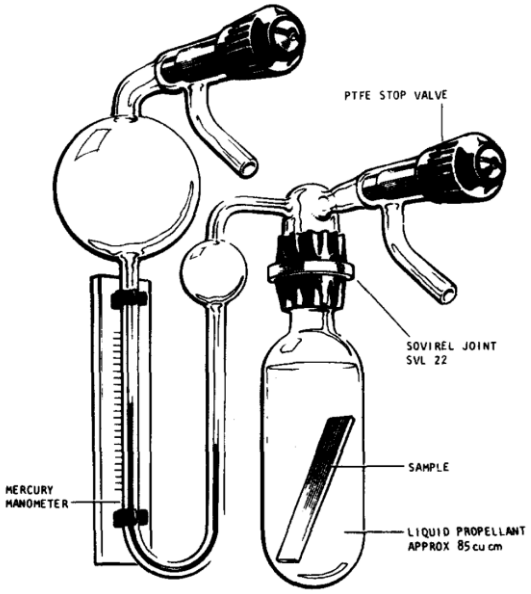

Figure 2.3 Pressure measurement equipment via mercury manometer (Bennett, Saw, & Sutton, 1979) Reproduced with permission from Elsevier

For static immersion tests, owing to its inert nature usually containers made of glass and teflon seated valves were utilized if possible. One such primitive piece of equipment consisted of a PTFE stop valve, glass test bulb, and mercury manometer (shown in Figure 2.3). However, later encountered that there were leaks around the sovirel joint at high temperatures and pressure recordings were severely affected by problems like bubble jam and fuel sticking within the column. For this reason, in improved design, a PTFE lined rubber gasket was placed within the sovirel joint to prevent gas leakage, and stainless steel pressure transducer replaced the mercury manometer (shown in Figure 2.4). Here, an aluminum connector between the pressure transducer and glass bulb was also attached with a stainless steel needle valve to release pressure before terminating the experiment. However, the pressure

build-up rates measured via the second design (Figure 2.3) were at least three times higher compared to the initial design (Figure 2.4), which was attributed to the decomposition of propellant on the metal surfaces of the relief valve, pressure transmitter, and aluminum connector. These misleading findings constrained the utilization of that improved design and some alterations were performed.

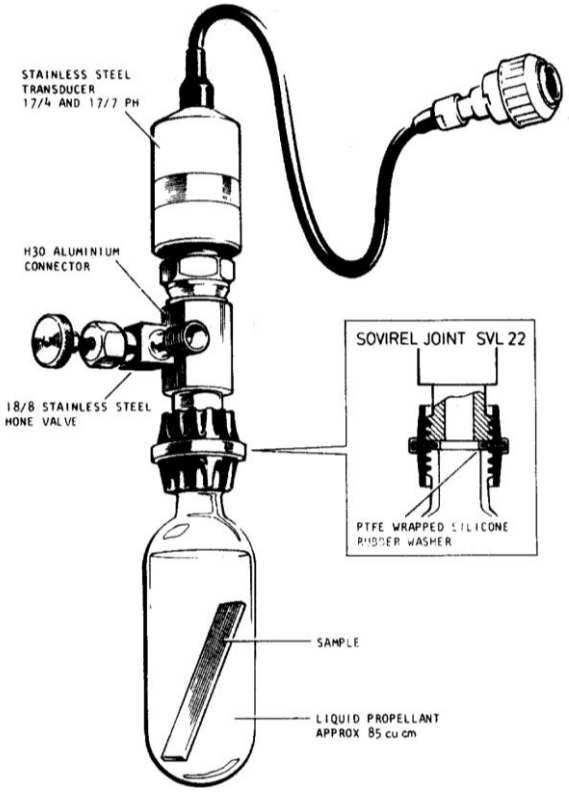

Figure 2.4 Pressure measurement equipment via transmitter (Bennett, Saw, & Sutton, 1979) Reproduced with permission from Elsevier

In the final design, the aluminum connecter along with the needle valve was removed and the stainless steel pressure transmitter was inverted upside down in such a way that propellant vapor would be in contact with the filled mercury pool. Lastly, the pressure relief method from the initial design was adapted, in other words, the PTFE valve was replaced by the steel needle valve (shown in Figure 2.5). This design was utilized for static immersion tests and the experiments mostly provided reasonable data. The pressure change data obtained from the latest test set-up provided similar findings compared to the initial set-up without the adverse deficits (Bennett, Saw, & Sutton, 1979).

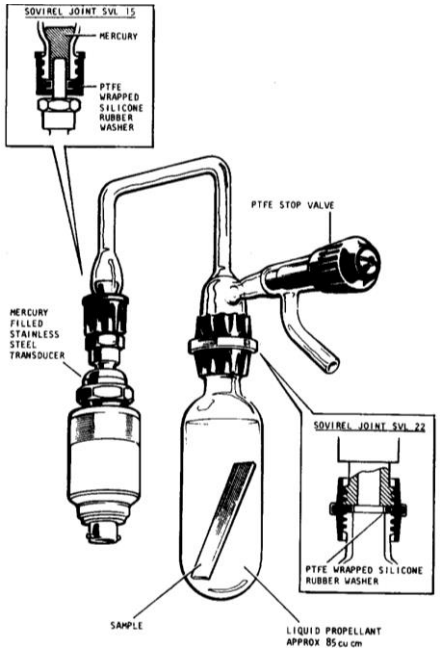

Figure 2.5 Pressure measurement equipment via mercury filled transmitter (Bennett, Saw, & Sutton, 1979) Reproduced with permission from Elsevier

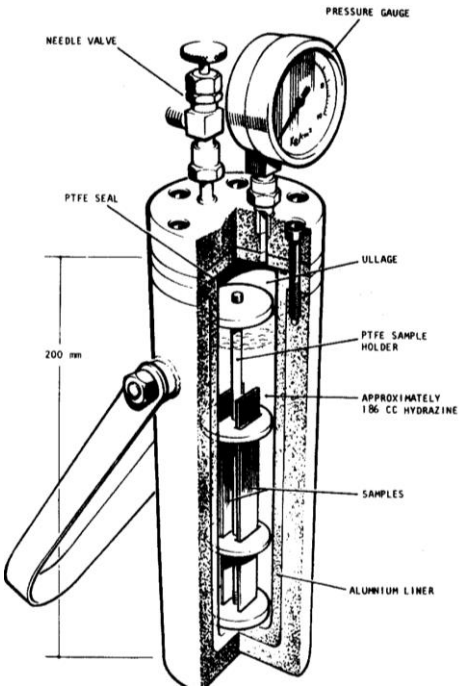

Figure 2.6 Aluminum plated pressure measurement vessel (Bennett, Saw, & Sutton, 1979) Reproduced with permission from Elsevier

In some static immersion tests, the decomposition pressure was well above the values that glass bulbs could withstand, for this reason in such cases tests were carried out in a teflon container in which placed inside an aluminum lined high tensile stainless steel vessel (shown in Figure 2.6). Similar to other designs, to release the pressure generated a stainless steel needle valve was attached on top of the lid. Additionally, to monitor pressure changes a stainless steel pressure gauge was utilized.

Static immersion tests were followed by storage properties determination tests by using sealed containers that had material of interest bodies on the inside and high tensile protective steel bodies on the outside. The vessel set-up was fitted with a diaphragm-equipped analog manometer and stainless steel vent valve that was mounted on the stainless steel cap (shown in Figure 2.7 and Figure 2.8).

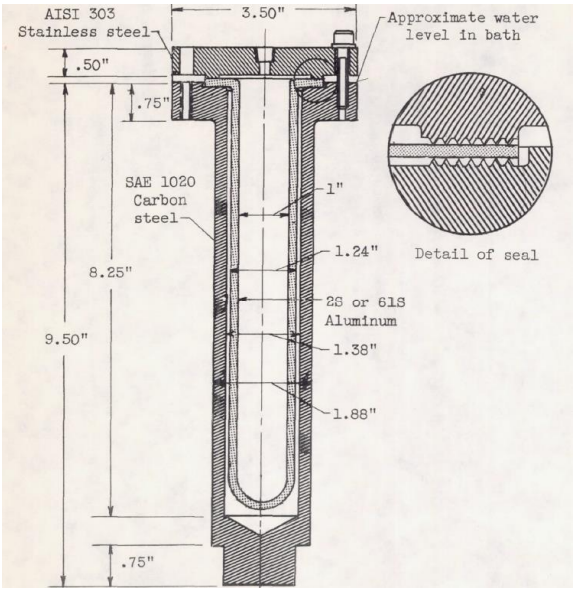

Figure 2.7 Engineering drawing of storage test vessel (Feiler & Morrell, 1952)

During storage tests at elevated temperatures, when the ullage space was roughly ranging from 5 to 15 percent pressures as high as 100 kilogram per square centimeter (98 barG) were encountered due to increased decomposition reactions from time to time. For this system, leak proofing was ensured via an extended lip of the inside tube which functioned as a gasket between the cap and outside body when these screws joined to each other.

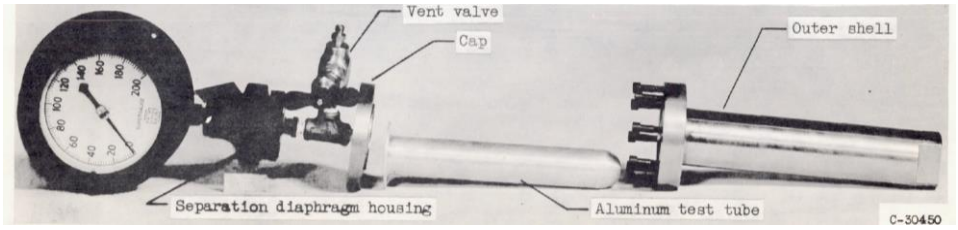

Figure 2.8 Disassembled view of storage test vessel (Feiler & Morrell, 1952)

At the end of storage properties tests, there were varying amounts of salts and corrosion formation depending on the conditions and propellant types. In some cases, the salt, corrosion, and adduct formation were intense (shown in Figure 2.9)where the pressure rise exceeded 150 kilograms per square centimeter.

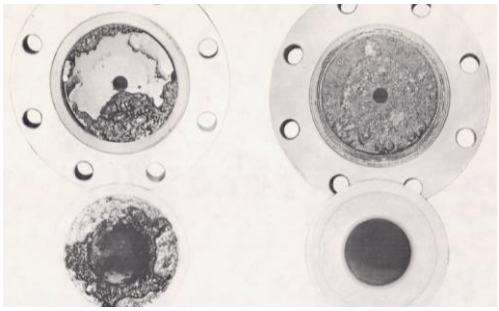

Figure 2.9 Corrosion on stainless steel caps and aluminum test tubes after 400-hour long storage of white fuming nitric acid at 77°C (Feiler & Morrell, 1952)

Substantially depending on the outputs of the static immersion and small-scale storage tests, the storage experiments are continued with medium-sized tanks that gradually start to converge into flight system configuration in terms of size and instrumentation (Figure 6.1 and Figure 6.2). By courtesy of these partially realistic experiments, the storage behavior of the propellant under investigation at elevated temperatures, ~60°C, is designated and as a result, the acceptability of the storage tanks being studied is evaluated. Later, pressure rate data obtained at high temperatures are linked to the pressure rise of the propellants at normal storage temperatures through the Arrhenius equation. This is primarily applied since tests conducted at or below normal temperatures require a considerably long time to produce useful data that consequently create inadmissible delays in the design and procurement steps (Sutton D. , 1986).

2.4 Propellant Storage Tank Designs and Propellant Feed Systems on Rockets Engines

Storage of liquid bipropellants within the rocket engine complex is accomplished via different shaped tanks where they are arranged in a different number of ways, whereas usually a single storage tank is employed to store monopropellants in the same manner. Apart from that, to have some command over the position of the entire system's center of gravity a great number of distinct tank designs can be used (shown in Figure 2.10).

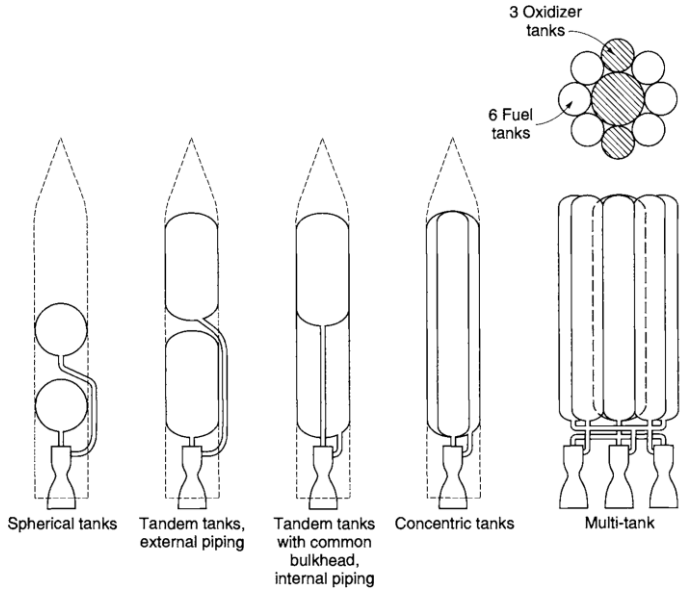

Figure 2.10 Common tank configurations for major liquid propellant rocket engines (Sutton & Oscar, Rocket Propulsion Elements, 2001) Reproduced with permission from John Wiley & Sons

Throughout the tank design process, one of the main aims is to achieve the highest expulsion efficiency or lowest vehicle inert mass. In other words, it is impossible to utilize the propellant in the system completely because a small amount of propellants are consumed as leftovers on the walls, and trapped in instrument connections. The expulsion efficiency for a typical tank design ranges from 97% to 99.7% in which the rest of the propellant is inconsumable and added to the inert mass of the vehicle. Theoretically, the sphere is the ideal propellant tank shape as it provides the smallest

tank weight in comparison to other geometrical shapes. However, the utilization of large spherical tanks for the primary propulsion system is impractical due to lateral space limitations in launch vehicles (Sutton & Oscar, Rocket Propulsion Elements, 2001). For this reason, larger tanks are generally manufactured in cylindrical forms with alternating dome shapes at the ends (shown in Figure 2.11) (National Aeronautics and Space Administration, 1974).

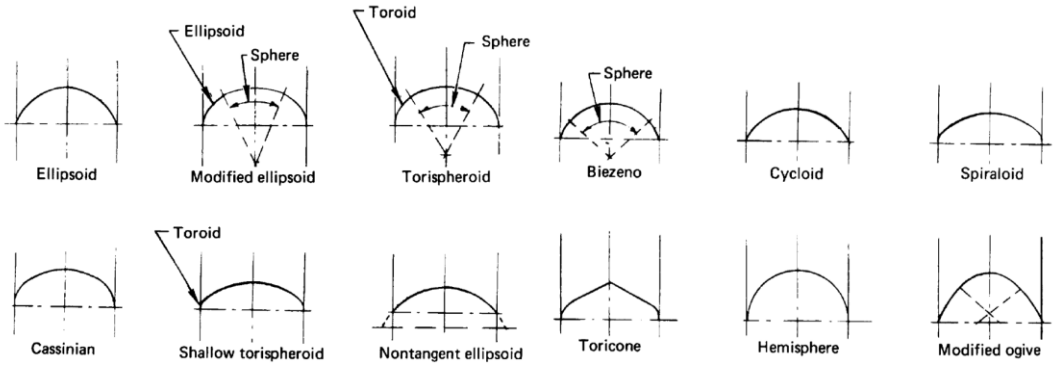

Figure 2.11 Common end closure of liquid propellant storage tanks (National Aeronautics and Space Administration, 1974)

Both turbopump and high-pressure gas feed system's liquid propellant storage tanks directly connect to the propellant feed system via related piping. The feed systems, in other words, rocket propulsion systems mainly consist of numerous complex valves, turbines, gas generators, pumps, sensors, precombustion chambers, and a thrust chamber at the end (shown in Figure 2.12). Depending on the engine cycle such as gas generator, staged combustion, or expander, the diversity, and the quantity of these equipment changes. However, the primary principle is to supply the desired amount of propellant into the combustion chamber at all times regardless of the supply or ignition system. For instance, the Space Shuttle's main engine consists of two distinct precombustion chambers in which each one is assembled onto another turbopump. Additionally, the main pumps' boosting pressure is provided by extra two turbopumps called booster pumps. However, the turbines of the booster pumps are driven by liquid oxygen and liquid hydrogen. This is just a specific example that each flight system has its unique propulsion and ignition system (Sutton & Oscar, Rocket Propulsion Elements, 2001).

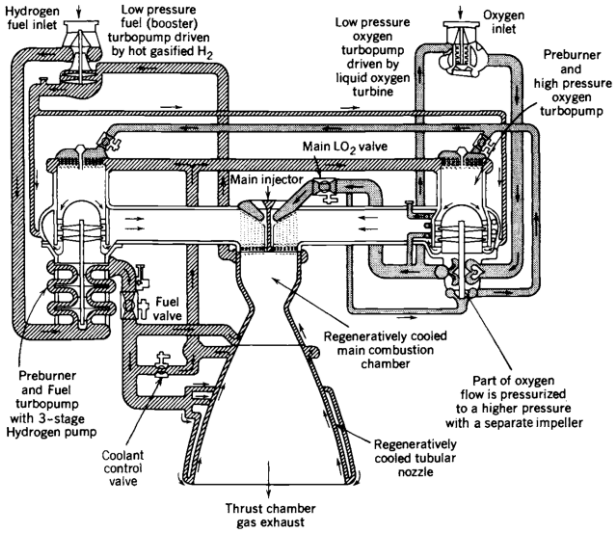

Figure 2.12 Propellant feed system of Space Shuttle main engine's staged combustion cycle (Sutton & Oscar, Rocket Propulsion Elements, 2001) Reproduced with permission from John Wiley & Sons

2.5 Parameters that Affect the Storage of Liquid Propellants

Liquid propellant storage is sensitive to discrete parameters such as ullage ratio, construction material of the vessel, surface treatments, pressurization gas type, storage temperature, initial blanket gas pressure, presence of additive chemicals, contaminants in propellant and blanket gas, the solubility of blanket gas in the propellant, and vessel material surface area to volume of test media ratio. Unfortunately, there is no single, yet effective parameter set, which could provide the most convenient storage conditions, but each affects one another for better or worse in some ways. For instance, low temperatures are desired for reduced chemical reactions during storage, but ensuring low temperature requires continuous infrastructure upkeep and maintenance inside the storage facility, which leads to substantial expenses. Such trade-offs between those parameters are loudly pronounced and great care must be taken during the test period. For this reason, each parameter ought to be carefully tested with one another, and accordingly, the most optimum yet cost-effective as well as applicable set of values shall be determined.

2.5.1 Ullage (Space) Ratio

Propellant storage tanks are almost filled only by leaving a small amount of space on top of the liquid, namely ullage volume, space, or ratio. Designers wish to constrain the amount of ullage space to the lowest value that will meet the pressure increases to be encountered during the storage period. Ullage volume determination may be simple to execute for those complexes that serve for short periods, but it is highly labor-intensive to attain the optimum amount for systems that will be sealed throughout years. (Sutton D. , 1986).

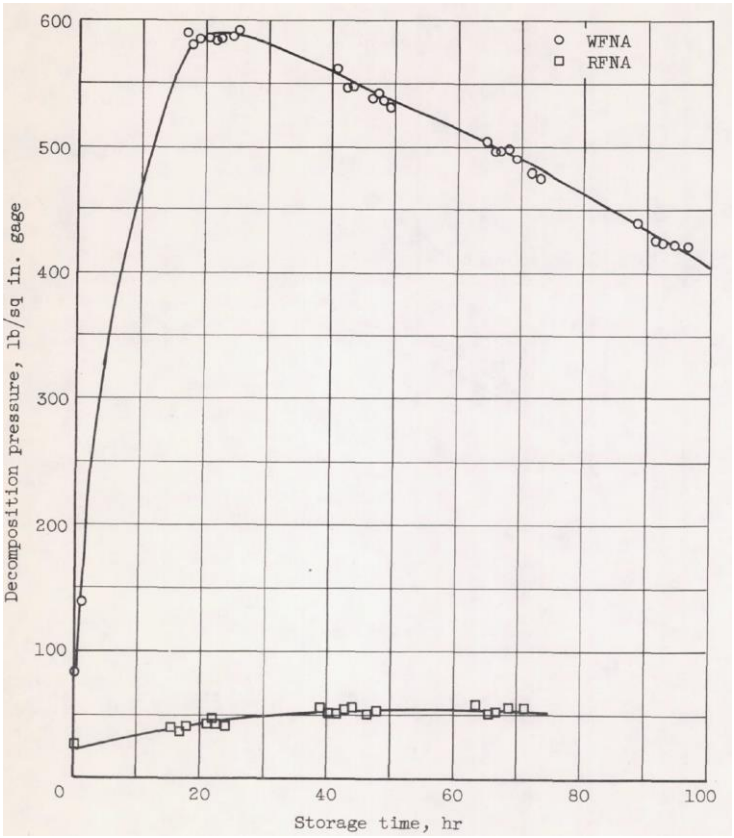

Figure 2.13 Decomposition pressure changes of RFNA and WFNA at 76.7°C and 16% ullage in aluminum vessels with steel caps (Feiler & Morrell, 1952)

Fundamentally, ullage space helps to compensate for thermal expansion of the propellant due to temperature changes, formation of gaseous chemicals due to reactions taking place between the propellant and tank material, and the emergence

of previously dissolved gases from the propellant. Depending on the propellant type 3 to 10 percent space is usually chosen as the ullage volume. The ullage volumes presented here only imply the initial values because once the propellant tanks are properly sealed the ullage space as well as resting pressure will continuously change due to changes in temperature and propellant content (Sutton & Oscar, Rocket Propulsion Elements, 2001). For instance, changes in decomposition pressures of RFNA and WFNA were determined at a constant temperature of 76.7°C when the initial ullage ratio was approximately 16% (shown in Figure 2.13). Here, the RFNA system experienced a slight pressure increase whereas the WFNA system underwent an extreme pressure rise. Pressure decrease in the WFNA storage experiment after a peak point was attributed to the oxidizing reactions consuming liberated oxygen that formed during decomposition (Feiler & Morrell, 1952). In other words, it was assumed that the system pressure was mainly controlled by two competing reactions namely corrosion and decomposition (Ladanyi, Miller, Karo, & Feiler, 1953).

2.5.2 Material Type of the Vessel

The material selection process is quite prominent in terms of compatibility as well as material properties such as physical, mechanical, acoustical, and thermal. Flight system designs are primarily affected by the material properties of the selected materials. Whereas the compatibility of disparate materials with liquid propellants can be based on either the degree that which the propellant influences the material or the degree that which the material influences the propellant, and sometimes both. In fact, regarding compatibility, there are perpetual reactions taking place between the materials and propellants. However, the acceptance limit for reaction and corrosion rate is applied up to a threshold value that defines the pair as compatible as long as it is not greater than that estimated value (Uney & Fester, 1972).

Approximately two thousand different types of both metallic and non-metallic materials were considered in the past. Specifically, some common steels, aluminum, nickel, and titanium alloys as well as numerous precious materials like pure gold,

tantalum, tungsten, and platinum were tested with propellants to obtain insight regarding the compatibility. As it turns out, most of these materials were portrayed as incompatible or did not provide required material properties along with machinability and weldability performances (American Institute of Aeronautics and Astronautics Liquid Propulsion Committee on Standards, 2001).

In cases in which an incompatible propellant material pair is utilized for long-term storage, depending on the extent of incompatibility, several evident changes are observed in both propellant and material. Firstly, the net weight of the test subject increases or decreases depending on reactions. Secondly, due to reactions serious etching, pitting, cracking, deposits, films, and stains form on the material surface. Lastly, because of the excess reactions taking place, solid crystalline deposits accumulate on the floor of the storage tanks over a long period and meanwhile propellant composition alternates continuously (Moran & Bjorklund, 1982).

After a while, in terms of metallic and non-metallic materials utilized for the construction of multifarious liquid propellant storage tanks, the selection was limited to only a handful of main categories like aluminum, nickel, stainless steel, titanium, and thermoplastic derivatives depending on the propellant type (given in Table 2-1). However, in addition to propellant content, processes such as welding, brazing, slugging, plating, and coating of the material significantly affect the rate and extent of surface reactions taking place (Moran & Bjorklund, 1982).

Table 2-1 Posttest results of compatibility ratings between diverse metallic materials and propellants (Moran & Bjorklund, 1982)

Duration (days)	MATERIAL Material	Configuration	Remarks	PROPELLANT Propellant	Remarks
3939	Al 6061-T6	Slug	Light corrosion; overall thick white film with cracking at the L/V area; light etching and no pitting.	Hydrazine	Slight decomposition; water-white.
3939	Ti 6Al-4V	Slug	No corrosion; overall thin film; no pitting.	Hydrazine	Slight decomposition; water-white.
4233	Al 2014-T6	Slug	Light corrosion; overall thick film; light etching; no pitting.	Hydrazine	Slight decomposition; water-white.
2980	Al 6061-T6	Slug-gold plated	Severe blistering of surface.	Hydrazine	Slight decomposition; light brown color.
3759	AISI 347	Weld-stress	No corrosion; thin overall film and no pitting seen in the weld zone. Light corrosion; thin overall film in the L and V areas and a thick film in the L/V area; no pitting seen in the heat-affected zone.	Hydrazine	Moderate decomposition; water-white.
3593	AISI 17-7 PH	Slug	No corrosion; thin overall film; no pitting.	Hydrazine	Slight decomposition; water-white.
3562	AISI 304L	Slug	No corrosion; very thin overall film; pitting.	Hydrazine	Very low decomposition; water-white.
2709	AISI 304L	Weld-stress	Light corrosion; thin film in the L/V and L areas and thick in the V area; light etching in the L/V and V areas and none in the L area; no pitting seen in the weld zone.	Hydrazine	Moderate decomposition; water-white.
3996	AISI 347	Slug	Light corrosion; thick overall film; light pitting approximately 10^{-6} in. diameter.	MMH	Slight decomposition; light brown color.
3996	Al 6061-T6	Slug	Light corrosion; thick overall film with cracking in the L/V and V areas; light etching; no pitting.	MMH	Slight decomposition.

Table 2-1 (cont'd)

3996	AISI 304L	Slug	Light corrosion; thin film in the L area and thick in the L/V and V areas with cracking in the L/V area; light etching in the L/V and V areas and none in the L area; light pitting in the L area and moderate in the L/V and V areas of about 10^{-6} in. diameter.	MMH	Slight decomposition; light yellow color.
3996	Ti 6Al-4V	Weld	Light corrosion; thick overall film; light pitting approximately 10^{-6} in. diameter.	MMH	Slight decomposition; light yellow color.
3996	AISI 304L	Weld	Light corrosion; thick overall film with cracking in the L/V area; light etching; no pitting.	MMH	Slight decomposition.
3996	Ti 6Al-4V	Slog-stress	Light corrosion in the L/V and V areas and none in the L area; thick overall film; light etching in the L/V and V areas and none in the L area; no pitting.	MMH	Slight decomposition; yellow-green color; dark sediment.
2443	AISI 347	Slug	No corrosion; thin film in the L/V area and very thin in the L and V areas; no pitting.	NTO	-
4147	Al 6061-T6	Slug	Light corrosion; thick overall film; light etching; no pitting.	NTO	-
4213	Ti 6Al-4V	Slug	Moderate corrosion; thin overall film; light etching; moderate pitting approximately 10^{-4} in. diameter.	NTO	-
4017	AISI 304L	Slug	Light corrosion; thin overall film; light etching in the L/V area only; no pitting	NTO	-
4147	AISI316	Slug	Light corrosion; thin film in the L/V and L areas and very thin in the V area; light etching in the L/V and L areas; no pitting	NTO	-
2246	AISI 17-4 PH	Slug	No corrosion; thin overall film; no pitting.	NTO	-
3199	Ti 6Al-4V	Weld-stress	Light corrosion and thin film in the L area; moderate corrosion and thick film in the L/V and V areas; light etching; light pitting in the L/V and V areas only of about 10^{-5} in. diameter.	NTO	-

2.5.3 Chemical Passivation Treatments

In simple terms, the formation of a chemically resistant film occurs spontaneously on the clean stainless steel surfaces when subjected to air or an oxygenated surrounding and this process is called passivation. Additionally, passivation refers to the removal of external free iron from the stainless steel surface via a chemical process. Here, free iron generally refers to the iron contamination on the surface, iron deposits caused by welding, and waste salts left from previous processes. Usually, the passivation process is performed with dilute nitric acid or citric acid solution (ASTM A967/A967M – 17, 2017). Once chemical treatments are applied, protective oxide film formation is enhanced significantly without adversely affecting the surface. At the end of complete passivation treatment, the material surface should not exhibit any physical deformation like pitting, blackening, or etching. However, surface damage and increased contamination might take place if the acid passivation step is executed improperly. For instance, if the passivation solution is utilized for prolonged periods and as a result becomes depleted then severe pitting on the steel surface might occur (ASTM A380/A380M – 17, 2017).

Corrosion formation is an important problem to avoid while employing stainless steel alloys for the space industry. Corrosion issues are pronounced especially for the storage of liquid propellants and wetted sections of propulsion systems. To enhance corrosion resistance, different chemical passivation treatments can be utilized and for this purpose several process steps can be followed if required (shown in Figure 2.14) (Parsons, Poyntz-Wright, Kent, & McManus, 2019).

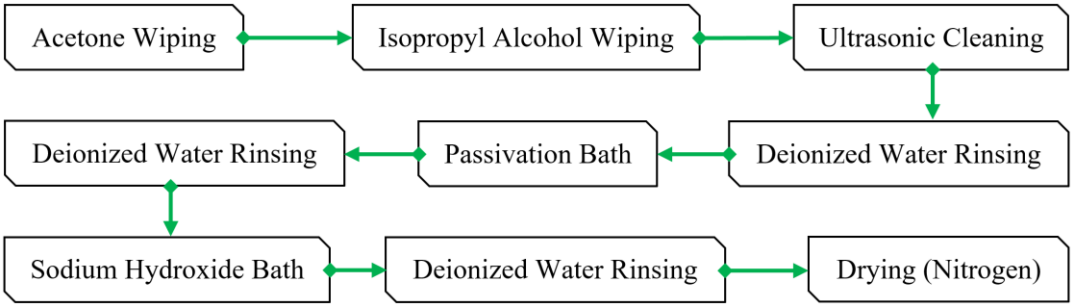

Figure 2.14 Process steps for stainless steel passivation (Parsons, Poyntz-Wright, Kent, & McManus, 2019)

The complete chemical passivation treatment steps slightly vary amongst people who operate. In other words, one does not have to follow each step but might carry out as one sees fit due to the nature of passivation application. Firstly, the material is cleaned from oil, grease, grit, dirt, particles, and other alien deposits found on the surface with a series of steps such as acetone wiping, isopropyl alcohol wiping, ultrasonic cleaning, and deionized water rinsing. Then, acid passivation is performed with a proper solution such as dilute nitric acid or dilute citric acid. Finally, passivated metal parts are neutralized by immersing in a dilute alkaline solution such as sodium dichromate, sodium peroxide, or sodium hydroxide. The neutralization process helps to accelerate passive oxide film formation but does not have any effect to free iron removal. During chemical passivation treatments, materials should be immediately rinsed with deionized water between every successive step after initial cleaning and to reduce staining they should not be allowed to dry naturally (ASTM A380/A380M – 17, 2017).

There are no generally accepted bath temperature, exposure time, and acid concentration parameters for both nitric and citric acid passivation treatments. The optimum passivation conditions strongly depend on the type of alloy being treated. Some featured acid passivation process parameters are recommended but the selection is left to the experimenter. For example, the citric acid solution containing from 4 to 10 weight percent could be used for at least 4 minutes at temperatures between 60°C and 70°C, whereas the same solution can also be employed for at least 20 minutes at temperatures between 20°C and 50°C. Additionally, other custom

concentrations, time, and temperature combinations are also possible but the results might vary (ASTM A967/A967M – 17, 2017).

Several verification tests are present and can be readily applied to determine the effectiveness of the chemical passivation treatment process. One of these is named boiling water immersion test, it is used to detect any free iron or anodic residue left on the material surface after passivation. The test is conducted by immersing the processed materials into an inert pot filled with deionized water. Then, the temperature of the water is raised to around 95°C then kept there for about 30 minutes while holding the parts immersed. After that, the heat source is switched off and the system is left to cool for approximately 3 hours. Later, the material is taken out of the pot and left on a piece of cloth to dry for about 2 hours. In the end, the processed parts shall not show any significant stain or rust on the surface (ASTM A967/A967M – 17, 2017).

2.5.4 Blanket (Pressurization) Gas Type

In the most general sense, blanket gases should not dissolve too much in the propellant and not condense during the storage period. Additionally, pressurization gases should be inert and do not react with the propellant (Sutton & Oscar, Rocket Propulsion Elements, 2001). Liquid propellants are slightly pressurized inside the run tanks throughout storage to decrease the oxygen content in the vapor to inhibit the formation of explosive mixture for flammable liquids and hinder air oxidation of the propellant (given in Table 2-2). For instance, a hydrazine-air mixture has a 4.7% lower explosive limit whereas a hydrazine-nitrogen mixture has a 38% lower explosive limit (Simpson, 1985). In addition, the use of inert padding gas precludes hygroscopic fuels like hydrazine from retaining moisture and slows down undesired catalytic reactions between highly reactive fuels and an oxygen-rich storage atmosphere. Furthermore, for strong oxidizing agents, an inert atmosphere helps to reduce the rate of undesired chemical reactions by inhibiting the formation of

corrosion on material surfaces in contact with propellant (American Institute of Aeronautics and Astronautics Liquid Propulsion Committee on Standards, 2001).

Table 2-2 Effect of diluent gas types on the LFL of hydrazine at 1 atm (American Institute of Aeronautics and Astronautics Liquid Propulsion Committee on Standards, 1999)

Diluent	**Temperature (K)**	**Lower Flammability Limit (% v/v)**
Argon[a]	373 – 393	28.1
Helium[b]	378 – 391	37.0
Nitrogen[a]	373 – 393	35.2

[a]Pannetir (1958)
[b]Scott, Burns, and Lewis (1949)

In the past, three main gases namely nitrogen, helium, and argon were utilized or at least experimentally tried as blanket gases for liquid propellant storage applications on the ground and launch vehicles. The primary common feature of these gases is that they are all chemically inert. In other words, they do not readily catalyze reactions and extensively dilute when in contact with energetic liquid substances (Marsh & Knox, 1970).

The utilization of inert diluting gases inside the storage system usually increases the autoignition temperature (Mullins & Penner, 1959). However, different blanket gases lead to varied property changes. For instance, in the hydrazine storage process, if argon and nitrogen are utilized, the autoignition temperature decreases up to 20%, but if helium is used, the autoignition temperature increases (American Institute of Aeronautics and Astronautics Liquid Propulsion Committee on Standards, 1999). Due to such reasons, numerous propellant flow and storage systems make use of helium gas for space applications (DeSain, Brady, Curtiss, & Greenberg, 2015).

2.5.5 Storage Temperature

Earth storable liquid propellants are typically stored at moderate temperatures of 10°C to 30°C when the chemical is relatively inactive to reduce the reaction rate, and amount of decomposition meanwhile prolonging the service life of the entire system (Bennett, Saw, & Sutton, 1979).

The chemical decomposition rate of liquid propellants is strongly dependent on ambient temperature (Simpson, 1985). In fact, as the temperature increases, the extent of catalytic reaction effects becomes more severe for shorter periods (Uney & Fester, 1972). For instance, controlled tests were performed with nitric acid by using stainless steel and aluminum alloys, which proved that increase in temperature appreciably accelerated the corrosion rate (shown in Figure 2.15) (Ladanyi, Miller, Karo, & Feiler, 1953). In addition to that, high temperatures could lead to a decrease in material compatibility. This phenomenon could be best explained by the possible change in reaction path at high temperatures compared to the ones at low temperatures. In other words, reaction kinetics at low temperatures could be considerably different from those at higher temperatures. Apart from that, findings obtained from high-temperature tests were somehow aimed to correlate with the low-temperature expectations. However, due to the possibility of change in reaction path, the extrapolated data would not overlap well with the low-temperature real-time exposure data (American Institute of Aeronautics and Astronautics Liquid Propulsion Committee on Standards, 1999).

In practice, the storage tests are generally conducted at high temperatures namely between 60°C and 90°C instead of nominal storage conditions which lies usually around 20°C. To be able to perform storage tests at low temperatures, highly sensitive data acquisition systems are required since the pressure build-up rate is quite slow and an extended experimental period in terms of years is necessitated. However, storage temperature and its effects on both the pressure rise and the ullage space are essential information that is essentially required at the very beginning of

project development. Owing to testing at high temperatures, the necessary data might be obtained in a considerably shorter time (Bennett, Saw, & Sutton, 1979).

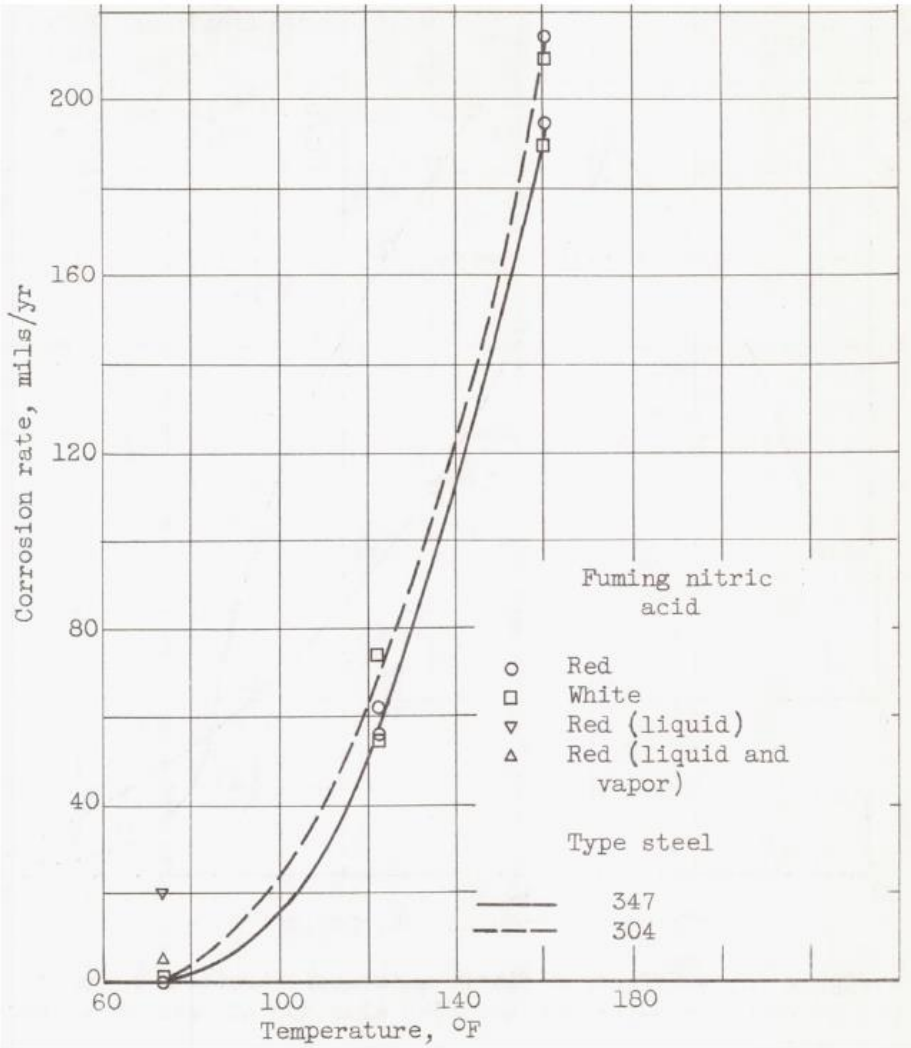

Figure 2.15 Temperature effect on corrosion rates of stainless steel in fuming nitric acids (Ladanyi, Miller, Karo, & Feiler, 1953)

2.5.6 Initial Blanket Gas Pressure

Liquid propellant storage tanks both on the ground and in launch vehicles are pressurized via an inert gas due to reasons discussed throughout in sections 2.5.4 and 2.5.9. The pressure value of the initial blanket gas directly affects the pressure rise

inside the vessel in the course of storage (American Institute of Aeronautics and Astronautics Liquid Propulsion Committee on Standards, 1999). For example, if higher initial pressures are employed as blanket gas to store hydrazine derivatives, then higher final pressures are observed at a constant volume environment according to the ideal gas law. However, increasing or decreasing initial gas pressure leads to several desirable and undesirable property changes. Such that, specific to hydrazine storage, if the gas pressure is decreased then the autoignition temperature increases (Benz, Bishop, & Pedley, 1988) but the minimum ignition energy decreases (Benz & Pippen, 1980). For instance, reduce in initial pressure of hydrazine decreases the upper flammability limit and increases the lower flammability limit. As a result, the flammability range is narrowed (American Institute of Aeronautics and Astronautics Liquid Propulsion Committee on Standards, 1999). In other words, changing initial pressure provides some safety benefits meanwhile inducing some safety issues.

2.5.7 Additive Chemicals

Chemical additives and sometimes inhibitors were tested and utilized to extend the propellants' storage life while suppressing the undesired characteristics like decomposition, corrosion, and deterioration. Meanwhile, those substances also served the purposes of improving ignition performance, ignition delay reduction, and increasing the specific impulse of propellant pairs (Ladanyi, Miller, Karo, & Feiler, 1953). However, in some cases, additives used to inhibit corrosion rate or to reduce the freezing point of liquid propellants might adversely affect combustion kinetics that may lead to the formation of solid particles due to caking out (Terlizzi & Streim, 1956). For instance, hydrofluoric acid was added to fuming nitric acids to inhibit the rate of corrosion reactions taking place on the material surface where hydrogen fluoride formed insoluble metal fluoride molecules that firmly held onto the surface of the metal (Phelps, Lee, & Robinson, 1955).

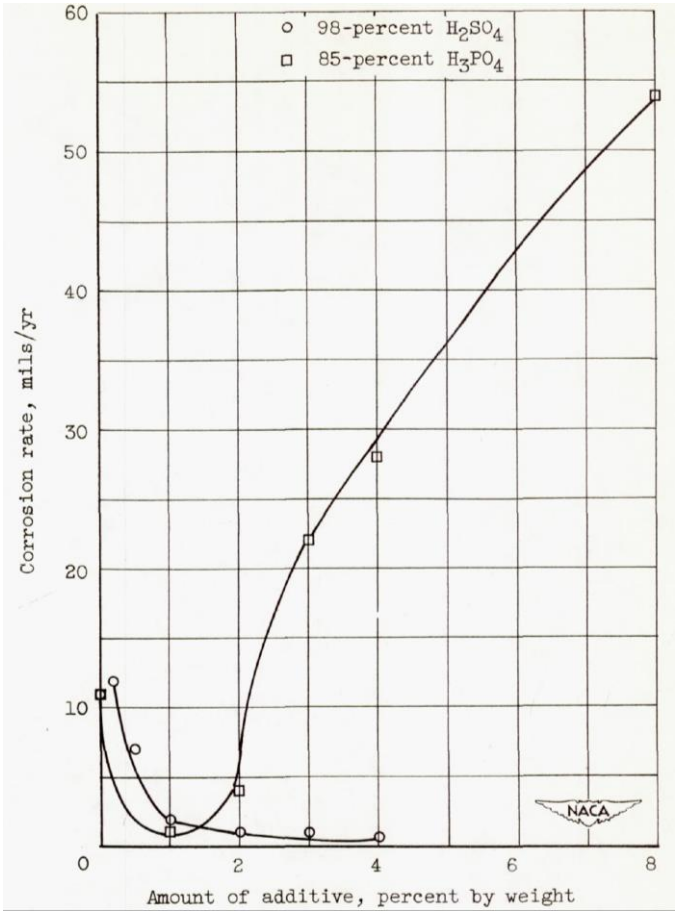

Figure 2.16 Effect of sulfuric acid and phosphoric acid additives on corrosion rate of mild steel in red fuming nitric acid (Ladanyi, Miller, Karo, & Feiler, 1953)

Effects of multifarious additives on corrosion rate, decomposition pressure rate, and propellant deterioration of stored liquid propellants have been extensively investigated. Accordingly, in terms of corrosion rate, while an increase in the amount of additive added positively affects the corrosion rate in some cases the opposite was observed in other cases. Later concluded that corrosion rate specifically depends on the type and amount of additive utilized. For instance, once sulfuric acid and phosphoric acid were individually added into red fuming nitric acid to inhibit corrosion of mild steel, as the amount of added sulfuric acid increased, a continuous decrease in corrosion rate was obtained, however, for phosphoric acid right after 1 percent value, corrosion rate accelerated substantially (shown in Figure 2.16) (Ladanyi, Miller, Karo, & Feiler, 1953).

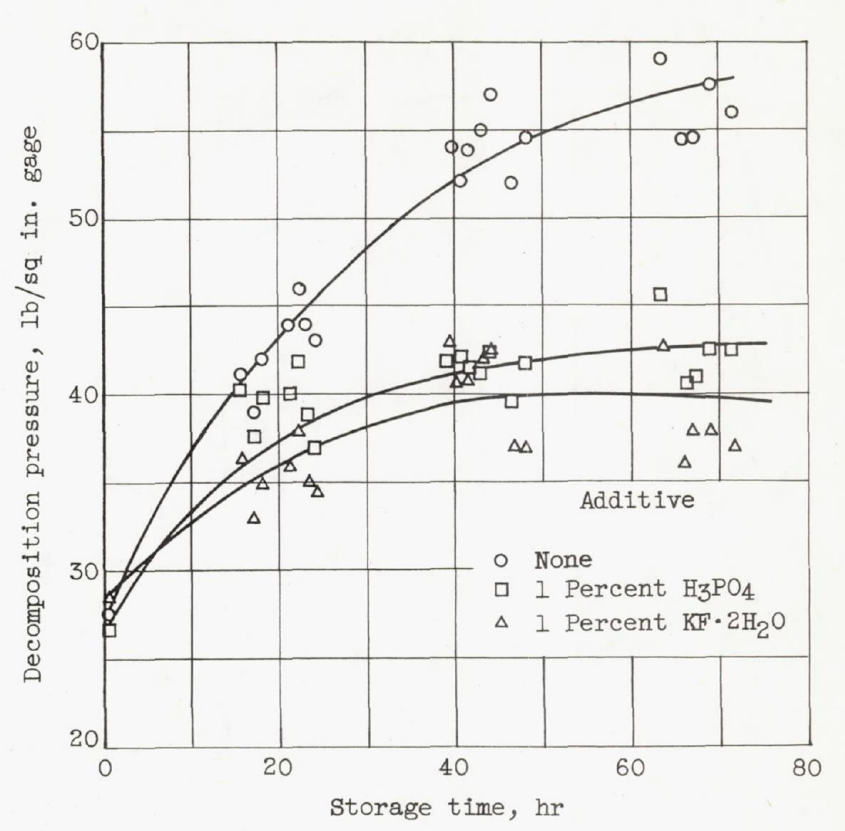

Figure 2.17 Effect of $KF \cdot 2H_2O$ and H_3PO_4 additives on decomposition pressures of red fuming nitric acid (Feiler & Morrell, 1952)

Decomposition pressures of red fuming nitric acid during short-term storage with and without $KF \cdot 2H_2O$ and H_3PO_4 additives were tested (shown in Figure 2.17). Consequently, $KF \cdot 2H_2O$ was found to be quite effective compared to H_3PO_4 and without additive cases to inhibit pressure rise inside the steel vessels. Concerning propellant deterioration, after 100-hour storage tests of propellant grade white fuming nitric acid with and without additives, some noticeable changes in their composition were detected (given in Table 2-3). At this stage, it could be stated that $KF \cdot 2H_2O$ was more effective compared to H_3PO_4 for white fuming nitric acid storage (Feiler & Morrell, 1952).

Table 2-3 Effect of potassium fluoride dihydrate and phosphoric acid additives on white fuming nitric acid composition (Feiler & Morrell, 1952)

Detail	Component (Weight Percent) HNO_3	NO_2	Water + Nonvolatiles	Nonvolatiles	Corrected Water
Before Storage					
Without Additive	**95**	**2.2**	**2.8**	**0.1**	**2.7**
AFTER Storage					
Without Additive	**86.4**	**10.2**	**3.4**	**0.97**	**2.4**
+ 1 % $KF \cdot 2H_2O$	**88.8**	**5.3**	**5.9**	**1.47**	**4.4**
+ 1 % H_3PO_4	**89.0**	**6.8**	**4.2**	**0.61**	**3.6**

2.5.8 Contaminants in the Propellant and Storage Atmosphere

The presence of impurities in the storage material surface, liquid propellant, and blanket gas significantly affect the decomposition and deterioration of the propellant during the storage period. Some specific metal oxides and ions accelerate catalytic reactions taking place markedly. For instance, cupric, ferric, and chromic ions drastically catalyze hydrazine decomposition into nitrogen and ammonia gases under a nitrogen atmosphere (Simpson, 1985).

The extent of pressure rise, and decomposition rate of fuels directly depend on the type of impurity present and the construction material of the vessel. For instance, when chromium ($Cr(N_2H_3CO_2)_3 \bullet 2H_2O$) and manganese ($MnCl_2 \bullet 4H_2O$) based complexes were introduced separately and together into hydrazine stored in glass vessels at 43°C, they conspicuously did not induce or accelerate homogeneous decomposition rate. On the other hand, the presence of relatively minute amounts of carbon dioxide impurity (20-ppm bottom threshold value) in the hydrazine could lead to the formation of hydrazine carboxylic acid ($CH_8N_4O_2$) (see (2.2)), which substantially increased homogeneous decomposition rate. The reaction rate increase was attributed to metal ions leached from the stainless steel material surface due to the formed carbazic acid's corrosive impact (Bellerby, The Effect of Some Dissolved Metal-Ion Contaminants on the Homogeneous Decomposition Rate of Anhydrous Hydrazine, 1985). Additionally, when stainless steel vessels were used, the change

in decomposition rate, metal corrosion, and the resulting rise in ullage pressure was determined to be a direct function of the carbon dioxide amount added. However, in glass vessels, carbon dioxide impurity presence was detected to have a little effect on the rate of decomposition and ullage pressure rise. In other words, interactions between carbon dioxide and hydrazine were strongly assisted by surface catalytic reactions (Bellerby, The Chemical Effects of Storing Hydrazine Containing Carbon Dioxide Impurity in Stainless Steel Systems, 1983).

$$2N_2H_4 + CO_2 \rightarrow N_2H_5{}^+ \bullet N_2H_3CO_2{}^- \qquad (2.1)$$

Liquid propellants of oxidizing origin also exhibit similar behaviors compared to liquid fuels. Such that, chloride, water, and oxygen impurities were individually added to nitrogen tetroxide in which different materials were tested. Accordingly, different metallic materials like aluminum, stainless steel, and titanium showed varied responses in terms of corrosion rate and propellant deterioration (shown in Table 2-4) (Martin Marietta Corporation, 1977). From diverse experimental data, it was clear that any dissolved or suspended contaminants present in the storage vessel adversely affected the material compatibility and effective storage life of propellants (American Institute of Aeronautics and Astronautics Liquid Propulsion Committee on Standards, 2001).

Table 2-4 Physical changes of one & four month metal specimens before and after propellant removal (Martin Marietta Corporation, 1977)

Added Impurity	**Material Type**	**Appearance of One Month Capsules**		**Appearance of Four Month Capsules**	
		Before Propellant Removal	**After Propellant Removal**	**Before Propellant Removal**	**After Propellant Removal**
None	Aluminum	No noticeable corrosion	No noticeable corrosion	No noticeable corrosion	Some oily substances on bottoms of tubes.
	Stainless Steel	No noticeable corrosion	No noticeable corrosion	No noticeable corrosion	Some gelatinous material on the bottoms of the tubes.
	Titanium	No noticeable corrosion	No noticeable corrosion	No noticeable corrosion	A few crystals on the walls of the tubes.
H_2O	Aluminum	Specimens covered with white salts.	Specimens covered with white salts.	White crystals on bottom of tubes. Specimens covered with white salts.	Specimens covered with white salts. Some crystals on walls and bottoms of tubes.
	Stainless Steel	Specimen were black with few black crystals on them. Greenish colored immiscible droplets on the sides of tubes.	Specimen were black with few black crystals on them. Greenish colored immiscible droplets on the sides of tubes.	Specimen were black with few black crystals on them. Greenish colored immiscible droplets on the sides of tubes.	Black salt crystals on specimen. Green oily substance on walls and bottom of tubes.
	Titanium	Specimens slightly spotted.	Specimens slightly spotted.	No noticeable corrosion	Small amount of oily substance on bottoms of tubes. Clear crystals on walls of tubes.
O_2	Aluminum	Slight spotted discoloration of specimens.	Slight spotted discoloration of specimens.	Slight discoloration.	Slight spotted discoloration of specimens. Yellow crystals at tops of the tubes. White powdery coating on the walls of the tubes.
	Stainless Steel	Specimens were black. Some yellow crystals on specimens and walls of the tubes.	Specimens were black and had some yellow crystals on them and on the tube walls.	Specimens were black. Reddish-brown crystals on walls of tubes above the liquid.	Specimen were black. Reddish-brown crystals on the walls of the tubes.
	Titanium	No noticeable corrosion of the specimens. Tube walls covered with a yellowish-white material.	No noticeable corrosion of the specimens. Tube walls covered with a yellowish-white material.	No noticeable corrosion	No noticeable corrosion

2.5.9 Solubility of Blanket Gases in Liquids

The concept of solubility could be defined in several different forms. Simply, it can be illustrated as a solute property to dissolve in a solvent substance. Here, the solute can be a solid, a liquid, or a gas substance. In this section, mainly the solubility of gases in liquids will be examined. The gas solubility in a liquid solvent is also called dissolution. Fundamentally, the value of solubility of a gas in a liquid is affected by the temperature and pressure along with the chemistry of the substances involved. However, the generalization of dissolution properties of different solutes in distinct solvents regarding the temperature and pressure changes is more deceptive than it seems. Furthermore, without experimental data, it is also not easy to comment confidently on the solubility of a known gas and liquid pair. In other words, one needs to determine the solubility change of a gas in liquid depending on the alternating temperature and pressure. However, the solubility of a gas solute in a liquid solvent might exhibit non-ideal and parabolic outcomes. For instance, the solubility of oxygen in water at constant pressure first decreases up to temperatures around 390K, and then as the temperature rises the solubility starts to increase drastically (shown in Figure 2.18). On the other hand, under similar conditions, helium solubility in water shows a slow but almost steady increase at low temperatures, and then a steep increase at elevated temperatures regardless of pressure values (shown in Figure 2.19). Indeed, there seems to be a ground-rule stating that "gas solubility in liquid decreases with increasing temperature", but this proposition does not hold all the time. According to J. Carroll (1999), this pseudo rule is only valid for a limited temperature range. From thermodynamics,

$$\left(\frac{\partial \ln H_{ij}}{\partial T}\right) = \left(\frac{-\Delta h_{sol}^{\infty}}{RT^2}\right) \tag{2.2}$$

Assuming constant enthalpy of solution, the equation (see (2.2)) simplifies as following (see (2.3)),

$$\ln H_{ij} = A + \frac{B}{T} \tag{2.3}$$

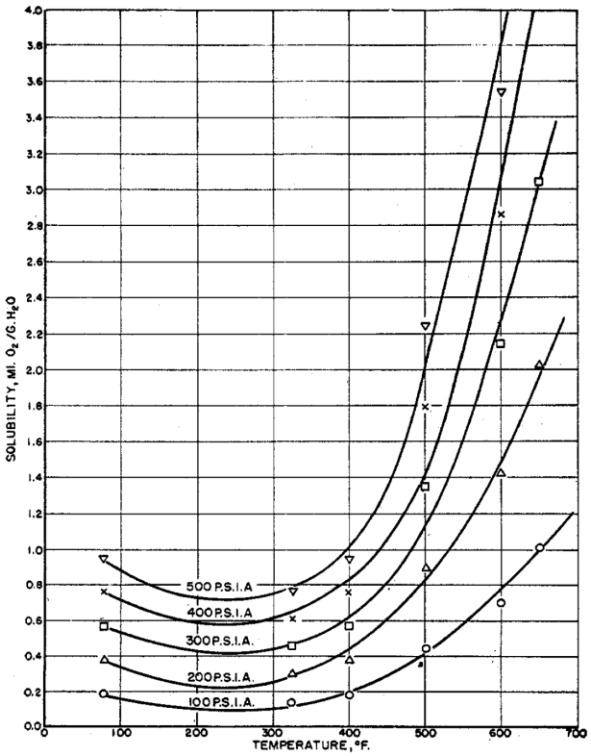

Figure 2.18 Oxygen Solubility in Water as a Function of Temperature at Constant Pressure (Pray & Minnich, 1952) Reproduced with permission from ACS Publications

At this stage, it is important to remember that regarding the sign of the heat of the solution no assumption was made. In fact, in reality, it can be either negative or positive. Additionally, the heat of the solution is not constant, which is the first assumption. As a result, depending on these facts, Henry's constant could be either decreasing or increasing function of temperature. For this reason, the common practice is to get empirical solubility data concerning temperature. Then, Henry's constants are computed and they are placed in a semi-experimental structure as given (see (2.4)) where A, B, C, and D are constants (Carroll, 1999).

$$\ln H_{ij} = A + BT + \frac{C}{T} + D\ln T \tag{2.4}$$

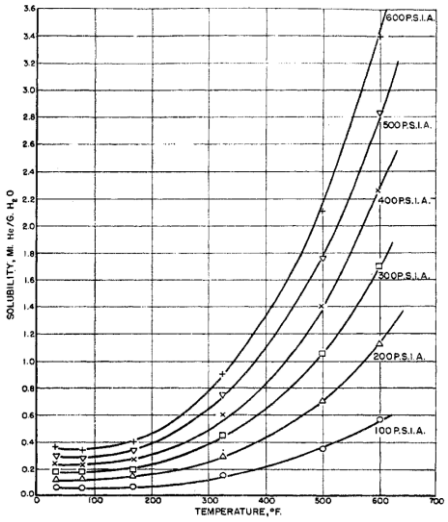

Figure 2.19 Helium Solubility in Water as a Function of Temperature at Constant Pressure (Pray & Minnich, 1952) Reproduced with permission from ACS Publications

The literature data about the solubility of gases in liquid propellants are rather scarce, furthermore, there are some contradictory results like the one stated by DeSain et. al. (2015). According to DeSain et. al. (2015), who compared the solubility results obtained by Chang et. al. (1968), the literature data presented by Chang et. al. (1968) was not overlapping, and the degree of difference was strongly pronounced. DeSain et. al. (2015) attributed these major differences to contamination of the liquids, variations of chemical composition, and poor quality of the measurement devices (DeSain, Brady, Curtiss, & Greenberg, 2015). However, another study done by Clever et. al. (1956) showed that the one-thousandth of the impurity (usually the difference between standard and analysis grade) in the tested gases has almost no detectable effect on the measured solubility (Clever, Battino, Saylor, & Gross, 1956). DeSain et. al. (2015) concluded that, except for a handful of data, their solubility results do not reach an agreement with the ones provided by Chang et. al. (1968). As a result, for important applications, it is a rational sense to measure the solubility of gases in the liquid of interest with respect to pressure and temperature precisely. For instance, the solubility data as a function of temperature and pressure helps to understand the behavior encountered during dosage, preservation, and pressurization of liquid propellants (DeSain, Brady, Curtiss, & Greenberg, 2015).

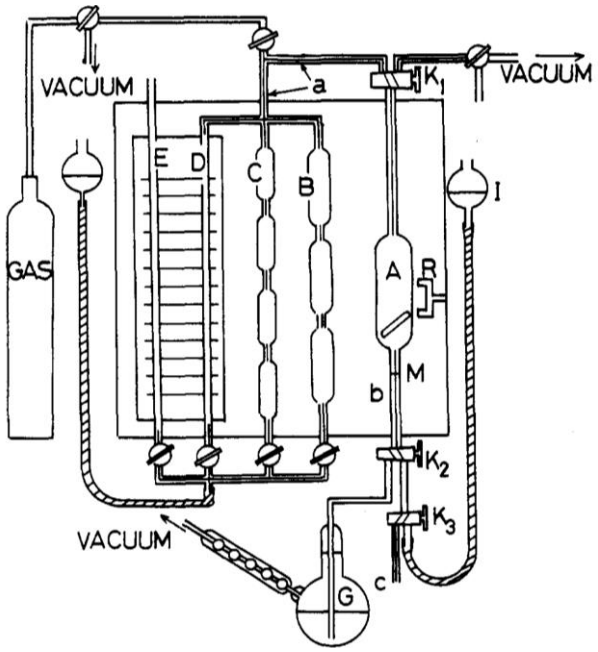

Figure 2.20 Solubility Determination Test Apparatus (Tokunaga, 1975)
Reproduced with permission from ACS Publications

Throughout the past, similar apparatus (Figure 2.20, Figure 2.21, and Figure 2.22) were employed by independent researchers to measure the solubility of inert gases like helium, nitrogen, and argon in liquid propellants such as hydrazine derivatives and hydrocarbon-based fuels. Fundamentally, they were all used to acquire solubility data with respect to temperature and pressure, but their working principles and experimental methods were partially different from one another. Additionally, it should be taken into account that different solubility determination approaches like Bunsen solubility coefficient, Henry's Law constant, and Ostwald absorption coefficient were also utilized. However, measurement methods, steps, and alternatives are beyond the scope of this work and no further discussion will be made regarding these topics. The reader might find the elaborate experimental procedures and techniques in the articles of figures named Solubility Determination Test Apparatus.

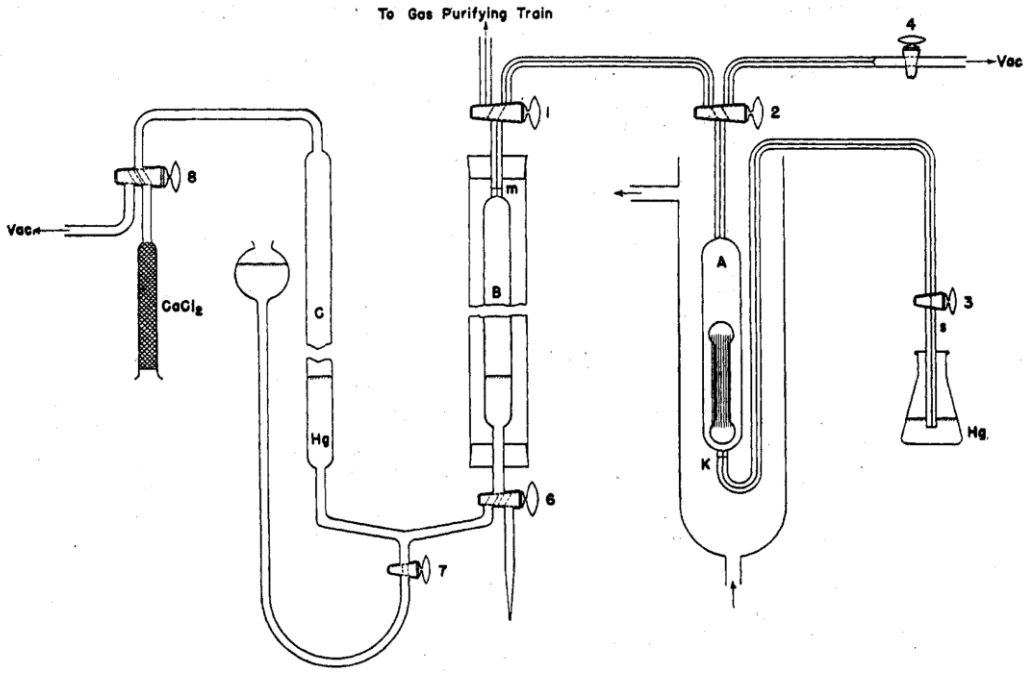

Figure 2.21 Solubility Determination Test Apparatus (Kretschmer, Nowakowska, & Wiebe, 1946) Reproduced with permission from ACS Publications

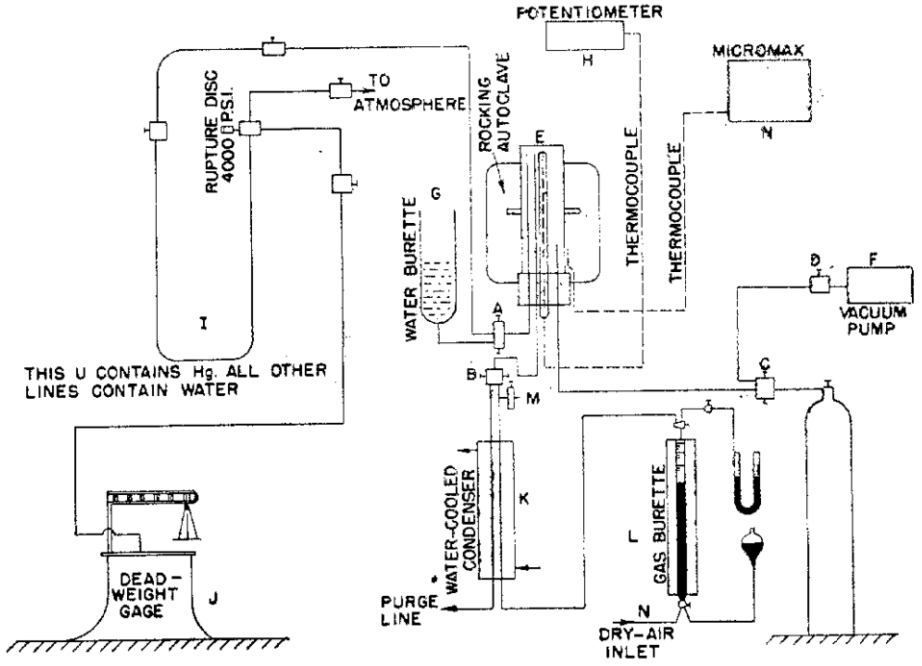

Figure 2.22 Solubility Determination Test Apparatus (Pray & Minnich, 1952) Reproduced with permission from ACS Publications

When it comes to the dissolution of pressurizing gas in the propellant there are several noteworthy issues pronounced. Firstly, excess dilution of propellant due to the excessive dissolution of blanket gas, which in turn affects the fuel composition and ignition performance negatively. Secondly, excess dissolution of gases in propellants leads to inefficiencies in the pressurization system in other words total inert gas and hardware mass required scales up extensively. For instance, nitrogen dissolves greatly in liquid oxygen for this reason; almost two and a half times more nitrogen is necessitated to provide the same amount of displacement when compared with the equivalent amount of water. Based on the above discussion, helium gas is usually utilized to provide protective cover, precluding performance degradation of propellants and redundant mass increase of inert systems (Sutton & Oscar, Rocket Propulsion Elements, 2001). The main reason for choosing helium, as mentioned above, is that it dissolved much less in nitrogen tetroxide than nitrogen, which is another commonly utilized inert gas. That is, at low temperatures (0°C) helium is almost 60 times less soluble than nitrogen, while at moderate temperatures this ratio is about 50 times. The solubility status for IRFNA is markedly similar to that of nitrogen tetroxide, only the numerical values and gas ratios differ (given in Table 2-5). This fact simply makes helium preferable over nitrogen for a large number of space applications (Martin Marietta Corporation, 1977).

Table 2-5 Nitrogen and helium gas solubility in N_2O_4 and IRFNA at 1 atm (Martin Marietta Corporation, 1977)

Conditions		**Liquid Propellant Type**	
		N_2O_4	**IRFNA**
Temperature (°C)	**Blanket Gas Type**	**Solubility (ppm)**	
0°C	**Helium**	3.0	0.73
	Nitrogen	182	24
25°C	**Helium**	4.3	0.86
	Nitrogen	203	62.8

According to the result obtained by Marsh & Knox (1970), the extent of gas solubility in rocket fuels is rather similar to those in oxidizers as discussed above in detail. Such that, Marsh & Knox (1970) experimented and extrapolated the amount of dissolution data of inert helium, argon, and nitrogen gases in rocket grade hydrazine fuel (Marsh & Knox, 1970). Accordingly, helium was the least soluble and argon was the most soluble inert gas in hydrazine as nitrogen was in between (shown in Figure 2.23).

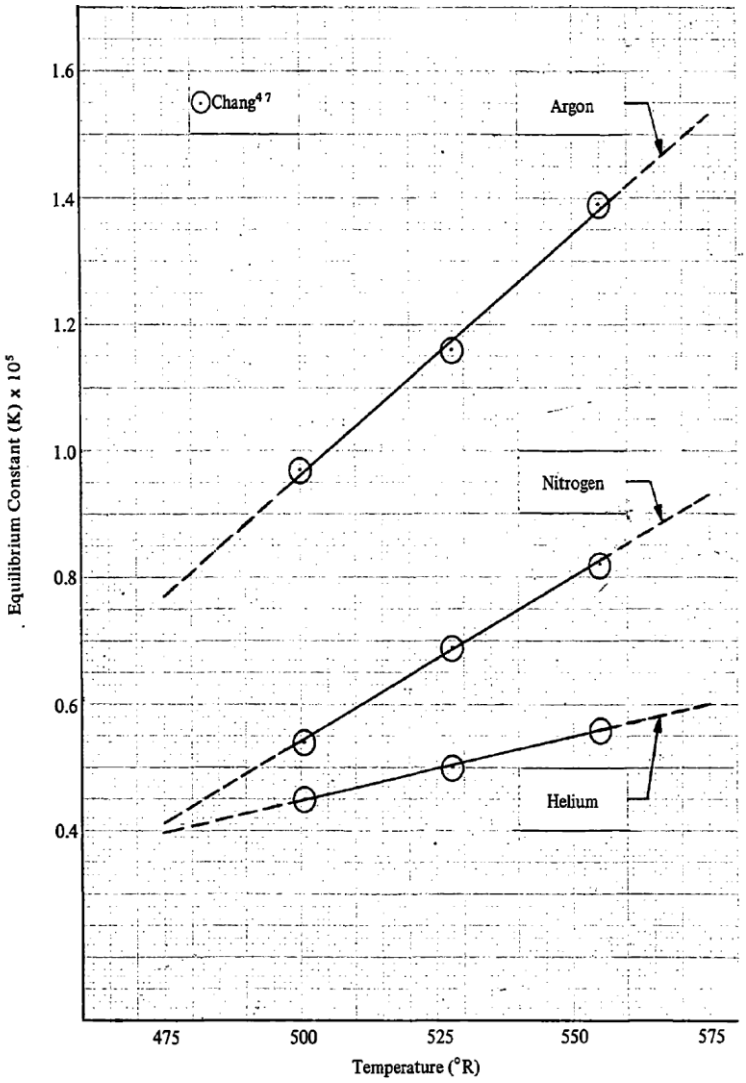

Figure 2.23 Helium, nitrogen & argon gas solubility in liquid hydrazine as a function of temperature (Marsh & Knox, 1970)

2.5.10 Vessel Material Surface Area to Volume Ratio

The literature data regarding the effects of internal vessel surface area to vessel volume ratio on the storage life of propellants is reasonably scarce. One study performed by Mellor et. al. (1991) detected a change in the dissolved iron concentration depending on the surface area to volume ratio. Nevertheless, that change did not affect the corrosion rate (mass loss) (Mellor, Smith, & Klach, A Parametric Study of Factors Affecting the Corrosion of Stainless Steel by MON Oxidizer, 1991). On the other hand, ASTM designation G31 – 72 (1999) states that the ratio of test medium volume to total surface area affects the end results. Such that, if the ratio is not large enough then the corrosivity of the solution may appreciably alter throughout the test which might lead to misleading data (ASTM G31 - 72 (Reapproved 1999), 1999) . Apart from those, as the total available surface area increases then the reaction rate increases since the material surface acts as a catalyst (American Institute of Aeronautics and Astronautics Liquid Propulsion Committee on Standards, 1999). Additionally, an increased surface area significantly accelerates the chemical reactions taking place to an extent where flammable propellants like hydrazine may spontaneously ignite if enough air is present (Safety Office - John F. Kennedy Space Center, 1965). However, the relation between surface area and volume in regard to storage is beyond the scope of this study and there will be no further discussion.

2.6 Empirical Methods Utilized to Determine Storage Materials and Conditions of Liquid Propellants

It is equally crucial to be able to correctly predict the total pressure generated at any time, the pressure build-up rate, and the maximum pressure that could occur inside the sealed propellant vessels (American Institute of Aeronautics and Astronautics Liquid Propulsion Committee on Standards, 1999).

Liquid propellant storage tanks employed in launch vehicle systems are designed in such a way that they can withstand up to certain pressures (Sutton & Oscar, Rocket Propulsion Elements, 2001). These values are called the design pressure and the maximum allowable working pressure. The former simply refers to the worst possible pressure and temperature scenario in which the fluid might apply to the tank enclosure. The latter is defined as the highest pressure that the tank could retain without failure, beyond this point the equipment becomes unpredictable and subjects to untimely failure.

Empirical methods quoted in literature by Uney et. al. (1972) and Sutton et. al. (1986) focused on the pressure build-up rate of the sealed propellant systems. In fact, solely the rate of pressure rise made it possible to restrict some alternatives by eliminating unsuitable combinations to fullest extent. In other words, change in pressure with respect to time could be utilized to distinguish ideal conditions. Here, the experiments could be either limited to the amount of time or the value of pressure rise at a constant temperature environment. In other words, the experimenter could set either a time or a pressure limit then each experiment would be terminated when the time was up, or the pressure reached that value. However, due to safety reasons, the experiment needed to be terminated if the pressure inside the vessel ever reaches the design pressure of the MPVs. In this research, time limited approach was applied and the tests were terminated after approximately 600 hours had passed.

CHAPTER 3

MATERIALS AND EXPERIMENTAL PROCEDURE

Determination of ideal conditions for liquid propellant storage requires apparatuses manufactured with high-end quality and maximum precision to achieve better results. In this concept, purchased equipment usually belonged to the high accuracy category whereas state-of-the-art systems were used during the manufacturing of the machined auxiliary parts. Similarly, experimental procures were prepared in such a way that controlled experiments could be followed in an orderly fashion while reducing accuracy problems and increasing empirical precision. In the first half of this chapter, materials and design were discussed while in the second half the experimental procedures were covered.

3.1 Experimental Set-up, Materials and Equipment Hardware

In literature, independent of the amount of propellant in question, storage tests were always performed in an isolated environment due to the dangerous nature of the liquid fuels and oxidizers. The experimental set-up mainly consisted of a compact cylindrical, spherical, or sometimes elliptical vessel, pressure measurement device, constant temperature medium, relief system, and safety apparatus. In the material category, stainless steel, aluminum, and titanium derivatives were the main choices of interest due to their desired physical, mechanical and thermal properties.

3.1.1 The Test Vessel Design, Auxiliary Components and Procurement

The portrayed pressure vessels and test set-ups in the literature were primarily dependent on the resources and allocated time of the research teams. Nonetheless, many of them usually started with relatively small cylindrical vessels, which had an

average volume of 20 to 150 ml and excess pressure ratings as high as 300 bar at 25°C. To conduct the previously mentioned experiments with concentrated nitric acid, a similar test set-up named non-stirred pressure vessel (NSPV) (shown in Figure 3.1) was designed in parallel with the literature design (shown in Figure 2.7 and Figure 2.8) (Feiler & Morrell, 1952).

The first prototype of the non-stirred pressure vessel was manufactured from stainless steel AISI 304L (UNS S30403) due to the ease of availability and machinability compared to other types of stainless steel and titanium alloys. The vessel was equipped with a relief valve (Ham-Let, model H-900-HP-SS-N-1/4-C) and a diaphragm sealed analog manometer (Wika, model 71228096). The objective behind this initial prototype was to achieve a system that could endure pressures as high as 300 bars and to provide a sealed environment for storage experiments. However, as expected, the first design had its design flaws such as leaks at elevated pressures (60 bar) between the steel surface and PTFE sealing gasket and around the needle valve connections as well. As a result, the initial design was renewed substantially (shown in Figure A.1) to make the system more convenient and less susceptible to failures. The renewed design of NSPV was superior compared to the previous one in terms of leaks and functionality, however, eleven distinct components made CNC manufacturing rather costly as well as time-consuming.

After that, due to budget and time constraints, the work continued with an alternative design called mini pressure vessel (MPV) (shown in Figure B.1) which consisted of only three distinct components that required CNC machining, and the rest were commercially available market products. Here, the vessel was directly connected with a male connecter (Ham-Let, model 768LG_1/2X3/4) and sealing was secured with a gasket (Ham-Let, model SS-GA-LG_3/4-FKM) and PTFE tape (manufactured under the compliance of EN-751-3).

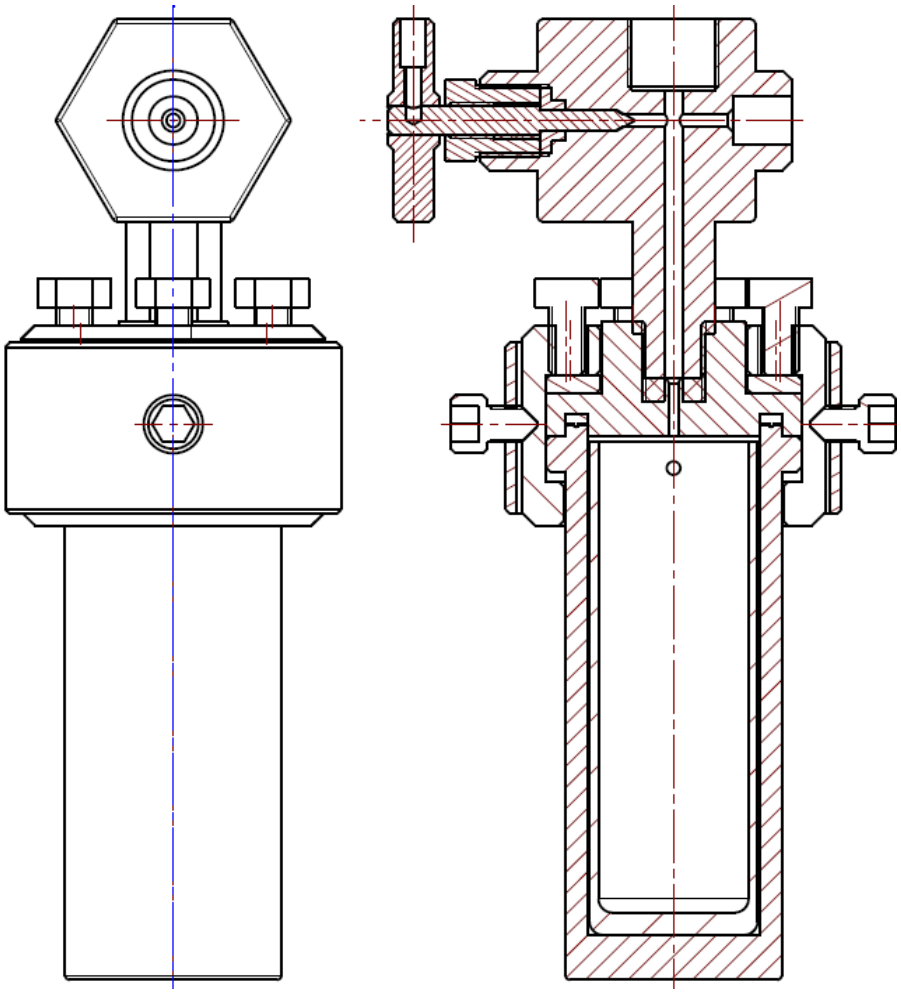

Figure 3.1 Detailed engineering section view of the first test set-up prototype

3.1.2 NSPV (Non-Stirred Pressure Vessel) (Equipment A)

An updated Non-Stirred Pressure Vessel (shown in Figure A.1) was designed right after the failed attempt of the first prototype. Compared to its predecessor, new NSPV was well designed and precisely toleranced. Additionally, it was easier to assemble as well as disassemble owing to its nicely oriented ergonomic layout of components. However, as stated earlier, it was expensive and time-consuming to produce. For this reason, another alternative called Mini Pressure Vessel (MPV) was pursued. More details regarding this design were given under the following headings in this section.

3.1.2.1 NSPV Qualification and Pressure Rating Tests

The storage tests were conducted to determine the optimum storage conditions for a specific type of liquid propellant. Due to the nature of these experiments, the high-pressure build-up was expected and also observed from time to time unless the tests were conducted inside a glass container with a small sample material inside.

To create a safe and sound experimental environment, external pressure vessel bodies were mainly manufactured from high tensile stainless steel whereas the inner tubes were manufactured from several materials like PTFE, low alloy steel, high alloy steel, and non-ferrous materials (nickel, aluminum, copper). Accordingly, NSPV external body was manufactured from stainless steel AISI 304L with a wall thickness of approximately 4.8 mm.

A pressure rating test was initiated at atmospheric conditions and room temperature. First, the system was filled with hydraulic oil, and the pressure was gradually increased with increments of 50. The plot of test data was obtained during the pressure-rating test (shown in Figure A.13), it was observed that the vessel withstood pressures up to 250 bar and no plastic deformation was detected in the post-test examination performed by a caliper (Mitutoyo, model 500-181-30). The pressure-rating test was repeated two times more without changing any conditions and after each test, the same examinations were conducted. As a result, there was no detectable leak and significant change in dimensions. To stay on the safe side, the pressure resistance of the vessel was rated at 200 bar at 25°C.

3.1.2.2 Disadvantages of NSPV

It was proven via pressure rating tests that second prototype of NSPV's unique design was reliable and leakproof. However, as previously stated, the manufacturing of eleven different pieces was quite pricey, approximately every unit costing around 1200 euros excluding the instrumentation. Additionally, there were literature images (shown in Figure 3.2) regarding the aftermath of storage condition tests that due to

the corrosive nature of concentrated nitric acid, wetted parts of the vessel corroded extensively even after one experiment (Feiler & Morrell, 1952). As a result, the possibility of replacement expense of corroded components was taken into consideration as a result the design was renewed. More details regarding the new design, called MPV, were provided in the proceeding sections.

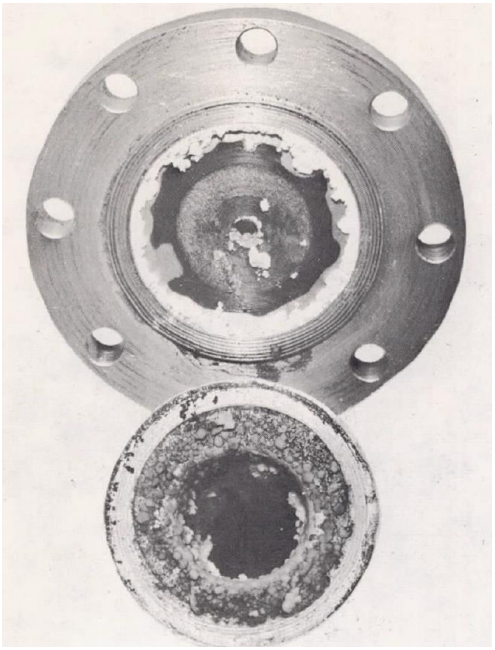

Figure 3.2 Aftermath corrosion on the test tubes after 100-hour storage of WFNA at 76.7° C (Feiler & Morrell, 1952)

3.1.3 MPV (Mini Pressure Vessel) (Equipment B)

After it had been decided that NSPV was not practical due to manufacturing time as well as upkeep expenses, the Mini Pressure Vessel (shown in Figure B.1) was designed. When compared to NSPV, MPV was small in terms of inner diameter and usable volume. However, it consisted of only three CNC machined parts and only one of which, namely the mini vessel body, required tight tolerances. Furthermore, the manufacturing time and upkeep costs decreased substantially (almost 85 percent). Here, the design was kept undemanding so that assembling as well as disassembling would be simple.

Figure 3.3 Mini Pressure Vessel Body with Pressure Measurement and Relief System (PMRS) attached (whole unit is MPV fixture) (see Table B.1 for detail)

3.1.3.1 MPV Qualification and Pressure Rating Tests

Due to the same reasons described earlier in the NSPV section, a pressure rating test was conducted at atmospheric conditions and room temperature. The steps followed here were similar as for the NSPV. However, for MPV the upper-pressure limit was set at 150 bar at 25°C and 30 bar increments were applied each consecutive time (shown in Figure B.5). During the pressure-rating test, it was monitored that, the vessel withstood pressures up to 150 bar and no plastic deformation was detected in the post-test examination performed by a caliper (Mitutoyo, model 500-181-30). The pressure-rating test was repeated one more time without making any alterations and after that, the same measurements were conducted via caliper. In the end, upon inspection there was no detectable leaks and significant change in dimensions. To have a safety factor of 1.5 at best, the pressure resistance of the MPV vessel was rated 100 bar at 25° C.

3.1.4 Advantages of MPV over NSPV

Both vessels were designed to create a safe test environment while operating at high pressures up to 100 bar at 50°C. Later it was experienced that the NSPV design was bulky, costly, hard to handle and there were numerous subcomponents. For this reason, a smaller and relatively less complex design with only three CNC machined parts was engineered while not sacrificing functionality. Besides, MPV parts were easier to manufacture, additionally, quality control and tolerance checks of machined components were less time-consuming. Lastly, the required parts for MPV to function were substituted via commercial shelf products which in return decreased expenses appreciably.

3.1.5 Pressure Data Acquisition

In literature, it was evidently and repetitively stated that to determine the optimum storage conditions of liquid rocket propellant, one must attentively monitor pressure changes and fluctuations with respect to time throughout the test duration. Even though there were two distinct experimental approaches, called pressure limited and time-limited, the fundamental objective was to decide and determine the storage conditions by gathering pressure data. For this purpose, two types of pressure data acquisition equipment called analog manometer and pressure transmitter was utilized over the years. In this research, an analog manometer was used in the early stages of preparation, but actual experiments were conducted by using a pressure transmitter (Trafag, model FPT.8235).

3.1.5.1 Diaphragm Sealed Analog Manometer

Analog manometers with or without a diaphragm seal were commonly used in the early days of propellant storage tests. Although they provided reliable pressure data in the beginning, there were some problems regarding the data recording frequency and corrosion of wetted parts inside the manometer in the following stages. Regarding the data recording frequency, the experimenter had to record the values personally due to the manual nature of data entry, and that could result in sparse and unevenly distributed data sets. In terms of corrosion of wetted parts inside the manometer, some mechanical disruptions may occur after a while, and that might lead to false or misleading data collection.

In the early stages of experimental planning, it was considered to utilize a Wika analog manometer model 233.50 together with a Wika diaphragm seal with threaded connection model 990.10, however, it was switched to a contemporary pressure transmitter due to evenly distributed data recording difficulties and corrosion risk of wetted parts inside the manometer.

3.1.5.2 Flush Membrane Pressure Transmitter

Acquiring pressure data with respect to time is the most prominent stage of storage condition tests. Any systematic inaccuracy might lead to a waste of a great deal of time, money, and most importantly equipment. To prevent this possibility, all the mini pressure vessels were equipped with a factory-calibrated Trafag flush membrane pressure transmitter with diaphragm seal model FPT.8235. The pressure measurement sensor is highly precise and accurate that could operate within ± 0.4% error limit at 25°C. Furthermore, it is supported by thin-film-on-steel technology that eliminates the potentiality of corrosion of sensitive components inside the transmitter. Under normal working conditions, this transmitter was expected to provide evenly distributed high-frequency pressure data with respect to time without the experimenter's effort or involvement at any stage once the tests were successfully initiated.

3.1.6 Constant Temperature Cabinet

Optimum storage condition determination tests required a temperature-controlled isolated environment. For this purpose, all the tests were conducted inside a Nuve model TK 120 test cabinet that could simulate desired environmental conditions via adjusting humidity and temperature. Here, the effect of distinct climatic conditions was tested by artificially creating desired environments.

The test cabinet is capable of providing temperatures between -10°C to 60°C and the interior is covered with stainless steel sheet while high-density polyurethane is present between the inner and outer frames. The insulation between frames ensures temperature and humidity stability while internal air circulation provides uniform temperature and humidity distribution within the cabinet. The system can operate for 40 days in the desired step and can be programmed up to 9 different steps each could be repeated from once to 99 times. In other words, once the system is set to operate, no external intervention is required.

3.1.7 Citric Acid

Citric acid treatment was performed for a selected group of materials to compare the presence and to determine the effectiveness of this treatment. The analysis grade citric acid monohydrate, $C_6H_8O_7 \cdot H_2O -\ M_w = 210.14\ g/mol$, utilized in all the treatments was purchased from Sigma-Aldrich / Merck. Throughout the experiments, the 1 kg citric acid plastic container made by HDPE was stored under recommended storage conditions. The lot, catalog, and CAS no of citric acid were K52067944 103, 1.00244.1000, and 5949-29-1, respectively.

3.1.8 FEP (Fluorinatedethylenepropylene) Narrow-Mount Bottle

During the propellant storage tests, 500 ml narrow-mount containers made of FEP were employed to preserve white fuming nitric acid. All the FEP bottles, catalog no. NG-1600-0016, utilized throughout tests was purchased from Thermo Scientific.

Historically, FEP had first been produced in the mid-1950s by Dupont and was introduced on the market in 1960. It is a molten copolymer of perfluoropropylene (PFP) and tetrafluoroethylene (TFE) and possesses similar mechanical, chemical, and thermal properties to those of PTFE. Labware that is produced by using FEP is almost transparent, and its surface is quite non-porous. However, space storable liquid propellants including but not limited to hydrazine derivatives, and nitrogen tetroxide permeates through FEP at relatively low rates, usually less than $3.0\ mg/in.^2 * hr$, (Uney & Fester, 1972). This phenomenon was extensively taken into consideration for TFE-based bladders, liners, and coating designs (Cuddihy, 1971).

3.1.9 Analytical Balance

Weight change of storage test tubes were closely monitored prior to and after the storage experiments. The change in weight, either a decrease or an increase, is the

direct result of chemical reactions taking place between the material and liquid propellant. By using weight change data, some important computations such as decomposition rate of the propellant and corrosion rate of the material in terms of time could be obtained. For such calculations, weight data up to one-thousandth precision is usually desired in terms of milligrams. In order to achieve this requirement and preclude any weighting errors from occurring inadvertently, Mettler Toledo model XPR206DR analytical balance was utilized throughout the research providing exceptional accuracy with 0.01 mg readability.

3.2 Experimental Procedure

Experimental procedure primarily compromises activities such as test matrix preparation, data acquisition interface modeling, pretest activities, tensile specimen tests, and finally storage tests. Each segment is discussed throughout the following sections in this chapter.

3.2.1 Test Matrix

At the far beginning of this research regarding the optimal storage condition determination of white fuming nitric acid, there were nine nearly independent parameters. They were ullage ratio, the material of construction, temperature, initial pressure, pressurization gas type, presence of surface treatment, presence of additive, internal surface area, and internal surface area to interior volume. Each parameter had different alternatives in variable numbers within itself. Such that, simply a great number of distinct temperatures, ullage ratios, construction materials, additives, surface treatment techniques, and so on were among the options. As a result, the total number of test combinations would be pronounced in the tens of thousands that would be quite impractical to follow. For this reason, some eliminations, limitations, and contractions had been applied to test conditions (given in Table 3-1). After all, the master test matrix was matured to its final state with thirty-two experiment sets.

In addition to the master test matrix (given in Table 3-4), a control test matrix with four control tests were also investigated prior to initiation of the master test matrix experiments (given in Table 3-5). This was also performed for safety reasons and to have an insight into storage test fundamentals.

Table 3-1 Experimental conditions to be tested of the master test matrix for the effects of liquid propellant storage

Test Parameters	**Test Alternatives**			
Material	AISI 316L	Alloy 904L	Al 5083-H111	Al 6061-T6
Temperature (°C)	50	-	-	-
Pressure (BarG)	2.5 – 3.2 barG	-	-	-
Blanket Gas	Helium	Nitrogen	Air	-
Ullage Space (%)	13.0	19.0	-	-
Passivation	With	Without	-	-
Additive	Without	-	-	-
Internal Surface Area (cm^2)	~83.13	-	-	-
Internal Surface Area (cm^2) to Interior Volume (cm^3) ratio	~2.23	-	-	-

As could be seen from the table above, some parameters like temperature, additive, and pressure have only one alternative whereas others like material and blanket gas have at least two different alternatives. These selections were performed by taking literature information into account. For instance, high temperature accelerated reaction rates which reduced required test time. Similarly, inert pressurizing gases inhibited reactive atmosphere formation which helped to protect instruments at the top. As a result, a test matrix compromised of 32 controlled experiments were prepared in which the effect of distinct parameters would be analyzed. Here, some tests were repeated two times to check the reliability and reproducibility of storage tests.

In section 2.6, two primary test methods namely pressure limited and time-limited were evaluated. In this research, the test matrices that show the experimental results were given in related sections of chapter 4.

3.2.2 Data Acquisition System

Pressure data acquisition was performed by employing a simple yet effective platform. Such that, the primary hardware was comprised of a NI chassis (model cDOQ-9181) and an analog input module (model NI-9208) (shown in Figure 3.4), where these hardware combinations were powered by Labview Visual Instrument Engineering Workbench. The system was prepared in such a way that it could obtain and record current data with a frequency of 1 hertz, meaning that data recorded at every second. Then the obtained current data could be converted into pressure data with respect to time. Later, that data pair could be utilized to plot the pressure build-up rate as a function of time at a constant temperature.

Figure 3.4 Pressure data acquisition system powered by National Instruments

3.2.3 Pretest Activities

Before the propellant storage tests were initiated, series of pretest activities were conducted on the relevant parts and apparatus. In order not to create discrepancies between the ultimate results, the same pretest steps for the different parts were followed under the same conditions to the greatest extent (shown in Figure 3.5).

As a whole, pretest activities were compromised of several sub-stages. Firstly, it started with washing the relevant parts with conventional detergent at 40°C. Secondly, they were washed with technical grade isopropyl alcohol and acetone, respectively. Then, the parts were kept in an ultrasonic cleaning bath at 25°C for about an hour to ensure that the impurities in hard-to-reach spots would be removed. After washing the parts with room temperature distilled water and drying them in the oven at 100°C for two hours, the initial pre-test section was concluded. Essentially, the activities performed up to this point were executed for all the vessel parts.

One of the test parameters was the effect of passivation on the propellant storage. To identify its influence, half of the test tubes and the tensile specimens were chemically passivated with the citric acid solution as described in section 3.2.3.1. After this step, each test tube was weighted via analytical balance. Then the assembly of mini pressure vessels was carried out with the parts of which the preparations were completed. Following the final assembly, the helium leak test was conducted to ensure the safety and accuracy of the test. In the case of the successful helium leak test, a two-stage weighting process used to measure the total dead volume of each vessel assembly. First the empty assembly and then the assembly filled with distilled water were weighted, and the difference between these two results provided the approximate total volume of the whole system (detailed in 3.2.3.2). As a result, the final assembly was ready to be used for the propellant storage experiments.

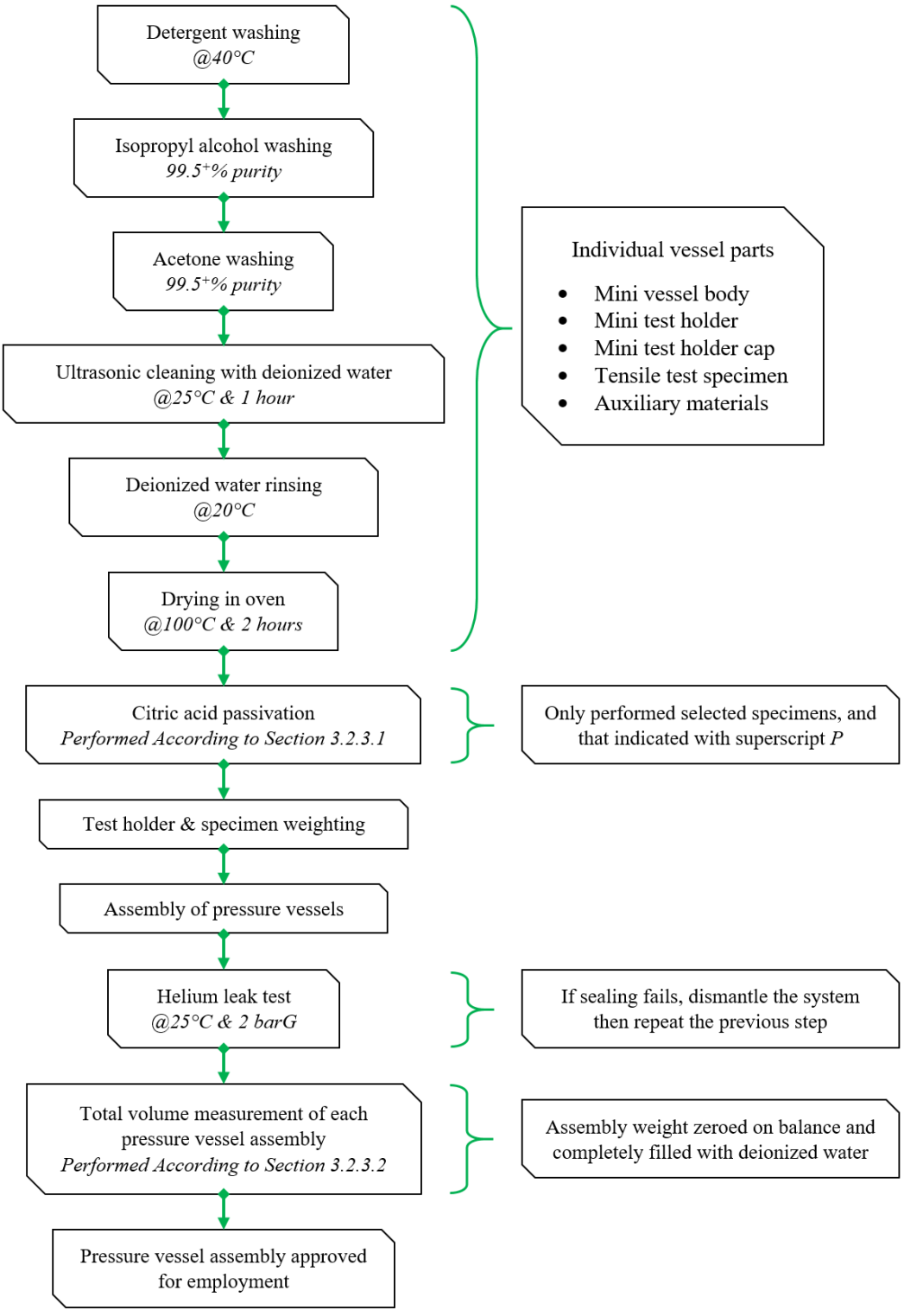

Figure 3.5 Pretest activities performed during propellant storage experiments prior to test initiation

3.2.3.1 Citric Acid Passivation

As previously discussed in section 2.5.3, there was no agreed method of use on metal passivation with acid solutions. Passivation performance is directly dependent on the temperature of the passivation solution, its concentration, and the duration of the operation, apart from the type of acid used and the structural properties of the material treated.

The central focus of this research was to characterize storage conditions of white fuming nitric acid by alternating disparate parameters, for this reason, no in-depth experimentation was done for establishing an excellent acid passivation technique. In fact, based on literature indications, citric acid was chosen as the passivation medium while the concentration, temperature, and duration conditions were selected as 10% (w/w), 60°C, and 90 minutes, respectively.

In the process of preparing passivation solution, citric acid monohydrate mentioned in section 3.1.7 was mixed with type III distilled water according to designation ASTM D1193 – 91. After that, the solution was mixed with a magnetic stirrer for about 15 minutes meanwhile its temperature was raised to about 60°C. Finally, the parts to be passivated were completely immersed in the mixture and were kept there for about 90 minutes meanwhile the temperature was kept constant.

Passivated parts were removed from the solution after exactly 90 minutes of total immersion then washed with deionized water two times, finally dried for an hour in the oven at 100°C. In the end, each passivated part was packed individually in vacuum-sealed bags and kept there until used in storage tests.

3.2.3.2 Total Dead Volume Determination of MPV Assembly

Storage tests were practiced by using mini pressure vessels, in total 16 identical MPVs were assembled by using the same parts. Following the end of the assembly process, the helium leak test according to designation ASTM F2391 – 05 (2016) was

applied to each final assembly system. In the helium leak test, procedure A was pursued where the fixture was externally scanned for helium leaks with a sniffer and the design was rated leak-proof with average leaks of 10^{-6} cc/sec/atm. Upon the successful completion of the helium leak test, the total dead volume of each vessel assembly was determined simply by using distilled water. Such that, the weight of empty and dry MPV fixture was zeroed on an analytical balance, and it was filled with type III distilled water at 20°C, here the final value on the balance would give the total available volume of the design fixture. Here the fixture consisted of a vessel body, test tube, sealing cap and PMRS (Pressure Measurement and Relief System). Important to state that the variations amongst external dimensions of test tubes and sealing caps were roughly 20 micrometers, for this reason, all the tubes were assumed identical and dead volume calculations were performed by using the same test tube (shown in Table 3-2). This process was individually carried out for each final MPV assembly. To reduce the variations during storage tests, the vessel body and the PMRS were used in pairs from this point on. Additionally, the same method used to find the usable volume of each test tube when closed with the sealing cap. Arithmetic mean of all the usable volume measurements of tubes were taken as the total volume of an individual tube (37.32 ml, calculated from Table 3-4 and Table 3-5) in the calculation of Internal Surface Area (cm2) to Interior Volume (cm3) ratio.

Table 3-2 Total Dead Volume of MPV Fixtures

MPV#	**Total Dead Volume (ml)**	**MPV#**	**Total Dead Volume (ml)**	**MPV#**	**Total Dead Volume (ml)**	**MPV#**	**Total Dead Volume (ml)**
1	5.39	5	5.37	9	5.35	13	5.37
2	5.41	6	5.38	10	5.39	14	5.34
3	5.43	7	5.44	11	5.36	15	5.38
4	5.46	8	5.47	12	5.44	16	5.37

All the values are averages of three consecutive measurements performed at 20°C.

3.2.4 Test Fluid Preparation

White fuming nitric acid was utilized as the test fluid in this research. The chemical composition of the white fuming nitric acid was shown in Table 3-3. The content of nitrogen dioxide and water were measured, and the amount of nitric acid was computed by balance assuming that no substantial pollutants and non-volatiles were present (30 mg/L dissolved metal concentration). When WFNA was not used, it was preserved at room temperature in FEP bottles. Before conducting storage tests with WFNA, only chemical characterization was carried out to specify nitrogen dioxide and water content. These composition tests, near-infrared absorption spectroscopy, were performed by an accredited laboratory located at Roketsan. Apart from that, to minimize the thermal effects as much as possible during propellant filling into the storage vessels, the filling operation was carried out when the temperature of the liquid was roughly equal to the test equipment temperature.

Table 3-3 Chemical composition of White Fuming Nitric Acid

Chemical Composition Type	Nitric Acid, HNO_3	Nitrogen Dioxide, NO_2	Water, H_2O
Composition (wt. %)	96.6	1.43	1.97

3.2.5 Experimental Steps of Storage Tests

In the course of storage tests, the same experimental steps were followed, and detailed stages of experimental steps were shown in Table C.1. White fuming nitric acid storage experiments carried out within the scope of this research were conducted by limiting the total test time to approximately 600 hours.

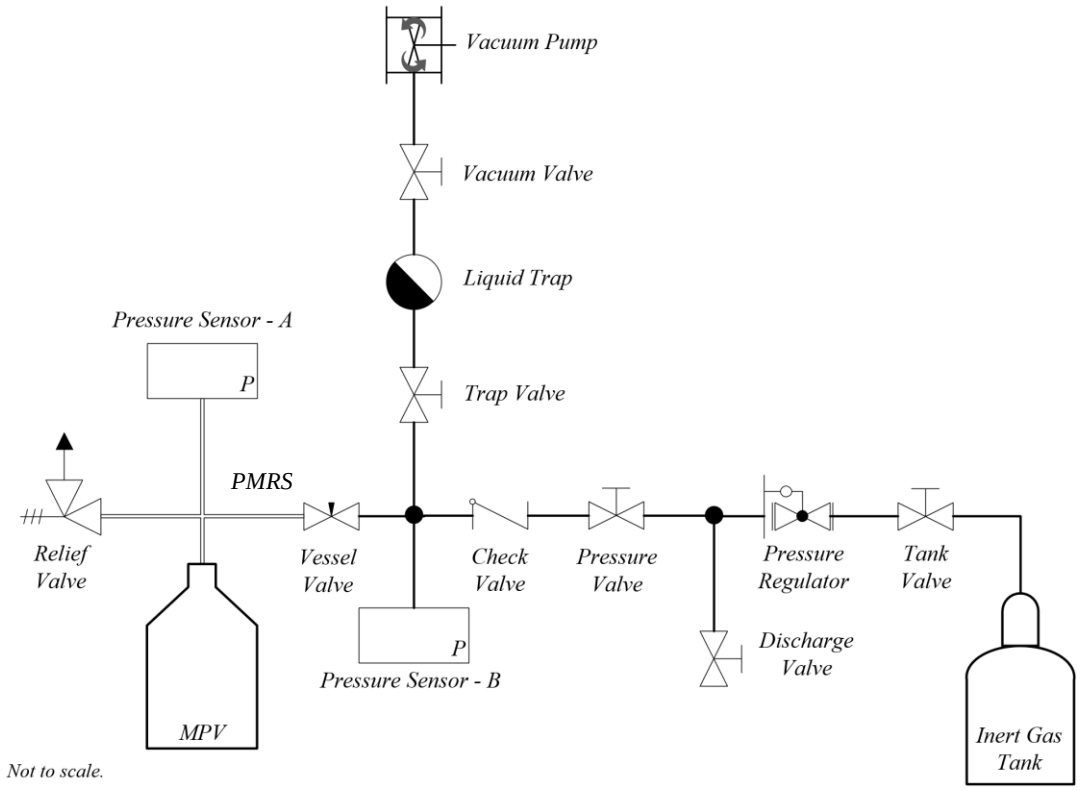

Figure 3.6 Schematic of Vacuum & Pressurization System (VPS) and Mini Pressure Vessel (MPV) fixture

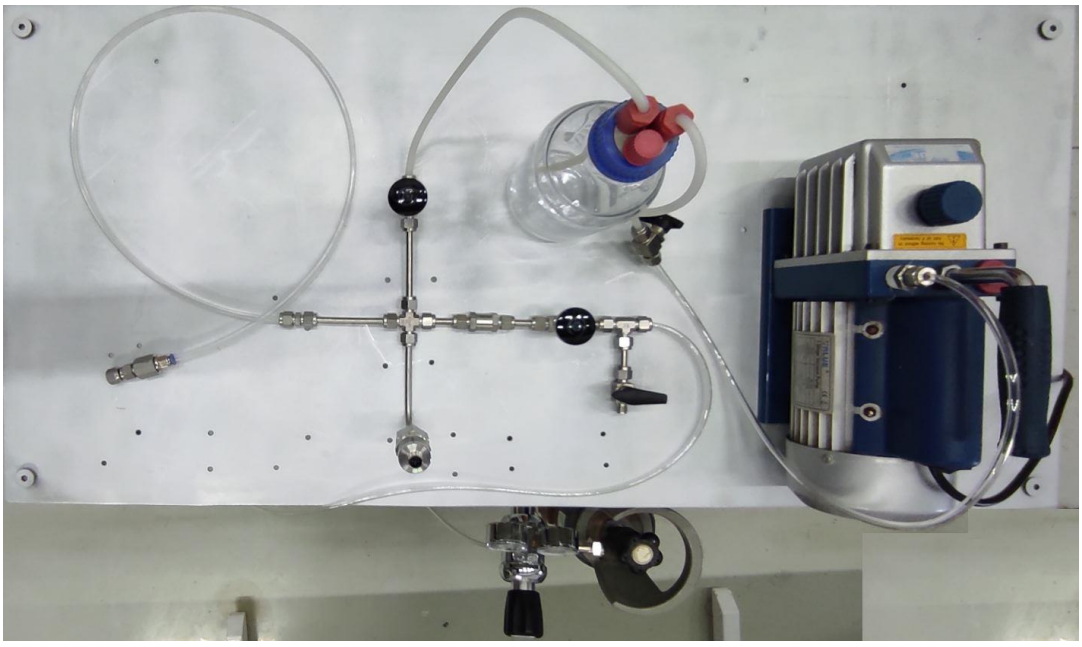

Figure 3.7 Installation of the Vacuum & Pressurization System (VPS)

3.2.6 Storage Tests

Liquid propellants continuously undergo spontaneous decomposition and deterioration reactions throughout the storage period inside propellant tanks. The extent and rate of these reactions are influenced by several factors including but not limited to variables given in the first column of Table 3-1. In consequence of these reactions, depending on the propellant type gaseous side products such as nitrogen, ammonia and oxygen are formed which eventually leads to pressure rise. In some cases, peak pressure could reach as high as the upper design limit of the propellant system which might lead to termination of the propellant storage enforcedly.

Controlled storage tests were executed by using mini pressure vessels (MPVs) (shown in Figure 3.3) to have a reliable foresight about the individual effects of these parameters on pressure build-up rate. These tests were carried out by the same material alternatives that the tensile tests were executed (given in Table D.1). Since an increase in temperature usually led to an acceleration in the reaction rate, the storage tests were performed at elevated temperatures of 50°C to reduce the required test length. Helium and nitrogen were used as blanked gases since modern rocket industry was heavily using these gases mostly. Each test vessel was pressurized with one these gases by using VPS (shown in Figure 3.6 and Figure 3.7) so that the internal pressure of the vessel would lie between 2.5 and 3.3 barG. Half of the storage test tubes were citric acid passivated at specified conditions provided in section 3.2.3.1 while the other half were not subjected to any processing after manufacturing. The total internal surface area of each tube was ~83.13 cm^2, which was taken from the computer-aided manufacturing program and no further measurement was conducted on test tubes. Before and after the experiments mass of each storage test tube was measured and the corrosion rate in terms of mm per year was computed via designated ASTM standard (ASTM G31 - 72 (Reapproved 1999), 1999). As ullage space, two different alternatives, 13.0 and 19.0 percent were evaluated at 20°C. No additive chemical was utilized in order not to increase the complexity of interpreting

test results. The behavior of four different materials, AISI316L, AISI904L, Al5083-H111 and Al6061-T6, were analyzed. Additionally, the presence of citric acid passivation were also investigated. Finally, a single type of test vessel was used for reasons similar to that of the use of an additive chemical.

Each MPV fixture were placed inside the reactor rack (shown in Figure 3.8) after completing steps given in Table C.1. Then, the storage tests were initiated one at a time by securing the connection between the pressure sensor and data transmission cable coming from data acquisition system. At the end, the time-dependent pressure data collection were initiated via Labview software.

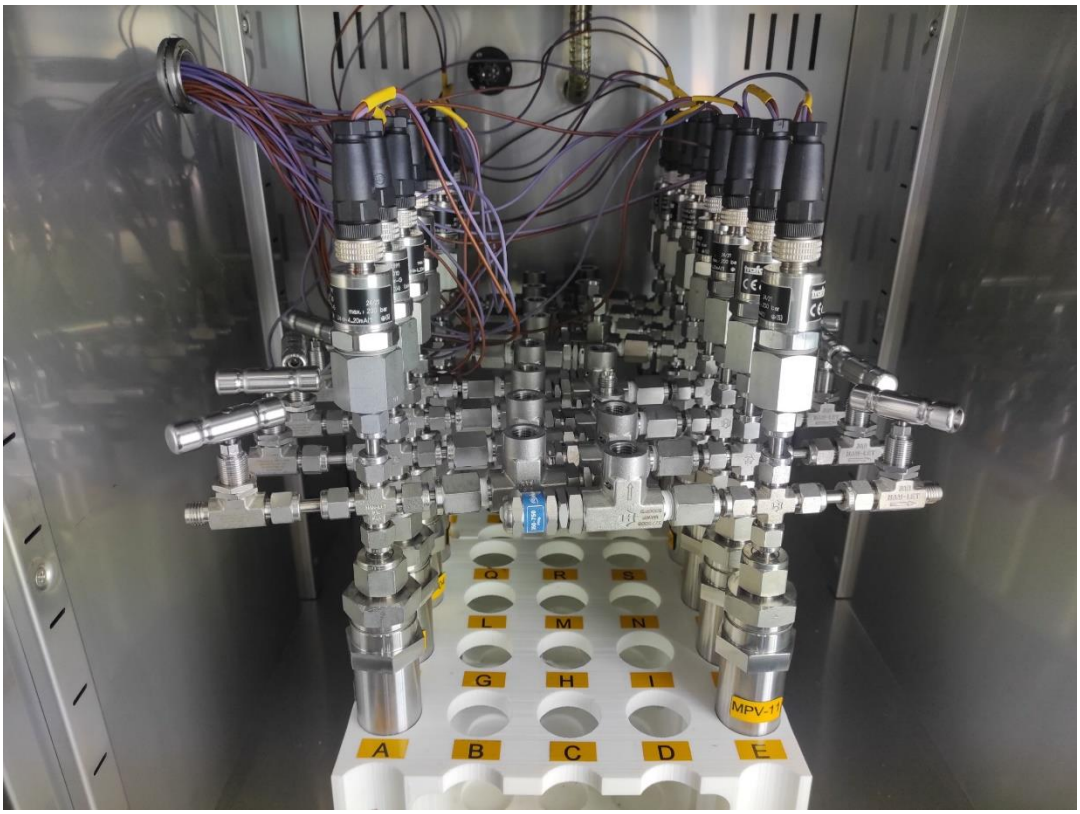

Figure 3.8 Arrangement of the reactors inside the thermal cabinet after the experimental steps of storage tests (Table C.1) were completed

Table 3-4 Detailed control test matrix exercised for the WFNA storage tests

Tube Detail				**Test Conditions**						
Marking[1]	**Usable Volume @ 20°C (ml)**	**Exposure Time[2] (Hours)**	**Material**	**Temperature (°C)**	**Initial Pressure @ 20°C (barG)**	**Pressurizing Gas[3]**	**Total Dead Volume @ 20°C (ml)**	**Ullage Space[4] @ 20°C (%)**	**WFNA Volume[5] @ 20°C (ml)**	**WFNA Mass[6] @ 20°C (g)**
PTFE-01	37.39	663	PTFE	50	2.63	He	5.46	13.0	37.28	56.07
PTFE-02	37.50	663	PTFE	50	2.71	N_2	5.47	13.0	37.38	56.23
PTFE-03	37.44	663	PTFE	50	2.55	He	5.44	19.0	34.73	52.24
PTFE-04	37.37	663	PTFE	50	2.47	N_2	5.37	19.0	34.62	52.07

[1] Tests were terminated for safety reasons when the pressure approached to the design pressure, a critical equipment failure encountered, or any major leaks detected. Marking of these tests were indicated in italic font format.

[2] Propellant storage tests were performed for about 600 hours (25 days) in a time-dependent status as explained in section 3.2.5.

[3] 99.999 Grade inert gases were utilized as initial pressurizing gas. The pressurization was performed via VPS according to details in section 3.2.5.

[4] Value of ullage space was set and it was the ratio of total empty volume to total available volume.

[5] WFNA volume was computed in a way to provide the desired ullage space (%).

$$\text{WFNA Volume} = (\text{Usable Volume} + \text{Total Dead Volume}) - (\frac{\text{Ullage Space}}{100} * (\text{Usable Volume} + \text{Total Dead Volume}))$$

[6] WFNA Density @ 20°C was measured via a “pycnometer” and determined as 1.504 g/ml at 20°C. Which was used to compute WFNA mass present inside the tubes at designated ullages.

Table 3-5 Detailed master test matrix exercised for the WFNA storage tests

Tube Detail				**Test Conditions**						
Marking[1, 2]	**Usable Volume @ 20°C (ml)**	**Exposure Time[3] (Hours)**	**Material**	**Temperature (°C)**	**Initial Pressure @ 20°C (barG)**	**Pressurizing Gas[4]**	**Total Dead Volume @ 20°C (ml)**	**Ullage Space[5] @ 20°C (%)**	**WFNA Volume[6] @ 20°C (ml)**	**WFNA Mass[7] @ 20°C (g)**
AISI 316L-01	37.30	562	AISI 316L	50	3.18	He	5.39	13.0	37.14	55.86
AISI 316L-02[P]	37.48	562	AISI 316L	50	2.89	He	5.41	13.0	37.31	56.12
AISI 316L-03	37.63	562	AISI 316L	50	3.16	He	5.43	13.0	37.46	56.34
AISI 316L-04[P]	37.40	562	AISI 316L	50	2.91	He	5.46	13.0	37.29	56.08
AISI 316L-05	38.01	663	AISI 316L	50	2.87	N_2	5.39	19.0	35.15	52.87
AISI 316L-06[P]	37.76	663	AISI 316L	50	2.76	N_2	5.41	19.0	34.97	52.59
AISI 316L-07	38.32	663	AISI 316L	50	2.85	He	5.43	19.0	35.44	53.30
Alloy 904L-01	37.65	562	Alloy 904L	50	3.31	He	5.37	13.0	37.43	56.29
Alloy 904L-02[P]	36.91	562	Alloy 904L	50	2.97	He	5.38	13.0	36.79	55.34
Alloy 904L-03	37.18	562	Alloy 904L	50	2.89	He	5.44	13.0	37.08	55.77
Alloy 904L-04[P]	37.24	562	Alloy 904L	50	3.00	He	5.47	13.0	37.16	55.89
Alloy 904L-05	37.26	663	Alloy 904L	50	2.94	N_2	5.37	19.0	34.53	51.93
Alloy 904L-06[P]	37.49	663	Alloy 904L	50	2.99	N_2	5.38	19.0	34.72	52.23
Alloy 904L-07	37.66	663	Alloy 904L	50	2.90	He	5.44	19.0	34.91	52.51
Al 5083-01	37.20	562	Al 5083-H111	50	3.03	He	5.35	13.0	37.02	55.68
Al 5083-02[P]	37.39	562	Al 5083-H111	50	3.02	He	5.39	13.0	37.22	55.98
Al 5083-03	36.89	562	Al 5083-H111	50	3.21	He	5.36	13.0	36.76	55.28

Table 3-5 (Cont'd)

Al 5083-04[P]	37.42	562	Al 5083-H111	50	3.27	He	5.44	13.0	37.29	56.08
Al 5083-05	37.49	663	Al 5083-H111	50	2.97	Air	5.35	19.0	34.70	52.19
Al 5083-06[P]	37.50	663	Al 5083-H111	50	2.73	Air	5.39	19.0	34.74	52.25
Al 5083-07	37.61	663	Al 5083-H111	50	2.83	N_2	5.36	19.0	34.81	52.35
Al 6061-01	36.76	562	Al 6061-T6	50	3.25	He	5.37	13.0	36.65	55.13
Al 6061-02[P]	36.82	562	Al 6061-T6	50	2.88	He	5.34	13.0	36.68	55.17
Al 6061-03	36.86	562	Al 6061-T6	50	3.06	He	5.38	13.0	36.75	55.27
Al 6061-04[P]	36.71	562	Al 6061-T6	50	3.18	He	5.37	13.0	36.61	55.06
Al 6061-05	36.78	663	Al 6061-T6	50	3.19	N_2	5.37	19.0	34.14	51.35
Al 6061-06[P]	36.87	663	Al 6061-T6	50	3.28	N_2	5.34	19.0	34.19	51.42
Al 6061-07	36.87	663	Al 6061-T6	50	3.29	He	5.38	19.0	34.22	51.47

[1] Tests were terminated for safety reasons when the pressure approached to the design pressure, a critical equipment failure encountered, or any major leaks detected. Marking of these tests were indicated in italic font format.

[2] Passivated tubes were marked with superscript P and Passivation was performed only half of the samples by following steps provided in section 3.2.3.1.

[3] Propellant storage tests were performed for about 600 hours (25 days) in a time-dependent status as explained in section 3.2.5.

[4] 99.999 Grade inert gases were utilized as initial pressurizing gas. The pressurization was performed via VPS according to details in section 3.2.5.

[5] Value of ullage space was set and it was the ratio of total empty volume to total available volume.

[6] WFNA volume was computed in a way to provide the desired ullage space (%).

$$\text{WFNA Volume} = (\text{Usable Volume} + \text{Total Dead Volume}) - (\frac{\text{Ullage Space}}{100} * (\text{Usable Volume} + \text{Total Dead Volume}))$$

[7] WFNA Density @ 20°C was measured via a pycnometer and determined as 1.504 g/ml at 20°C. Which was used to compute WFNA mass present inside the tubes at designated ullages.

CHAPTER 4

RESULTS AND DISCUSSION

Results obtained via storage tests were discussed in this chapter by evaluating the various outcomes, their relation to one another and how these outcomes were affected by the changes in storage condition variables. These outcomes would be listed as pressure change with respect to time, maximum pressure, corrosion rate, ignition delay times, chemical composition, and elemental analysis. In this regard, pressure change as a function of time were collected at 1-second intervals at 50°C for all the experiments listed in Table 3-4 and Table 3-5. Maximum pressure was highest numeric value that was observed during the long-term storage tests which was determined by analyzing the recorded time-dependent pressure data. Corrosion rate was calculated by using the data between the final and initial mass difference of test tubes and following the steps given in related ASTM designation (ASTM G31 - 72 (Reapproved 1999), 1999). Ignition delay experiments were performed by dropping 6µl of fresh fuel (Tetramethylethylenediamine) on to 300µl pool of stored oxidizer at room temperature (shown in Figure 4.13). Chemical composition of WFNA after storage was analyzed in terms of water, and nitrogen dioxide contents. Lastly, elemental analysis of stored WFNA was carried out to identify the type and amount of dissolved metals, which were transferred from the test tubes to the liquid medium due to surface reactions and permeation in cases where PTFE were used.

In total, five of the thirty two MPV fixtures failed the storage test due to major leaks, sensor malfunctioning or communication errors, part of these results and data were given to present the problems encountered during the research. For simplicity, superscript P was not employed in text but all the even numbered samples should be assumed passivated specimens.

As a result of the comprehensive nature of this investigation, the type and amount of data were abundant and arduous to follow. For this reason, one of the results belonging tube marked Al6061-03 would be analyzed step by step to make easy to track down the rest of the results.

Storage tests were initiated with Al6061-03 after successfully preparing the system with desired test conditions (given in Table 4-1).

Table 4-1 Test conditions for Al6061-03 tube

Marking	Initial Pressure @ 20°C (barG)	Pressurizing Gas	Ullage Space @ 20°C (%)
Al 6061-03	3.06	He	13.0

After the test period was complete, the time dependent pressure data collection was terminated and the stored propellant along with storage tube were taken out of MPV fixture. Some discoloration and precipitation within the WFNA (shown in Figure 4.1) and some corrosion on the inner surface of test tube was present (shown in Figure 4.2).

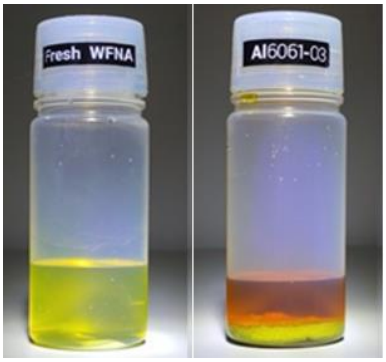

Figure 4.1 Visual state of WFNA before and after storage

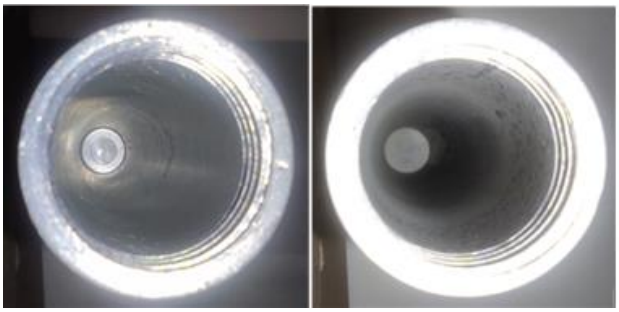

Figure 4.2 Extent of corrosion on Al6061-03 test tube

The pressure as a function of time graph was plotted with the data collected (given in Figure 4.3). By using the pressure data maximum pressure was found as 19.42 barG.

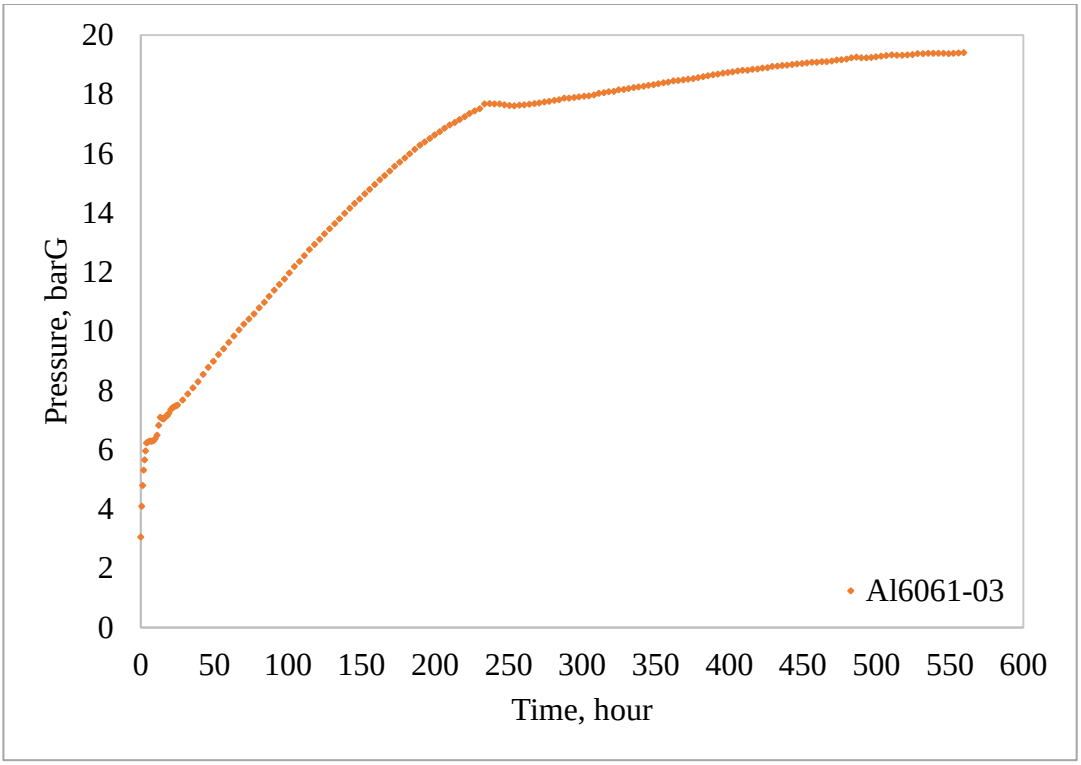

Figure 4.3 Pressure build-up rate of WFNA stored in Al6061-03 tube @ 50°C

By using the initial and final masses of Al6061-03 test tube, the mass loss rate and corrosion rate in terms of mm/year were computed (given in Table 4-2).

Table 4-2 Corrosion rate and mass loss of Al6061-03 tube

Tube Marking	Tube Mass @ ti (g)	Tube Mass @ tf (g)	Tube Mass Loss {ti (g) - tf (g)}	Actual Tube Mass Loss (%)	Corrosion Rate (mm/year)
Al 6061-03	64.12	63.62	-0.50	0.78	0.12

Stored WFNA in Al6061-03 were diluted 1 to 100 with distilled water then the presence and concentration of several dissolved metals were measured via ICP-OES device (shown in Table 4-3). It was found out that excess amounts of some metals diffused into stored liquid from the tube material.

Table 4-3 Elemental Analysis of Fresh and Stored WFNA in Al6061-03 tube

Tube Marking	ICP – OES Elemental Analysis (mg/L)								
	Al	Cr	Cu	Fe	Mg	Mn	Ni	Zn	Total
Fresh WFNA	20	0	0	10	0	0	0	0	30
Al 6061-03	900	4	30	900	140	50	230	2	2256

The chemical content of WFNA taken from the Al6061-03 tube was evaluated in terms of nitrogen dioxide and water concentration. It was found out that compared to fresh WFNA the concentration of water and nitrogen dioxide increased 1.5 and 7.5 times, respectively (shown in Table 4-4).

Table 4-4 Chemical Analysis of Fresh and Stored WFNA in Al6061-03 tube

Tube Marking	Chemical Composition (wt. %)	
	H_2O	NO_2
Fresh WFNA	1.97	1.43
Al 6061-03	2.90	10.74

Stored WFNA inside Al6061-03 tube was used in the ignition delay drop tests with fresh TMEDA and ignition lag in terms of ms (millisecond) was computed via high frame rate camera (shown in Table 4-5). Compared to fresh WFNA, shorter ignition delay times were recorded with WFNA stored in Al6061-03 tube.

Table 4-5 Ignition delay times between fresh TMEDA and stored WFNA in Al6061-03 tube

Tube Marking	Ignition Delay Times with Fresh TMEDA @ 20°C (ms)				
	Test #1	Test #2	Test #3	Test #4	Average
Fresh WFNA	27.1	27.1	25.0	25.0	26.0
Al 6061-03	12.5	8.3	8.3	8.3	9.4

In the following sections throughout chapter 4, the pressure, corrosion, composition and ignition data of all the test samples would be presented and discussed thoroughly in subsections.

4.1 Pressure Changes of WFNA Stored in PTFE Tubes

White fuming nitric acid is reactive consequently; exposure to inappropriate conditions would result in fire, explosion or toxic gas release. To preclude such incidents, in the first place, four distinct storage tests with PTFE tubes were conducted (for details see Table 3-4) to qualify the mini pressure vessel storage test fixture.

According to obtained pressure time data, MPV fixture was proved to provide a leak-free test environment. Additionally, it was clear from the plot that a decrease in ullage space would lead to a decrease in the rate of pressure rise amongst cases where only ullage space variable was altered (shown in Figure 4.4). Based on the results, pressure time data revealed that utilization of helium or nitrogen as ullage gas did not make much difference in the rate of pressure change or in maximum pressure. That behavior was because of the fact that nitric acid was not readily reactive with PTFE and only homogeneous decomposition took place. However, in some cases (PTFE-01 & PTFE-04) serious darkening in fluid color did occur and ICP-OES analysis verified that large amounts of Fe, Cr and Ni elements leached into the solution within the Teflon test tubes. The leaching was attributed to the molecular diffusion of liquid through the porous structure of PTFE material and to the acid vapor. in combination. This incident mainly attributed to the porous structure of PTFE material that would allow high permeation rates. Acid permeation through Teflon is dependent on thickness, quality, pressure and temperature. In fact, because of the elevated temperatures nitric acid permeation rate increased. However, in this case, no data was available regarding the quality, also defined as percent crystallinity, of PTFE tubes. On the bases of these results, excess presence of dissolved metals could be the outcome of poor quality Teflon employed during manufacturing. Surprisingly, tube marked as PTFE-03 was purchased from another supplier and it was only used as substitute to the original one because the actual tube that was intended to be used was thicker and could not fit inside the vessel body.

From the data presented in Table 4-6 and the post-experiment state of PTFE tubes, it was evident that no corrosion took place on the surface of Teflon tubes as expected but a slight yellowing and mass increase were detected due to adsorption and permeation for all the cases. As stated earlier, PTFE-03 was purchased from different supplier, on this account it could be taken as outlier. Among the remaining data, nearly identical mass gains were detected which could be interpreted as the direct result of total surface area of PTFE tubes accepting that the quality was similar. Concerning the pressure change rate, it could be stated that the equilibrium at 50°C occurred after about 500 hours assuming homogeneous thermal decomposition (see (1.2)) and insignificant corrosion. Lastly, there was a loss of connection with one of the pressure sensors (PTFE-04) around the 380th hour of the experiment. Later the system was examined and a short circuit on the sensor was detected.

Table 4-6 Mass and maximum pressure data of WFNA stored in PTFE tubes

Tube Marking	**Tube Mass @ t_i (g)**	**Tube Mass @ t_f (g)**	**Tube Mass Gain {t_i (g) - t_f (g)}**	**Actual Tube Mass Gain (%)**	**Maximum Pressure (barG)**
PTFE-01	53.14	53.21	0.07	0.13	14.86
PTFE-02	52.14	52.21	0.07	0.13	16.81
PTFE-03	51.70	51.75	0.05	0.10	14.08
PTFE-04	52.14	52.22	0.08	0.15	13.81

Ignition delay data, belonging to PTFE tubes, was evaluated in chapter 4.4 by associating them to the changes occurred in other variables.

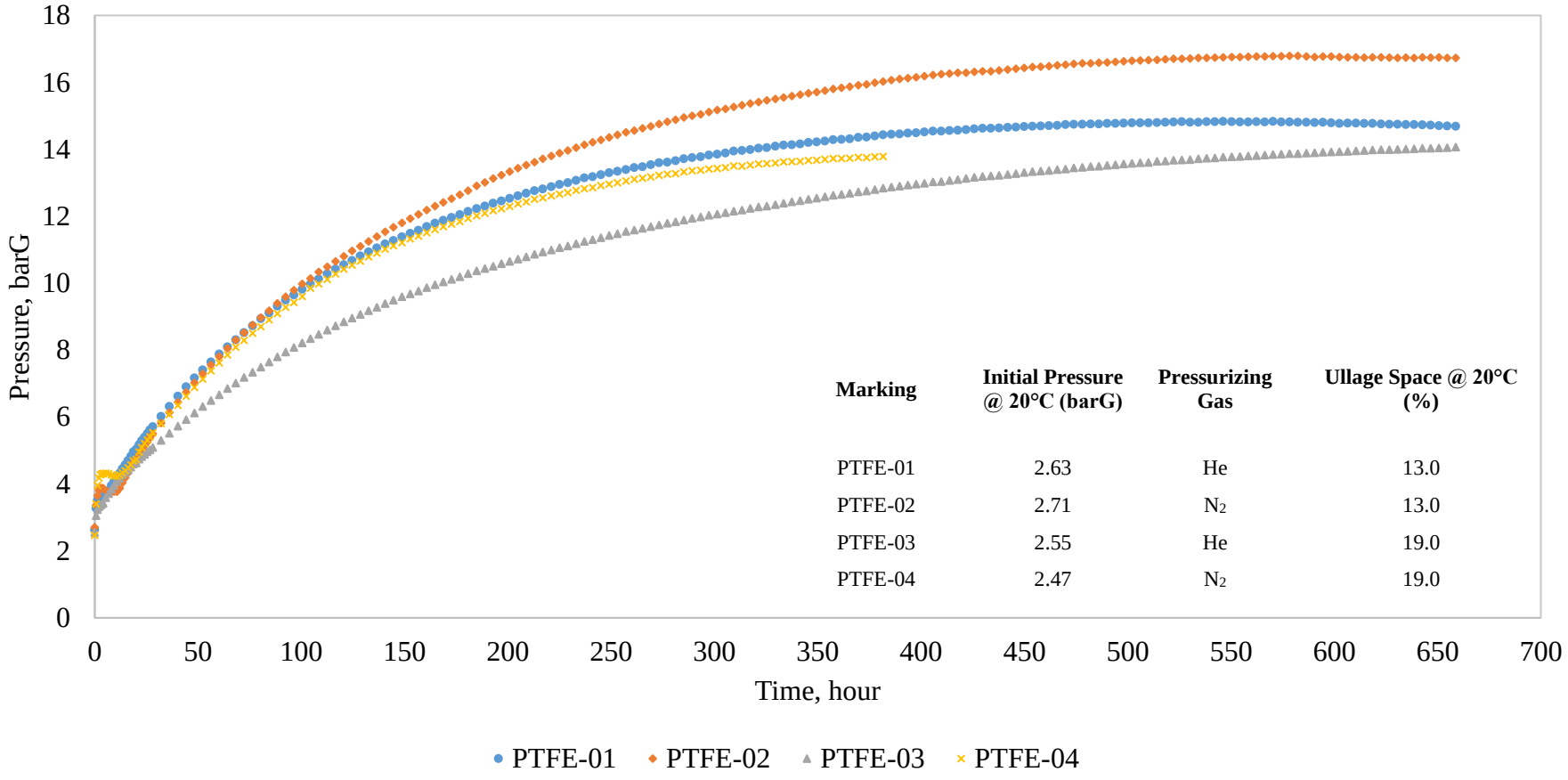

Marking	Initial Pressure @ 20°C (barG)	Pressurizing Gas	Ullage Space @ 20°C (%)
PTFE-01	2.63	He	13.0
PTFE-02	2.71	N_2	13.0
PTFE-03	2.55	He	19.0
PTFE-04	2.47	N_2	19.0

Figure 4.4 Time-dependent pressure data of WFNA stored in PTFE tubes @ 50°C

4.2 Pressure Changes of WFNA Stored in Metal Tubes

Intrinsic experimentation was initiated with four different metallic materials – AISI316L, AISI904L, Al5083-H111 and Al6061-T6 –under different conditions (shown in Table 3-5) after successfully qualifying mini pressure vessel fixture and data acquisition system. Experiments were conducted in a scientific control to minimize the number of affecting variables and create mostly binary comparison groups.

One of the primary acceptance constraints of the propellant storage tanks was the maximum pressure encountered throughout preservation (Sutton D. , 1986). For this purpose, the maximum pressure values were acquired from the time-dependent data recorded (shown in Table 4-7). Based on these results by considering only the maximum pressure values, no elimination was carried out because the propellant storage and propulsion flow systems on the flight vehicles could operate up to 40 barG.

Table 4-7 Maximum pressures recorded in successfully completed tests

Tube Marking	Maximum Pressure (barG)	Tube Marking	Maximum Pressure (barG)
AISI 316L-01	5.93	**Al 5083-01**	19.20
AISI 316L-02^{P}	5.49	**Al 5083-02^{P}**	17.08
AISI 316L-03	5.77	**Al 5083-05**	11.41
AISI 316L-05	4.69	**Al 5083-06^{P}**	9.49
AISI 316L-06^{P}	4.76	**Al 5083-07**	12.52
AISI 316L-07	5.14		
Alloy 904L-02^{P}	9.64	**Al 6061-02^{P}**	15.36
Alloy 904L-03	9.75	**Al 6061-03**	19.42
Alloy 904L-04^{P}	8.70	**Al 6061-04^{P}**	15.39
Alloy 904L-05	8.99	**Al 6061-05**	14.01
Alloy 904L-06^{P}	7.54	**Al 6061-06^{P}**	13.71
Alloy 904L-07	7.70	**Al 6061-07**	12.66

According to pressure data, within the first few hours a rapid pressure rise occurred in all the metal specimen tubes. That was due to expansion of pressurizing gas, increase in the vapor pressure of WFNA and expansion of liquid WFNA in which they were triggered by the rise in temperature. However, the rate of pressure rise its behavior and the maximum value that the pressure reached were different in all cases. For this reason, the experimental data were analyzed in sections by making comparisons with one another.

Tube pairs marked with AISI316L-01 & AISI316L-03, AISI904L-02 & AISI904L-04 and Al6061-02 & Al6061-04 were exposed to the identical test conditions. From the graphs presented in Figure 4.7, Figure 4.8 and Figure 4.9, respectively, it could be seen that identical test condition provided similar outcomes resulting that the desired conditions could be set properly and repeatability was not an major issue. Small pressure value variations between identical sets of experiments could be resulted from measurement tolerances, variation in defects found on the internal surface of tubes or minute propellant doping errors. In addition to all these, one likely reason could be that they failed to overlap perfectly would be the fact that the time elapsed between preparation and pressurization of each test was different from each other. Lastly, the initial pressure of each test was different in the magnitude of 0.3 barG from each other, which could also change the course of pressure rise behavior as stated in literature (Feiler & Morrell, 1952) (Ladanyi, Miller, Karo, & Feiler, 1953) (Sutton D. , 1986).

Half of the test tubes were passivated. To detect the effect of passivation binary experiments were conducted where the only difference was passivation variable. These tube pairs were marked with AISI316L-01 & AISI316L-02, AISI316L-05 & AISI316L-06, Al5083-01 & Al5083-02, Al5083-05 & Al5083-06, Al6061-02 & Al6061-03 and Al6061-05 & Al6061-06. From the data presented in Figure 4.7, Figure 4.9 and Figure 4.10, respectively, it could be seen that the passivation reduced the rate of pressure rise in most cases and the maximum pressure reached was either smaller than or equal to the ones that were not passivated. These pressure behaviors was attributed to the removal of contaminant and free elements from the metal

surface during passivation. However, an evident contradicting result was obtained amongst tube pairs marked with AISI904L-03 & AISI904L-02/04. Here, passivation helped to reduce rate of pressure rise in the beginning, however after about 200 hours (AISI904L-02) and 430 hours (AISI904L-04), the pressure value in non-passivated specimen became smaller than passivated ones (shown in Figure 4.8). The best explanation to this phenomenon would be poor practice during passivation of AISI904L-02, in fact, passivation quality was not evaluated, or one of the disturbances illustrated in the previous paragraph would be in presence. However, repetition tests would be helpful to fully understand the reasons behind this instance.

Two different ullage spaces – 13.0% & 19.0% – were evaluated by conducting binary experiments in which only ullage space variable was intentionally changed. These tube pairs were marked with AISI316L-03 & AISI316L-07, AISI904L-03 & AISI904L-07, and Al6061-03 & Al6061-07. Additionally, Al6061-07 test that was supposed to be used in binary comparison were failed and the pressure data was faulty after the first 250 hours. Based on the data depicted in Figure 4.7, Figure 4.8 and Figure 4.10 for most of the binary test pairs stated above increase in ullage space from 13.0% to 19.0% not only reduced rate of pressure rise but also it decreased the maximum pressure value. This was because there were more room for the expansion of nitric acid liquid and gases present in the sealed atmosphere. However, pressure data in AISI316L-03 & AISI316L-07 pair was slightly unpredicted mostly after the 200^{th} hour. The exact reason of these movements was not considered similar to one of the issues explained early on such as defects, measurement errors or quality but rather due to the nature of material itself. In fact, it was a known fact that the vapor of nitric acid was more corrosive and detrimental in nature compared to liquid form. In other words, it was a possibility that increasing ullage space had led to increase in surface area covered by vapor and that accelerated surface corrosion reactions. However, to accurately answer to that circumstance surface analysis of these test tubes shall be performed.

In the course of pressurization, high-grade helium and nitrogen were used as gases and binary experiments were carried out. Additionally, the effect of air was also

evaluated via two specific cases. The primary aim of using different gases was to detect any change taking place in the pressure rate behavior. In fact, in space industry helium happed to be the main choice of pressurizing gas because of the extreme inertness and occupying less room compared to nitrogen and argon. Storage tests provided four set of pairs that were marked with AISI316L-05 & AISI316L-07, AISI904L-05 & AISI904L-07, Al5083-05 & Al5083-07 and Al6061-05 & Al6061-07. As shown in Figure 4.7, Figure 4.8, Figure 4.9 and Figure 4.10, time-dependent pressure data would not be easily generalized. Meaning that, each of these pattern where the helium and nitrogen effect aimed to be analyzed unfortunately provided slightly diverse outcomes that in return made evaluation rather nonsensical. The best clarification to this data would be the presence of competing forces of solubility and heat capacity differences. As stated in literature section, dependent on temperature nitrogen was way more soluble in nitric acid compared to helium. However, the heat capacity of helium happened to be four times higher than what was for nitrogen per gram basis at constant volume environment. In addition, from the beginning to the end of storage process, temperature, vapor and liquid composition and surface structure was not stationary but rather dynamic. Due to these factors, it was not possible to differentiate the effects of using helium and nitrogen as ullage gas.

It was common and apparent from all the pressure as a function of time plots found in Figure 4.7, Figure 4.8, Figure 4.9 and Figure 4.10 that after passing through a peak point, pressure inside the vessel initiated to decrease. This phenomenon based upon the fact that the consumption rate of liberated oxygen molecules, which were coming from the homogeneous decomposition of nitric acid, by oxidation reactions exceeded rate of oxygen generation. However, as time went by to compensate the decrease in oxygen concentration nitric acid further decomposed according to equation (1.2). In the end, the chemical composition shifts occurred depending on the rate of surface catalytic reactions. As a result, nitrogen dioxide and water concentration of white fuming nitric acid escalated significantly. The complete chemical composition analysis data was given in Table J.1.

Figure 4.5 Leak through pressure sensor and PMRS connection occurred during with the Al6061-07 tube storage

In total five tests were failed to provide healthy data. The underlying reasons why they failed to meet the expectations were investigated. According to inspections executed on the failed systems, it was found that one sensor experienced short circuit, one lost communication in the middle of testing but it was operational at the end, three MPV fixtures experienced small to moderate leaks in different locations (shown in Figure 4.5 and Figure 4.6). The reason of the leaks was attributed to application of insufficient or excessive torque.

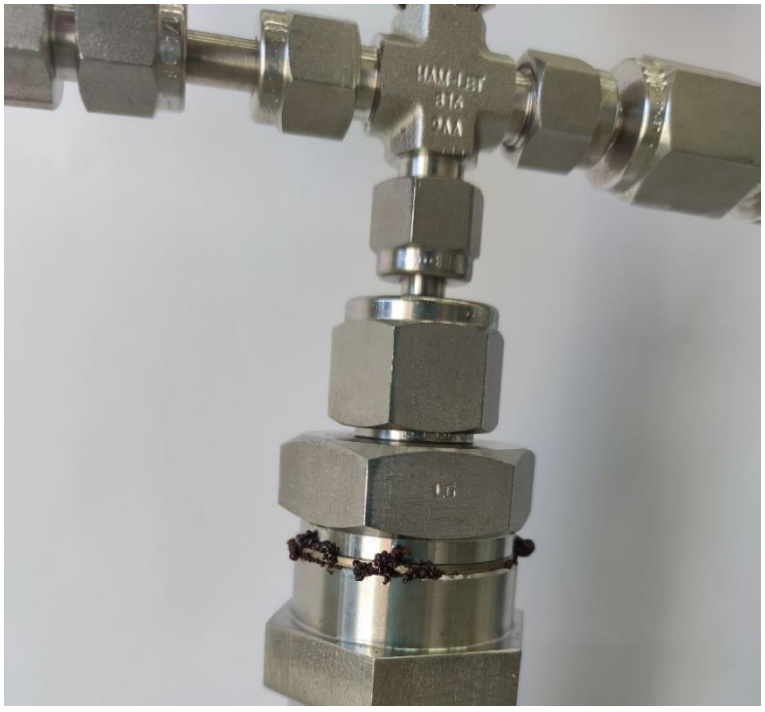

Figure 4.6 Leak through MPV body and PMRS connection occurred during with the PTFE-04 tube storage

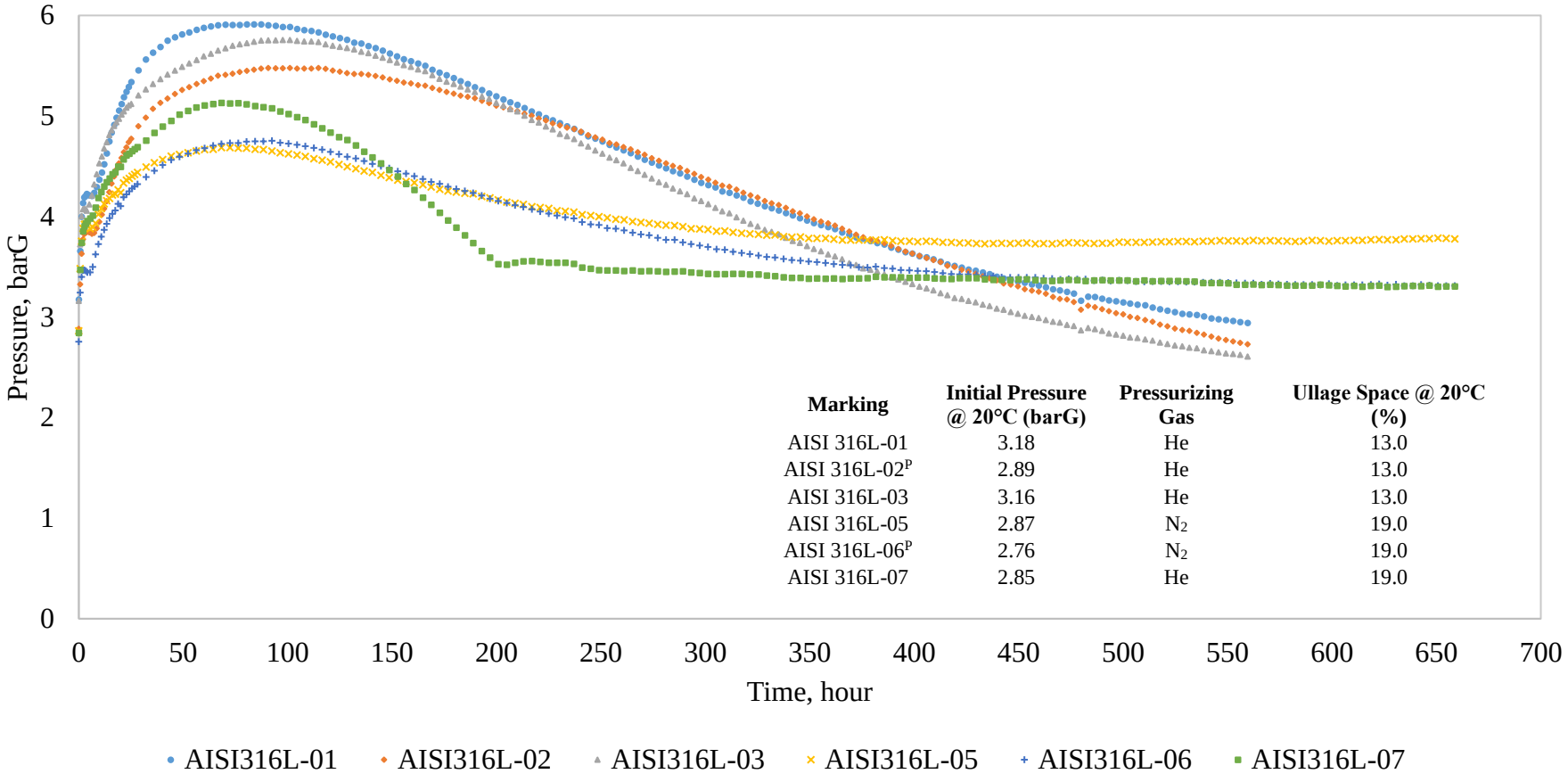

Marking	Initial Pressure @ 20°C (barG)	Pressurizing Gas	Ullage Space @ 20°C (%)
AISI 316L-01	3.18	He	13.0
AISI 316L-02^{P}	2.89	He	13.0
AISI 316L-03	3.16	He	13.0
AISI 316L-05	2.87	N_2	19.0
AISI 316L-06^{P}	2.76	N_2	19.0
AISI 316L-07	2.85	He	19.0

Figure 4.7 Time-dependent pressure data of WFNA stored in AISI316L tubes @ 50°C

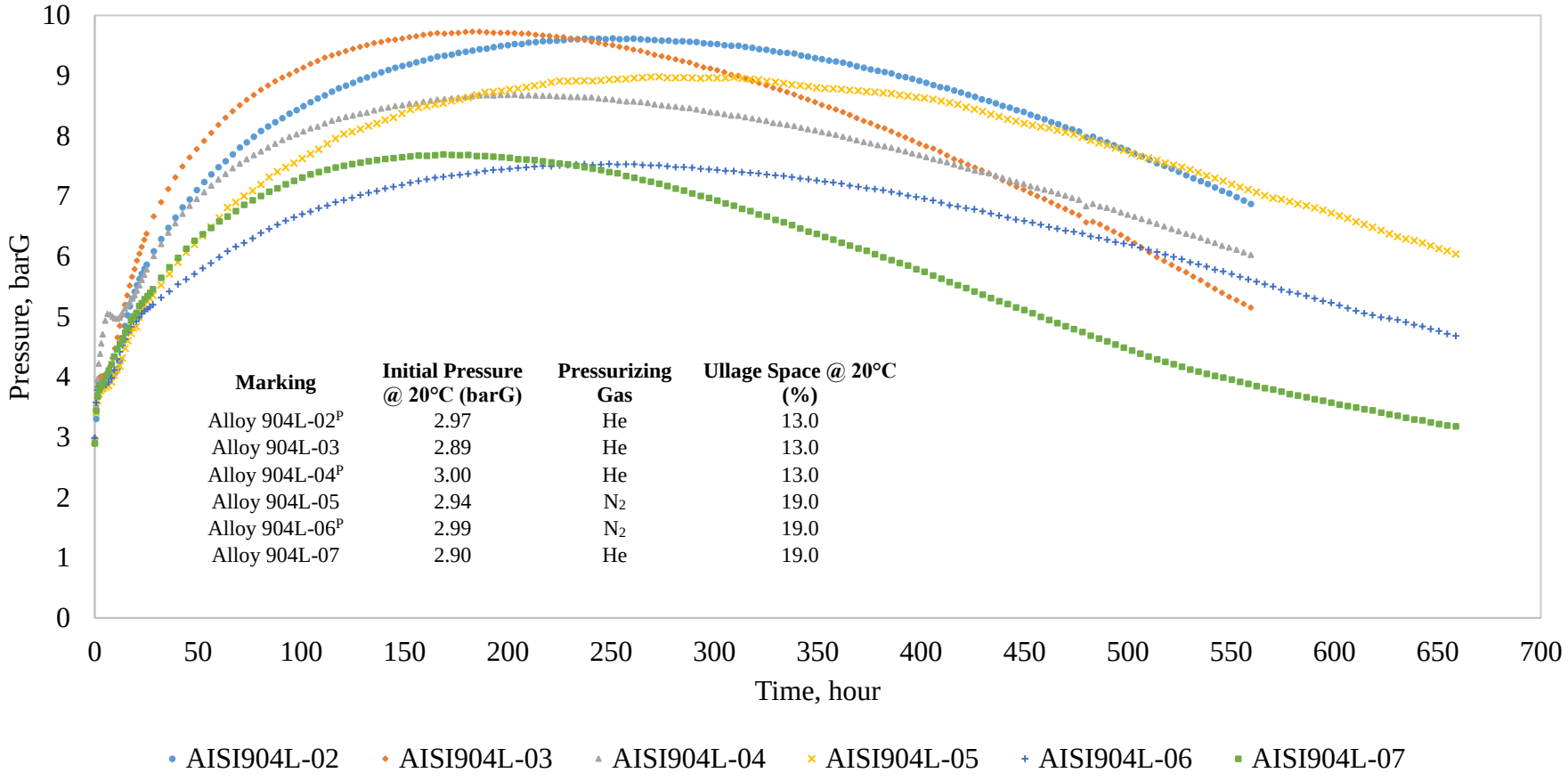

Marking	Initial Pressure @ 20°C (barG)	Pressurizing Gas	Ullage Space @ 20°C (%)
Alloy 904L-02[P]	2.97	He	13.0
Alloy 904L-03	2.89	He	13.0
Alloy 904L-04[P]	3.00	He	13.0
Alloy 904L-05	2.94	N_2	19.0
Alloy 904L-06[P]	2.99	N_2	19.0
Alloy 904L-07	2.90	He	19.0

Figure 4.8 Time-dependent pressure data of WFNA stored in AISI904L tubes @ 50°C

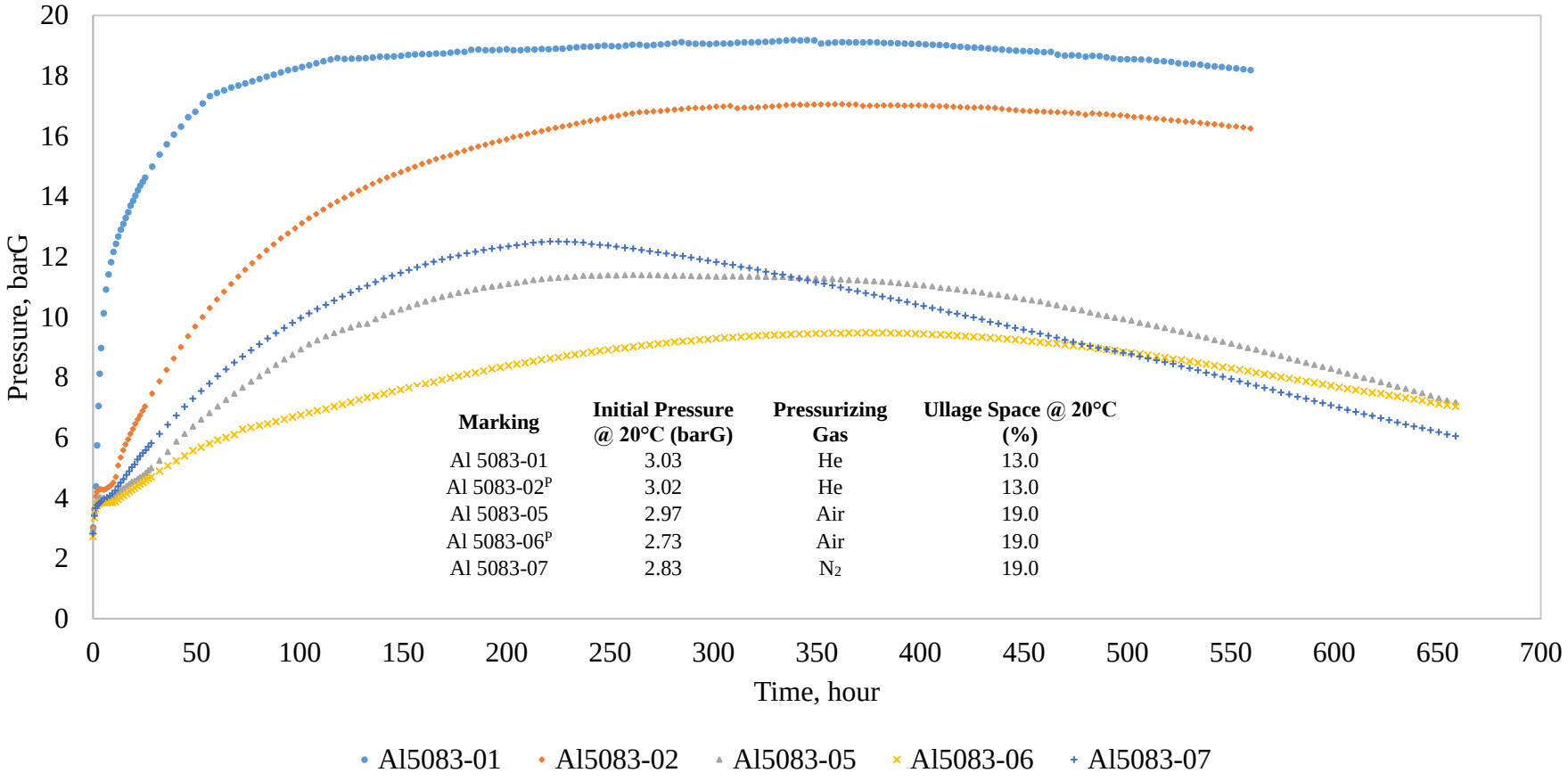

Marking	Initial Pressure @ 20°C (barG)	Pressurizing Gas	Ullage Space @ 20°C (%)
Al 5083-01	3.03	He	13.0
Al 5083-02^{P}	3.02	He	13.0
Al 5083-05	2.97	Air	19.0
Al 5083-06^{P}	2.73	Air	19.0
Al 5083-07	2.83	N_2	19.0

Figure 4.9 Time-dependent pressure data of WFNA stored in Al5083-H111 tubes @ 50°C

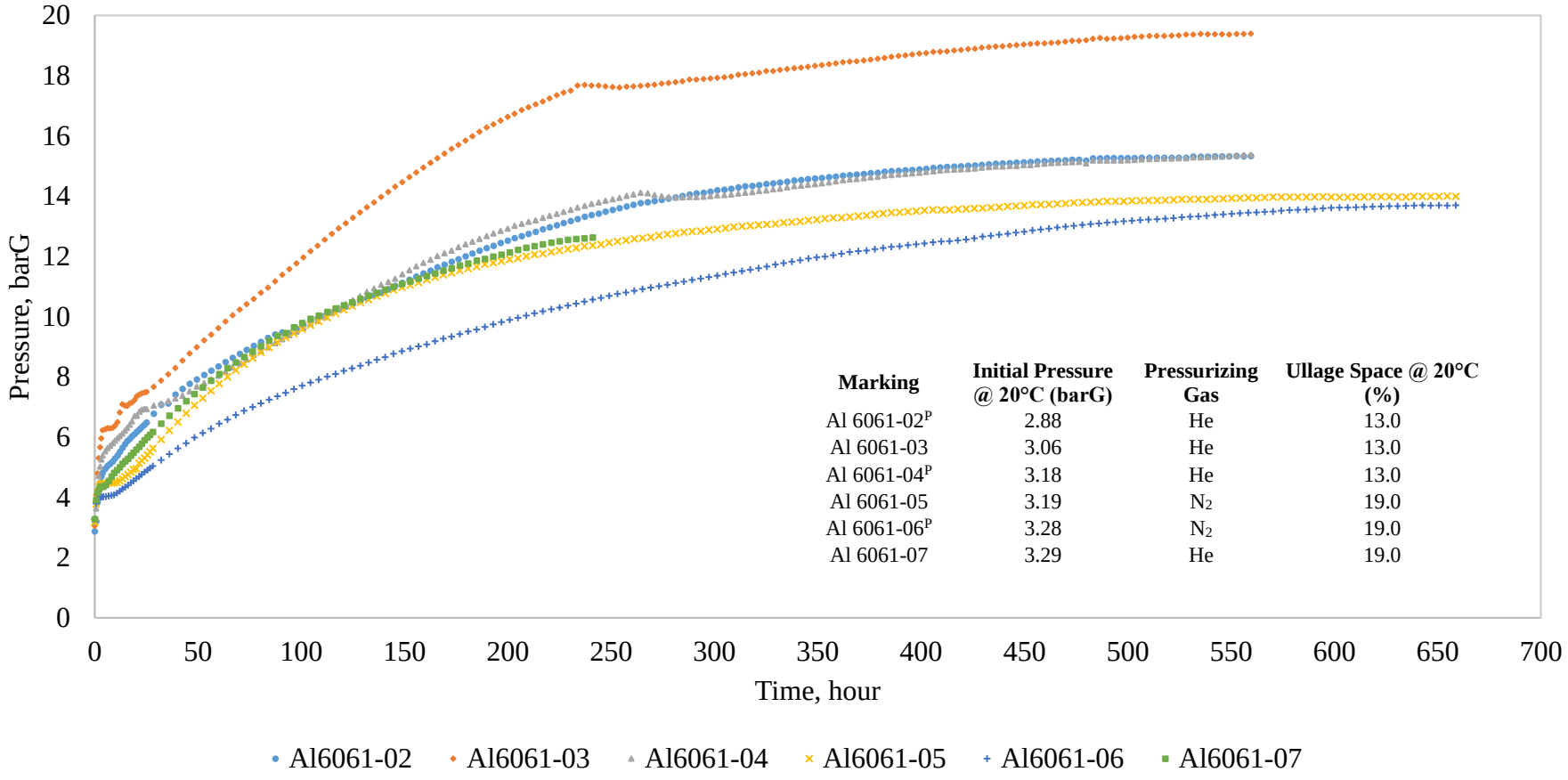

Marking	Initial Pressure @ 20°C (barG)	Pressurizing Gas	Ullage Space @ 20°C (%)
Al 6061-02[P]	2.88	He	13.0
Al 6061-03	3.06	He	13.0
Al 6061-04[P]	3.18	He	13.0
Al 6061-05	3.19	N_2	19.0
Al 6061-06[P]	3.28	N_2	19.0
Al 6061-07	3.29	He	19.0

Figure 4.10 Time-dependent pressure data of WFNA stored in Al6061-T6 tubes @ 50°C

4.3 Corrosion Rate and Mass Losses of Metallic Tubes

Nitric acid readily reacts with all of the metal elements (Al, Cr, Cu, Fe, Mg, Mn, Ni, Zn) constituting metallic tubes used in this investigation. However, the reaction path and products are affected by acid concentration and temperature. Additionally, the reactivity of each metal element is different from one another. These issues could create competing reactions, and since the concentration of the acid will be constantly changing, the reaction pathways may also change. This research aims to answer the overall effect of white fuming nitric acid on the selected few metals and establish a connection between corrosion rate, amount of dissolved metals and chemical composition change of nitric acid. The exact mechanism by which how elements behave in an invariably altering dynamic acid environment is beyond the purpose of this research.

There was a strong visual evidence of corrosion in variable amounts especially on the internal surface of test tubes (shown in Figure 4.11). The type of corrosion was different depending on the material type, but it was apparent from the rough images that pitting and etching was present. In addition to that, due to aggressive nature of nitric acid vapor there was some blackening, staining and spotting on the outer surface of the test tubes as well. The mass of each tube was measured before and after storage experiments. By using the mass difference data and the method provided in ASTM G31-72 standard, the corrosion rate of tubes were computed in terms of mm per year (given in Table G.1). Based on the test conditions, with a few exceptions, the corrosion rate was directly dependent on the type of material.

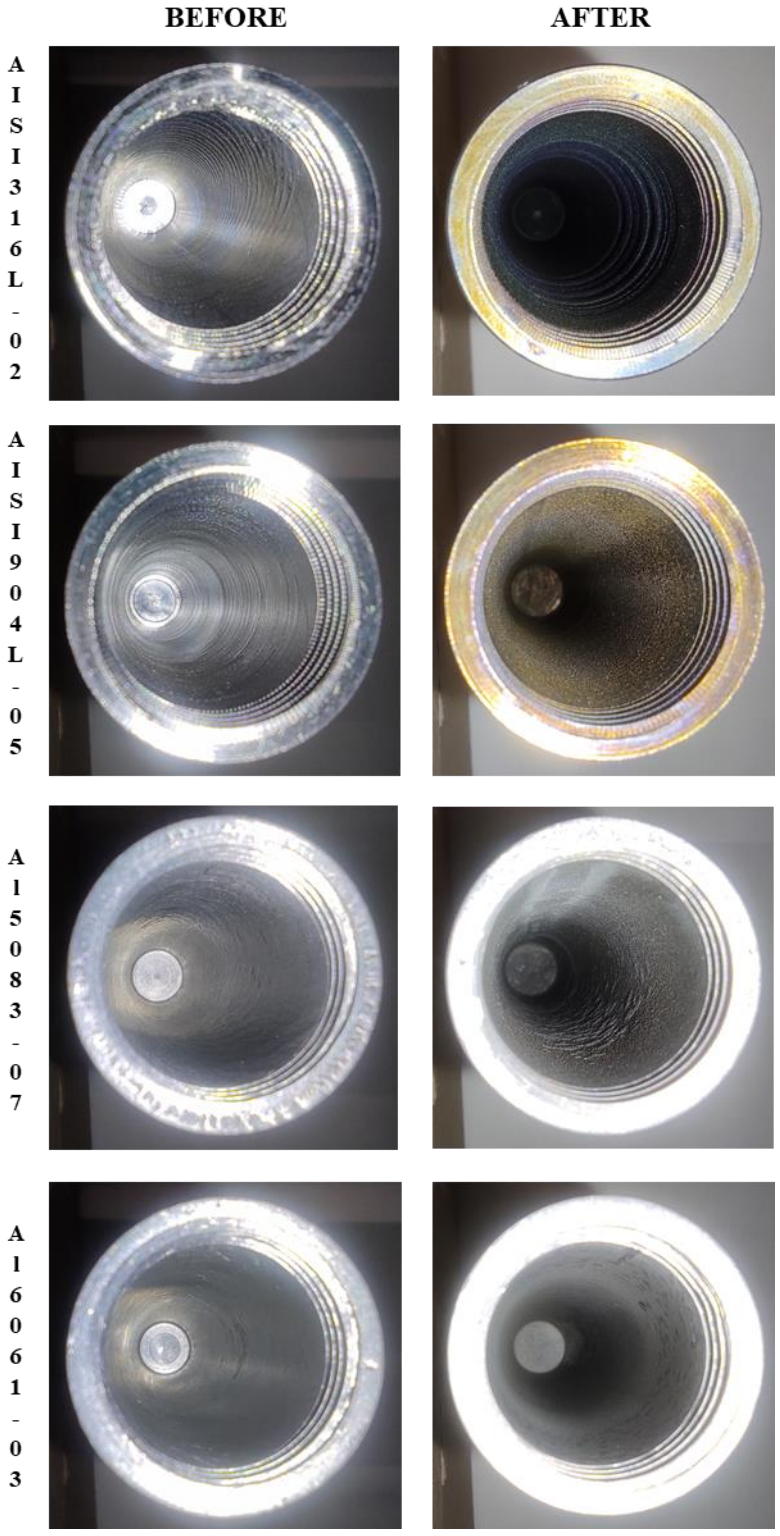

Figure 4.11 Extent of corrosion on various metallic test tubes under different conditions

Among the metallic materials investigated, when mass losses and corrosion rates were evaluated Al6061-T6 was relatively the most resistant to WFNA corrosion, whereas AISI316L showed the lowest resistance. The effect of the pressurizing gas type was not salient. For instance, almost identical corrosion rate values were computed for Al6061-T6 and AISI316L test sets among themselves. Another variable evaluated was the presence of passivation. Similar to pressurizing gas, there was not an explicitly recurring indication that could be used neither to support nor to refute the effect of citric acid passivation on corrosion rate of these four metals.

Another approach commonly used in the evaluation of oxidation of metals and alloys was Pilling-Bedworth ratio (PBR). This ratio was used to estimate the protection performance of oxide film forming on the surface. In fact, oxide film formation was required to increase the metal resistance to high temperature oxidation. In some cases, due to poor formation of oxide film spallation and cracking were caused as could be clearly seen in Al5083-07 test tube (shown in Figure 4.11). These surface defects could primarily caused by growth and thermal stresses generated in the oxide film (Xu & Gao, 2000). Additionally, oxide film formation on the interior surface and precipitated phases of each test tube were highly different. This phenomenon was attributed to the activity difference between alloying elements (Jiang, Lu, Liu, Liu, & Hou, 2021). However, to better understand the characteristic of oxide film and its structure, further microstructure surface analyses such as scanning electron microscopy (SEM) and energy dispersive spectroscopy (EDS) would be resorted.

The relation between corrosion rate and total dissolved metal concentration was evaluated. The related plot given in Figure 4.12. According to numerical results, in most cases increased metal concentration led to higher corrosion rates. However, the data belonging to Al5083-H111 tubes was contradictory where in all five cases the corrosion rate was the same, 0.5 mm, but there was up to two times difference between total dissolved metal content. Additionally, passivation did not affect corrosion rate in most cases, but it reduced the total dissolved metal concentration. This was attributed to the removal of free contaminants and elements from the metal surface.

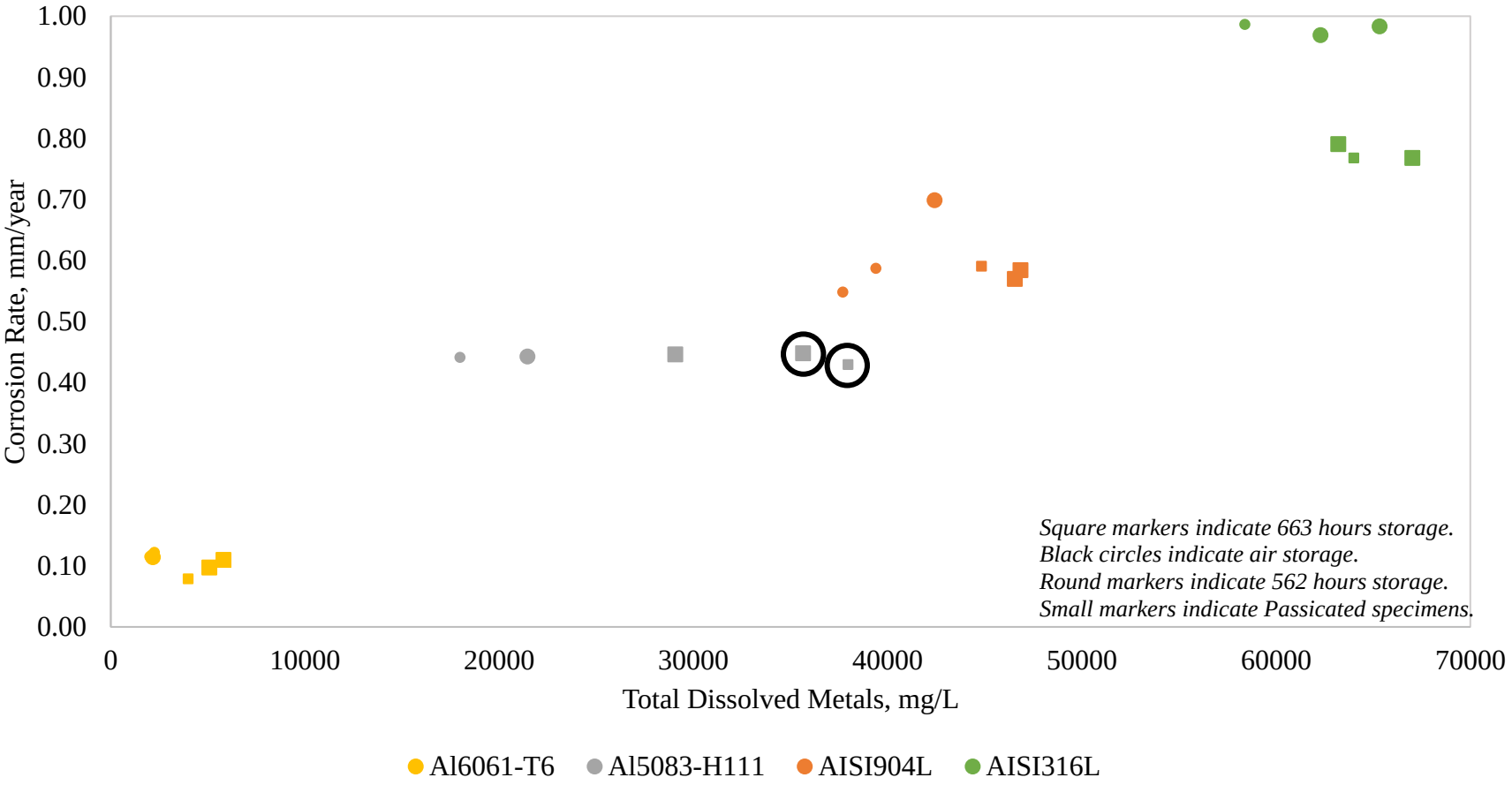

Figure 4.12 Variation of corrosion rate (mm/year) in metal tubes as function of total dissolved metal concentration (mg/L)

4.4 Ignition Delay Tests and Variation of Ignition Delay Times

Hypergolic propellants tend to ignite spontaneously when appropriate conditions are present. Some of these conditions are surrounding temperature, atmospheric pressure, propellant composition, mixing ratio and mixing rate. They especially affect the neutralization, nitration and redox reactions taking place between the fuel and oxidizer. In this regard, simple drop tests were conducted by using ignition delay set-up (shown in Figure 4.13). In this set-up, Brand Transferpette® model D-10 and D-1000 microliter pipettes were employed for fuel and oxidizer, respectively. Throughout ignition delay tests, Tetramethylethylenediamine (TMEDA) was chosen as the working fuel because it was considered perfect green alternative to replace hydrazine in bipropellant applications (Liu, Dasgupta, Zybin, & Goddard, 2011). In addition to that, propellant grade TMEDA was commercially available product.

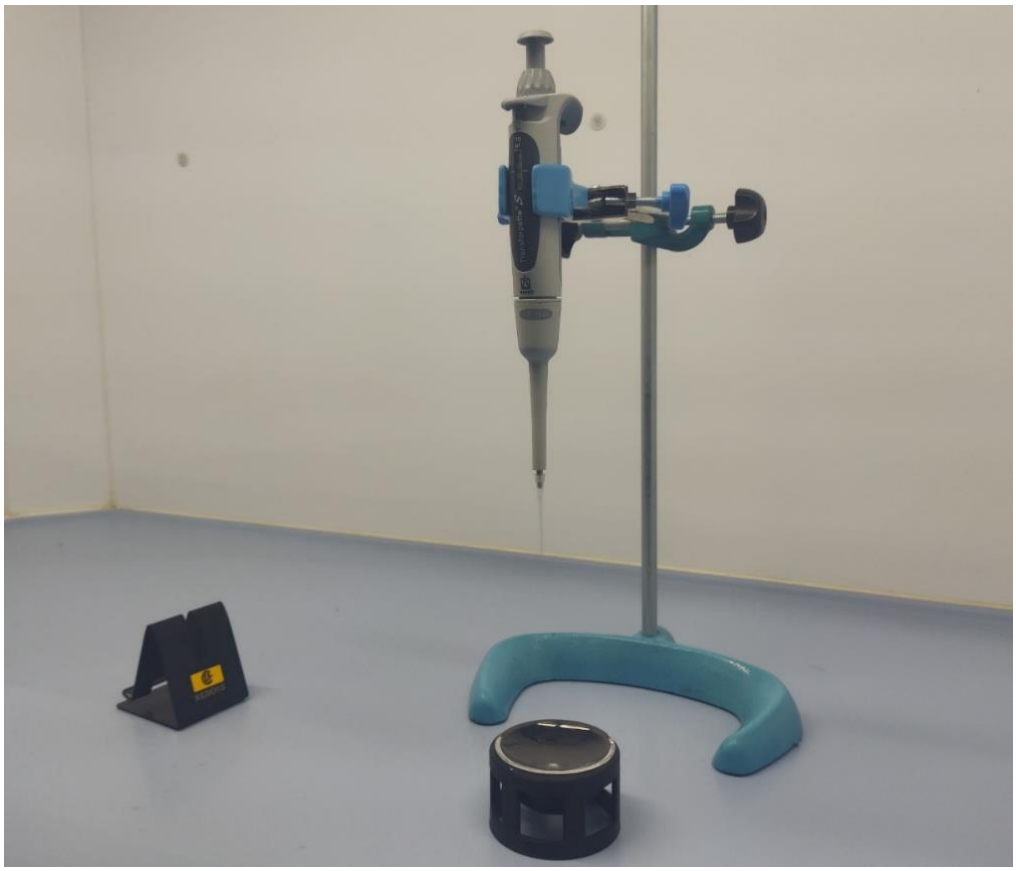

Figure 4.13 Ignition delay set-up via simple drop test

At the end of storage tests, WFNA samples were taken inside 250ml FEP bottles and kept at 20°C for the remainder of the investigation. Ignition delay tests were conducted by using these samples with fresh TMEDA. Bilateral interaction both between the variation of ignition delay times and total dissolved metals and between the variation of ignition delay times and chemical composition were interpreted.

During the ignition delay tests, 300µl of WFNA were used to create a pool in the watch glass and 6µl of TMEDA were dropped upon it from 115mm distance (shown in Figure 4.14). The tests were recorded with high-speed frame rate and ignition delays were computed by counting the number of frames elapsed between the first contact and first flame. Complete numerical results of ignition delay via drop tests were given in Table İ.1.

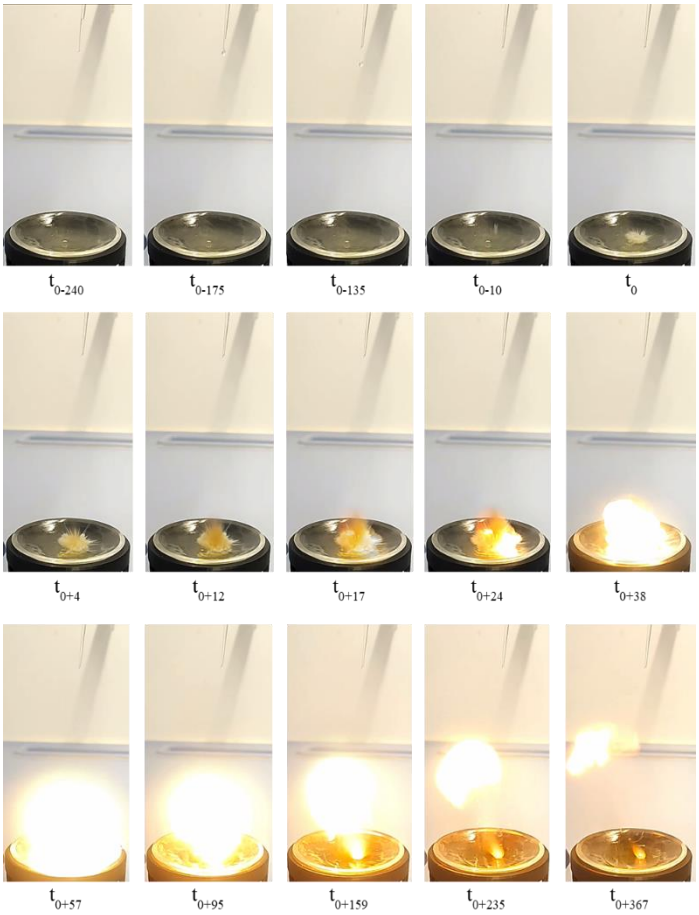

Figure 4.14 Ignition delay drop test with a pool of 300µl fresh WFNA and a single drop of 6µl fresh TMEDA (time indications are in ms)

Ignition delay times were analyzed with two different but analogous approaches. The first approach took into account the total amount of dissolved metals determined in the WFNA samples. When the variations in ignition delay times were compared with the total amount of dissolved metals, it was apparent that as the concentration of dissolved metals increased the ignition delay times were negatively affected in many cases. However, as shown in Figure 4.15 there were also some other instances where ignition delay of stored WFNA was less than the fresh WFNA, which had only 30 mg/L dissolved metals. For instance, all the ignition delay tests performed using the samples taken from the Al6061-T6 reactor tubes exhibited at least three times shorter ignition delay times. On the bases of these findings, two distinct postulates could be put forward. Former one being that, the presence of a specific type and amount of dissolved metal could be taking a role in the catalysis of the preignition reactions. From the data presented in Table H.1 and Table İ.1, it could also be conjectured that there would be threshold values for the concentration of dissolved metal type, which would be influencing the reaction rate positively up to a point. However, to shed light on the reasons for this phenomenon, continuation experiments would be needed in such a way that metal nanopowders (NPs) shall be added to the fresh WFNA then ignition delay tests under identical conditions would be performed. Latter one being that, due to vigorous decomposition reactions the chemical composition of the concentrated nitric acid would be altered in return it could accelerate or decelerate the ignition period. Which brought the second approach to the agenda.

In the second approach, unlike the previous one, the pivotal focus was given to the chemical composition of the nitric acid. For this purpose, the percent weight composition of nitrogen dioxide and water of all the liquid samples were analyzed (given in Table J.1). When the chemical composition and ignition delay times data were evaluated together (shown in Figure 4.16), there was not an unambiguous pattern between those. For instance, amongst tests samples (excluding fresh acid) the most interesting results were obtained in aluminum 5083 specimens. Although, the water and nitrogen dioxide contents of all the Al5083 samples were very close, it was determined that there were differences of up to 30 times between the ignition

delay times. Even though, it was clearly stated by various researchers that change in nitrogen dioxide and water concentration would affect the ignition delay times (Miller, 1953) (Hennings & Ladanyi, 1954) (Morrell, 1957) (Zung & Breen, 1970). In fact, such instances were presented for both open cup drop and small-scale engine cases by comparing white fuming and red fuming nitric acids with a number of organic fuels (Hennings & Ladanyi, 1954). However, the effect of increase in nitrogen dioxide and water concentration would be arduous to interpret since preignition reactions were also strongly dependent on the fuel type (Miller, 1953) (Morrell, 1957). Similar to the dissolved metal layout, further ignition delay experimentation would be necessitated with nitric acids having various nitrogen dioxide and water concentration with having dissolved metal no more than what fresh WFNA had in this study.

From the above discussion, there would be several possibilities that influences ignition. Such that, one or more elements could be acting as in the favor of ignition up to a certain concentration then they could begin to act inhibitively. In addition to the first proposition, some elements could assist ignition then they are alone but when they come together then opposite might take place. Analogically, similar arguments could also be stated for the bilateral interactions of chemical composition and ignition because when fresh WFNA gets involved data becomes much harder to justify. Only then, the exact factor that determines the ignition delay time could be specified with relative confidence.

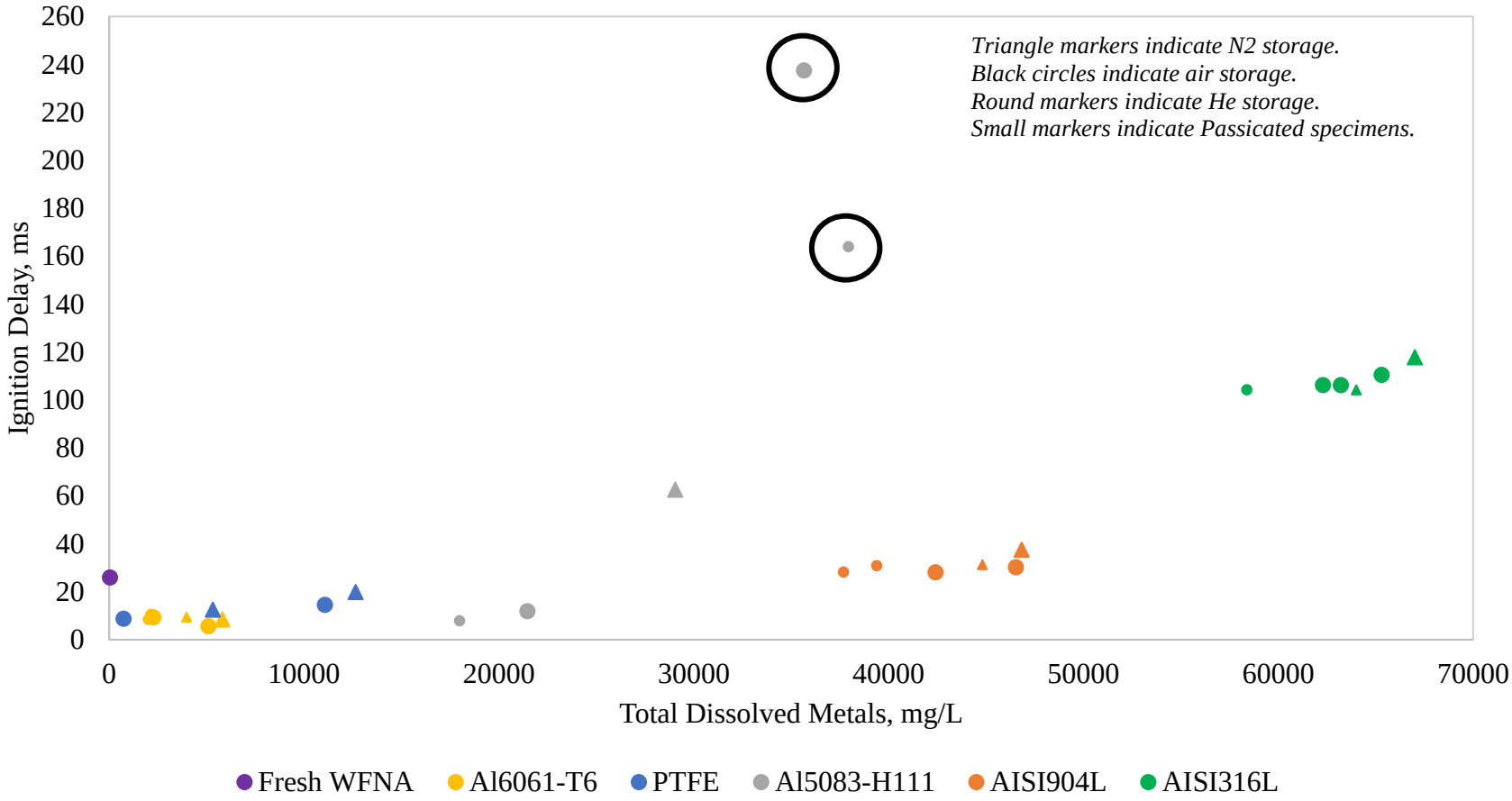

Figure 4.15 Variation of ignition delay times of WFNA with TMEDA depending on the amount of total dissolved metals

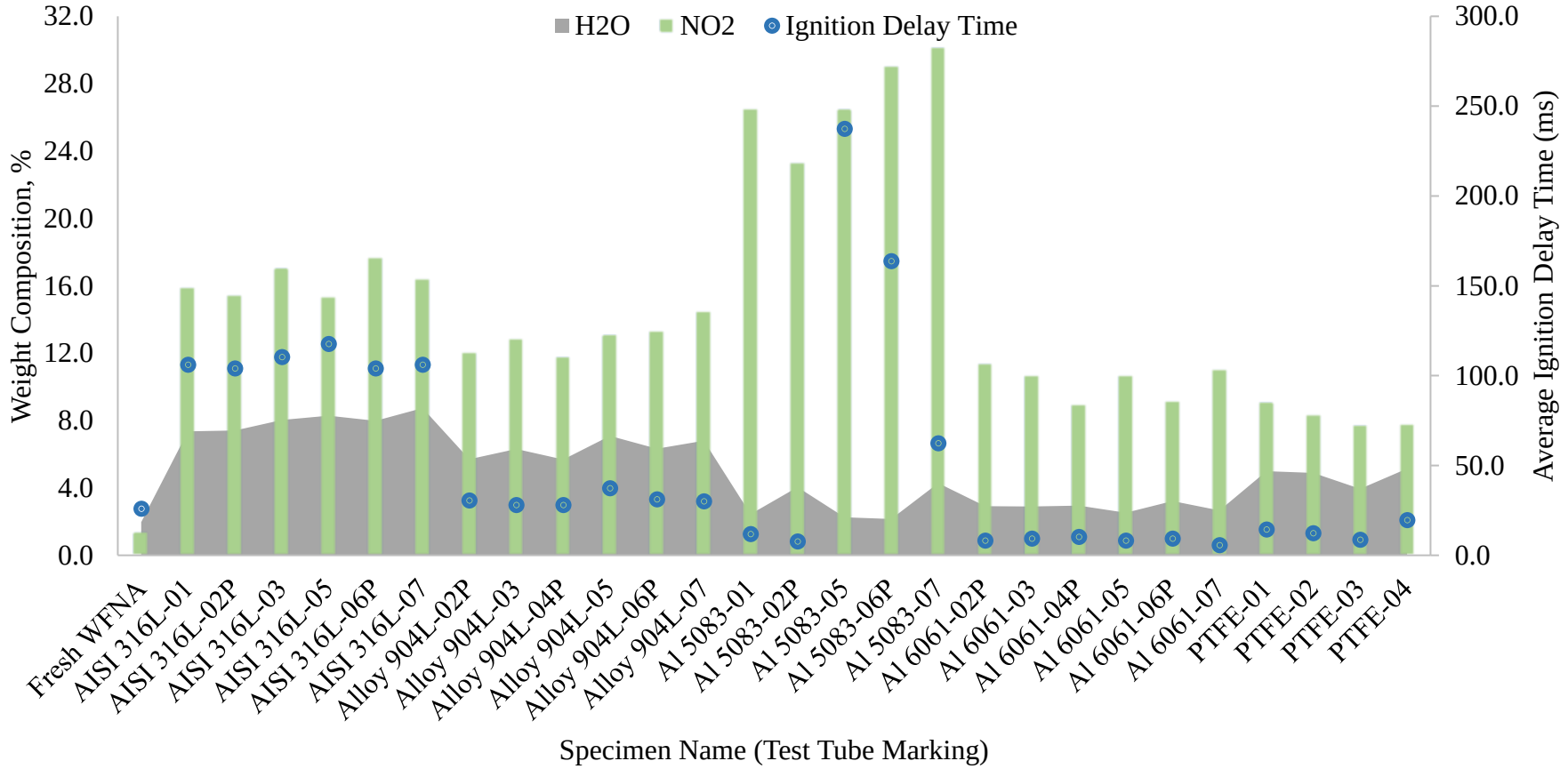

Figure 4.16 Variation of ignition delay times of WFNA with TMEDA depending on the chemical composition content

CHAPTER 5

CONCLUSION

The objective of this thesis was to determine the optimum storage materials and conditions of propellant grade WFNA. For this purpose, a custom pressure test vessel (MPV) was designed and two comprehensive test matrices – control & master – were prepared. In this regard, storage tests were performed at elevated temperatures of 50°C up to 600 hours inside MPV fixtures. In the course of experimental evaluation, five different materials – PTFE, AISI316L, AISI904L, Al5083-H111 & Al6061-T6 –, three different pressuring gases – helium, nitrogen & air –, two different ullage space values –, 13.0% & 19.0% –, and presence of citric acid surface treatment were investigated. At the end, by keeping the rest of the variables at a fixed value, the effect of each of the four variables on pressure rise and propellant stability were analyzed individually. After the post testing analyses, corrosion rate calculation of test tubes, ignition delay tests with fresh TMEDA, near-infrared absorption spectroscopy and ICP-OES analysis of stored propellant were performed. As a result, lowest corrosion rates were obtained with Al6061 tubes, similarly shortest ignition delay times were recorded with white fuming nitric acid taken from the Al6061 tubes. According to ICP-OES analysis, lowest total dissolved metal concentration belonged to Al6061 tubes. In terms of chemical composition, smallest changes in water and nitrogen dioxide contents were detected mostly in Al-6061 tubes. About storage conditions usually independent of storage material, larger ullage space values led to slower and smaller pressure rise and peak pressure values, respectively. Helium and nitrogen performances were overlapping but air exhibited significantly inferior performance. Lastly, passivation reduced pressure rise in most cases and the peak pressure was either smaller than or equal to the specimens that were not passivated. To sum up, Al6061 material exhibited superior performance compared to other metallic materials independent of the storage variables.

CHAPTER 6

FUTURE WORK

Empirical determination of the most optimal storage conditions would only suggest one that what should not be done but providing those conditions would not imply that the propellant would exhibit high performance and be applicable for missions. Accordingly, all the studies performed up to now were mostly empirical and theoretical studies as well as statistical analysis shall be performed to determine parameter-dependent and random variations.

6.1 Large Scale Long Term Storage Tests

Within the scope of this thesis, short-term behavior of white fuming nitric acid storage in small amounts were investigated under several varying conditions. Unfortunately, extrapolation of short-term data to present the long-term data would only be a serious fault. (Uney & Fester, 1972).

After the completion of storage tests with small tubes long-term storage of WFNA in analogous storage tank assemblies shall be conducted to assess the acceptability of the ultimate storage tanks and to obtain genuinely functional data for further computations. Accordingly, by using the long-term pressure-time data, stored propellants and the storage tanks, several prominent properties shall be obtained. These properties would be classified as physical and mechanical properties, ignition delay times, flow characteristics, and mass loss rates.

Analogous tanks were usually equipped with actual tank instruments and devices that were intended to take place on the final system (shown in Figure 6.1 and Figure 6.2). In this way, while testing the tank performance and overall compatibility, the response of each piece of equipment would also be tested in the same manner.

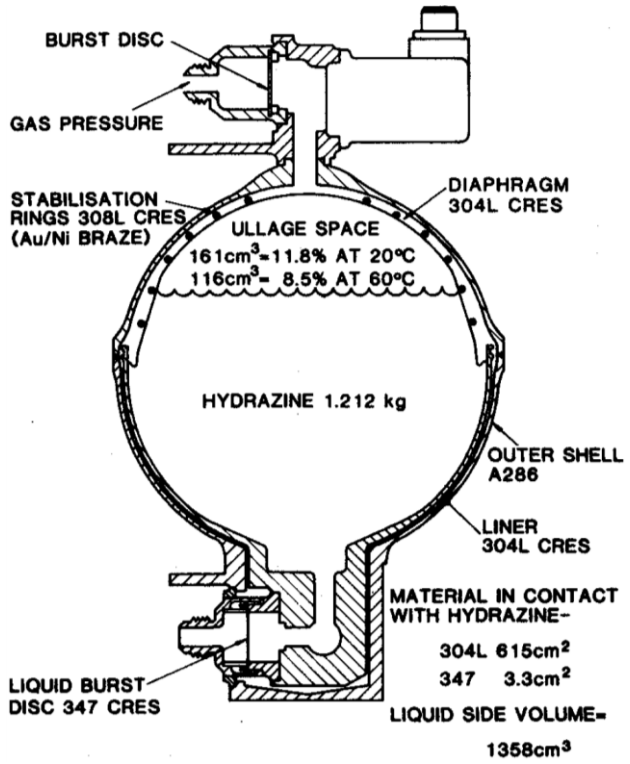

Figure 6.1 Gas Generator Hydrazine Storage Tank Layout (Sutton D. , 1986) Reproduced with permission from AIAA

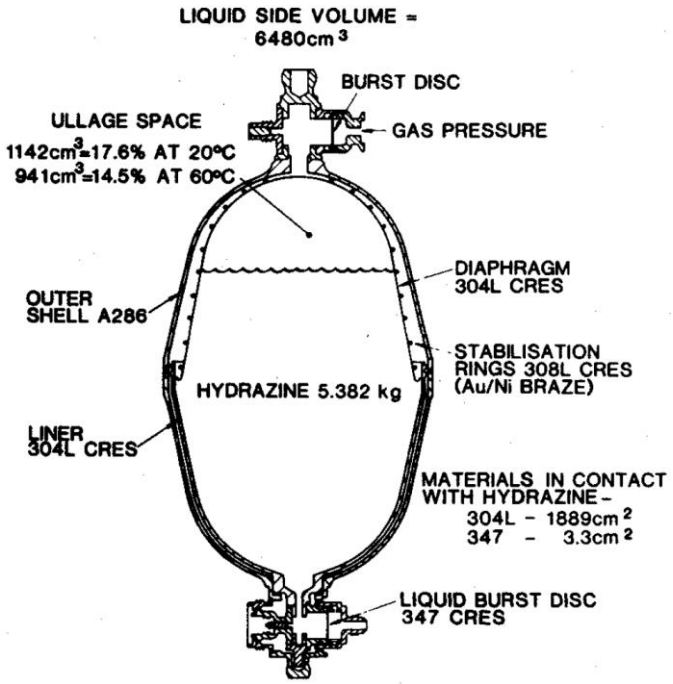

Figure 6.2 Attitude Control System Hydrazine Storage Tank Layout (Sutton D. , 1986) Reproduced with permission from AIAA

In the future, tensile specimens shall be tested with short-term and long-term static immersion tests as maintaining the surrounding conditions identical to optimum storage ones. Then, the changes in the composition, hardness, elongation, and tensile strength for short-term and long-term immersion samples shall be specified.

Once the optimum storage conditions of the WFNA were successfully determined, the next step should be the determination of reaction kinetics and ignition delay times with promising liquid fuels such as hydrazine or amine derivatives. For instance, specific to amines, in the course of the ignition period liquid state neutralization and nitration reactions are reasonably influential along with a follow-up oxidation reaction that is a slow and importantly rate-determining step (Schalla & Fletcher, The Ignition Behavior of Various Amines with WFNA, 1959).

At the end of this research study, only basic drop-tests was performed with a selected amine derivative to have an insight about the effect of storage on ignition lag. Further analysis regarding the ignition should be continued once the long-term stage of research reaches to an end.

Flow characterization, as well as flow-related problems of WFNA in the propulsion system, require intense investigation. At low temperatures, sludge, gel, or precipitate substances would cause flow blockage, valve seat clogging, excess pressure drop through filters, and flow restrictions through capillary tubes. On the other hand, at elevated temperatures, their solubility in the propellant increases and this leads to higher corrosion rates and decreased propellant performance along with a change in the propellant composition. Issues regarding the flow behavior shall be pursued under a few selected sets of conditions.

In this research, only mass loss of test tubes was calculated at the end of each experiment. Interpretation of this data alone would be misleading and might direct the experimenter into wrong conclusions. Overall, a series of analogous storage tanks should be tested under the identical conditions to the fullest extent. Meanwhile, one of the ongoing tests should be terminated with an equal time interval each time. At the end, mass loss with respect to time plots shall be obtained.

REFERENCES

American Institute of Aeronautics and Astronautics Liquid Propulsion Committee on Standards. (1999). Fire, Explosion, Compatibility, and Safety Hazards of Hypergols - Hydrazine. Reston, Virginia: AIAA. Retrieved November 11, 2021

American Institute of Aeronautics and Astronautics Liquid Propulsion Committee on Standards. (1999). Fire, Explosion, Compatibity, and Safety Hazards of Hypergols - Monomethylhydrazine. Reston, Virginia: AIAA. Retrieved August 22, 2021

American Institute of Aeronautics and Astronautics Liquid Propulsion Committee on Standards. (2001). Fire, Explosion, Compatibility, and Safety Hazards of Nitrogen Tetroxide. Reston, Virginia: AIAA. Retrieved May 8, 2021

ASTM A380/A380M – 17. (2017). Standard Practice for Cleaning, Descaling, and Passivation of Stainless Steel Parts, Equipment, and Systems. West Conshohocken, Pennsylvania, United States. Retrieved December 17, 2021

ASTM A967/A967M – 17. (2017). Standard Specification for Chemical Passivation Treatments for Stainless Steel Parts. West Conshohocken, Pennsylvania, United States. Retrieved December 24, 2021

ASTM F2391-05. (2016). Standard Test Method for Measuring Package and Seal Integrity Using Helium as the Tracer Gas. West Conshohocken, Pennsylvania, United States. Retrieved October 18, 2021

ASTM G31 - 72 (Reapproved 1999). (1999). Standard Practice for Laboratory Immersion Corrosion Testing of Metals. West Conshohocken, Pennsylvania, United States. Retrieved July 17, 2022

Bellerby, J. M. (1983). The Chemical Effects of Storing Hydrazine Containing Carbon Dioxide Impurity in Stainless Steel Systems. Journal of Hazardous Materials, 7, 187-197. Retrieved January 15, 2022

Bellerby, J. M. (1985, May 26). The Effect of Some Dissolved Metal-Ion Contaminants on the Homogeneous Decomposition Rate of Anhydrous Hydrazine. Journal of Hazardous Materials, 57-60. Retrieved January 5, 2022

Bennett, C. R., Saw, D. R., & Sutton, D. (1979). Laboratory Tests at Elevated Temperatures for the Prediction of the Rates of Pressure Rise in Hydrazine Tanks at Normal Storage Temperatures. Journal of Hazardous Materials, 23-44.

Benz, F. J., & Pippen, D. L. (1980). Autoignition Flammability and Explosion Properties of Hydrazine and Monomethylhydrazine. Chemical Propulsion Information Agency. Retrieved January 14, 2022

Benz, F. J., Bishop, C. V., & Pedley, M. D. (1988). Ignition and Thermal Hazards of Selected Aerospace Fluids. New Mexico: NASA Johnson Space Center White Sands Test Facility. Retrieved December 11, 2021

Boyd, W. C., & Brasher, W. L. (1989). A Perspective on the Use of Storable Propellants for Future Space Vehicle Propulsion. Johnson Space Center. Houston, Texas: National Aeronautics and Space Administration. Retrieved July 18, 2021

Braeunig, R. A. (2014, July 4). Basics of Space Flight. Retrieved from Rocket Propellants: http://www.braeunig.us/space/propel.htm

Carderelli, F. (2008). Materials Handbook: A Concise Desktop Reference (2nd ed.). London: Springer-Verlag. Retrieved 12 17, 2021

Carroll, J. J. (1999). Henry's Law Revisited. Chemical Engineering Process, 49-56. Retrieved December 29, 2021

Clark, J. C. (1972). Ignition! An Informal History of Liquid Rocket Propellants. (I. Asimov, Ed.) Rahway, New Jersey, United States of America: Quinn & Boden Company, Inc. Retrieved September 22, 2021

Clever, L. H., Battino, R., Saylor, J. H., & Gross, P. (1956). The Solubility of Helium, Neon, Argon and Krypton in some Hydrocarbon Solvents. Division of Physical and Inorganic Chemistry, 125th National Meeting of the American Chemical Society, (pp. 1078-1082). Kansas City, Missouri. Retrieved December 22, 2021

Crowl, D. A., & Louvar, J. F. (2014). Chemical Process Safety Fundamentals with Applications (3rd ed.). Massachusetts: Prentice-Hall. Retrieved March 18, 2021

Cuddihy, E. F. (1971). Solvent-Stress-Cracking and Fatigue Properties of Liquid Propellant Expulsion Teflon Bladders. Pasadena, California: Jet Propulsion Laboratory. Retrieved November 2, 2021

DeSain, J. D., Brady, B. B., Curtiss, T. J., & Greenberg, L. T. (2015, August). Solubility of Pressurant Gases in Liquid Hydrazine at Elevated Temperatures. Journal of Propulsion and Power, 31(4), 1193-1203. Retrieved December 30, 2021

Feiler, C. F., & Morrell, G. (1952). Investigation of effects of additives on storage properties of fuming nitric acids. Lewis Flight Propulsion Laboratory. Washington: National Advisory Committee for Aeronautics. Retrieved December 15, 2021

Hennings, G., & Ladanyi, D. J. (1954). Organophosphorus Compounds in Rocket-Engine Applications. Washington: NACA. Retrieved September 17, 2022

Jiang, Q., Lu, D., Liu, C., Liu, N., & Hou, B. (2021). The Pilling-Bedworth Ratio of Oxides Formed From the Precipitated Phases in Magnesium Alloys. (Y. Song, Ed.) Frontiers in Materials, VIII. Retrieved December 08, 2022

Kretschmer, C. B., Nowakowska, J., & Wiebe, R. (1946, May). Solubility of Oxygen and Nitrogen in Organic Solvents from -25 to 50°C. Industrial and Engineering Chemistry, 38(5), 506-509. Retrieved December 25, 2021

Ladanyi, D. J., Miller, R. O., Karo, W., & Feiler, C. E. (1953). Some Fundamental Aspects of Nitric Acid Oxidants for Rocket Applications. National Advisory Committee for Aeronautics, Washington. Retrieved March 14, 2021

Liu, W.-G., Dasgupta, S., Zybin, S. V., & Goddard, W. A. (2011, April 28). First Principles Study of the Ignition Mechanism for Hypergolic Bipropellants: N,N,N',N'-Tetramethylethylenediamine (TMEDA) and N,N,N',N'-Tetramethylmethylenediamine (TMMDA) with Nitric Acid. The Journal of Physical Chemistry, 5221-5229. Retrieved September 17, 2022

Marsh, W. R., & Knox, B. P. (1970). USAF Propellant Handbooks Hydrazine Fuels. Bell Aerospace Company, Division of Textron, Buffalo, New York. Retrieved December 12, 2021

Martin Marietta Corporation. (1977). USAF Propellant Handbooks Nitric Acid/Nitrogen Tetroxide Oxidizers. AFRPL-TR-76-76, Denver, Colorado. Retrieved February 22, 2021

Mellor, B., Smith, C. L., & Klach, I. (1991). A Parametric Study of Factors Affecting the Corrosion of Stainless Steel by MON Oxidizer. AIAA/SAE/ASME 27th Joint Propulsion Conference. Sacramento, California: AIAA. Retrieved January 17, 2022

Mellor, B., Smith, C. L., Carr, K. M., & Bellis, R. J. (1993). Hydrazine Storage in Critical Applications: A 10-Year Milestone. California: AIAA. Retrieved February 18, 2021

Miller, R. O. (1953). Ignition Delays of Some Nonaromatic Fuels with Low-Freezing Red Fuming Nitric Acid in Temperature Range -40°F to -105°F. Washington: National Advisory Committee for Aeronautics. Retrieved March 28, 2021

Mohammadi, K., & Gorji, M. (2013). Prediction of Amine-Based Liquid Rocket Propellant Shelf Life. Weinheim: Wiley. Retrieved May 14, 2021

Moran, C., & Bjorklund, R. (1982). Propellant/Material Compatibility Program and Results. Pasadena, California: Jet Propulsion Laboratory. Retrieved November 17, 2021

Morrell, G. (1957). Summary of NACA Research on Ignition Lag of Self-Igniting Fuel - Nitric Acid Propellants. Washington: National Advisory Committee for Aeronautics. Retrieved March 31, 2021

Mullins, B. P., & Penner, S. S. (1959). Explosions, Detonations, Flammability, and Ignition. London: Pergamon Press. Retrieved December 11, 2021

Musgrave, G. E., Larsen, A., & Sgobba, T. (2009). Safety Design for Space Systems. Jordan Hill, Oxford: Butterworth-Heinemann. Retrieved June 17, 2021

National Aeronautics and Space Administration. (1974). Liquid Rocket Metal Tanks and Tank Components. Ohio: NASA.

Parsons, S., Poyntz-Wright, O., Kent, A., & McManus, M. C. (2019, January 2). Green Chemistry for Stainless Steel Corrosion Resistance: Life Cycle Assessment of Citric Acid versus Nitric Acid Passivation. Materials Today Sustainability, 1-9. Retrieved December 7, 2022

Phelps, E. H., Lee, F. S., & Robinson, R. B. (1955). Corrosion studies in fuming nitric acid. Ohio. Retrieved December 15, 2021

Pray, H. A., & Minnich, B. H. (1952, May). Solubility of Hydrogen, Oxygen, Nitrogen, Helium in Water at Elevated Temperatures. Industrial and Engineering Chemistry, 1146-1151. Retrieved December 26, 2021

Safety Office - John F. Kennedy Space Center. (1965). Liquid Propellants Safety Handbook. Cocoa, Florida: NASA. Retrieved December 12, 2021

Schalla, R. L., & Fletcher, E. A. (1957). The Behavior of the System Triethylamine-White Fuming Nitric Acid under Conditions of Rapid Mixing. Sixth Symposium on Combustion. 6, pp. 911-917. Reinhold Publishing Corp. Retrieved November 24, 2021

Schalla, R. L., & Fletcher, E. A. (1959). The Ignition Behavior of Various Amines with WFNA. Lewis Research Center. Cleveland, Ohio: National Aeronautics and Space Administration. Retrieved November 4, 2021

Simpson, D. K. (1985). Safety and Handling of Hyzrazine. 22nd Department of Defence Explosive Safety Seminar, (pp. 947-968). California. Retrieved January 14, 2022

Skartvedt, G. (1969). Propellant Clogging and Flow Decam Problems Encountered in Liquid Rocket Propulsion Systems. Denver, Colorado: USAF/Martin Marietta Corporation Technology. Retrieved November 8, 2021

Sugur, V. S., & Manwani, L. C. (1983, July 15). Storage of Red Fuming Nitric Acid. Defence Science Journal, 33(4), 331-337. Retrieved July 17, 2021

Sutton, D. (1986). Acceptance Test for Tanks Used for Storage of Hydrazine. Jet Propulsion, 2(4), 291-295. Retrieved May 11, 2021

Sutton, G. (2006). History of Liquid Propellant Rocket Engines. Reston, Virginia, United States of America: American Institute of Aeronautics and Astronautics. Retrieved 7 15, 2021

Sutton, G., & Oscar, B. (2001). Rocket Propulsion Elements (7th ed.). New York: John Wiley & Sons, Inc. Retrieved 08 5, 2021

Terlizzi, P. M., & Streim, H. (1956, April). Liquid Propellant Handling, Transfer, and Storage. Industrial and Engineering Chemistry, 48(4), 774-777. Retrieved June 17, 2021

Tiffany, C. F., & Masters, J. N. (1967). Investigation of the Flaw Growth Characteristics of Ti-6Al-V4 Titanium Used in Apollo Spacecraft Pressure Vessels. NASA. Seattle, Washington: The Boeing Company. Retrieved April 26, 2021

Tokunaga, J. (1975). Solubilities of Oxygen, Nitrogen, and Carbon Dioxide in Aqueous Alcohol Solutions. Journal of Chemical and Engineering Data, 20(1), 41-46. Retrieved December 28, 2021

Uney, P. E., & Fester, D. A. (1972). Material Compatibility with Space Storable Propellants. Colorado: Martin Marietta Corporation. Retrieved November 22, 2021

Xu, C., & Gao, W. (2000). Pilling-Bedworth ratio for oxidation of alloys. 231-235. Retrieved December 07, 2022

Zung, L. B., & Breen, B. P. (1970). A Basic Study of the Ignition of Hypergolic Liquid Propellants. Irvine, California: National Aeronautics and Space Administration. Retrieved March 29, 2021

APPENDICES

A NSPV Engineering Design Details, Pressure and Leak Test Results

Assembled and section view of NSPV (shown in Figure A.1) is given together with each subcomponent's locations. Detailed technical properties and basic functions of each subcomponent are provided in this subtitle.

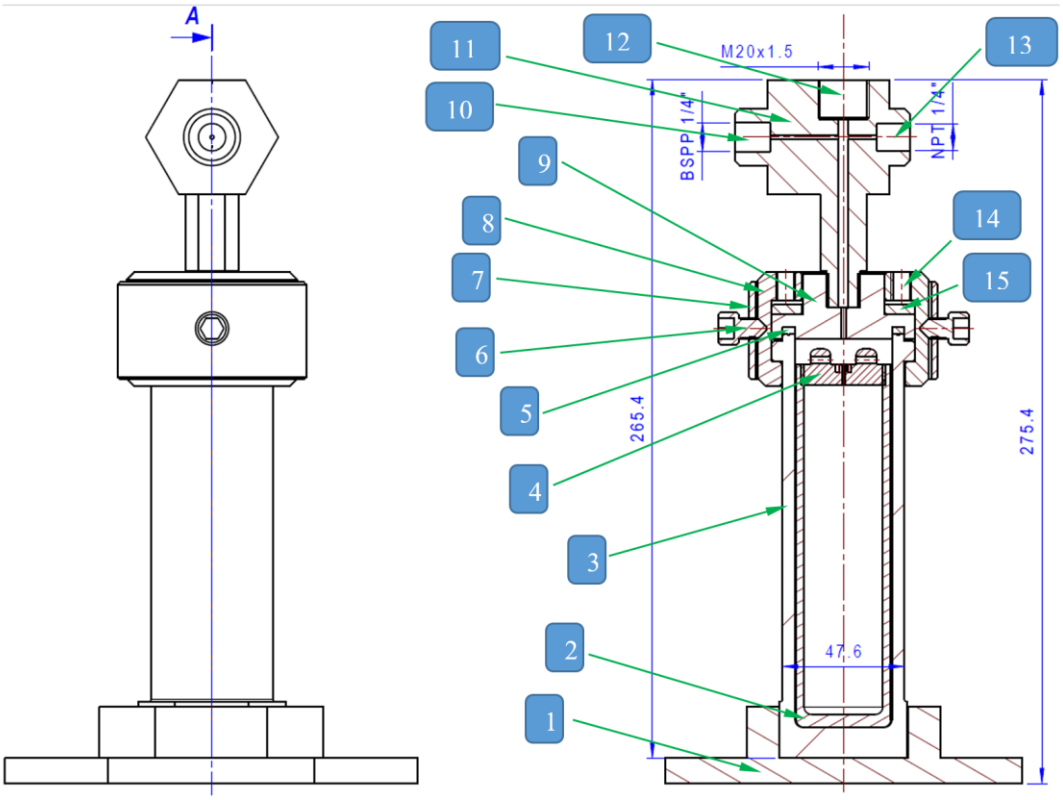

Figure A.1 Assembled and section view of NPSV

Component numbered one is named pedestal (shown in Figure A.2) and manufactured from stainless steel AISI 304L. Utilized to keep the system balanced and preclude it from being knocked over unintentionally applied forces.

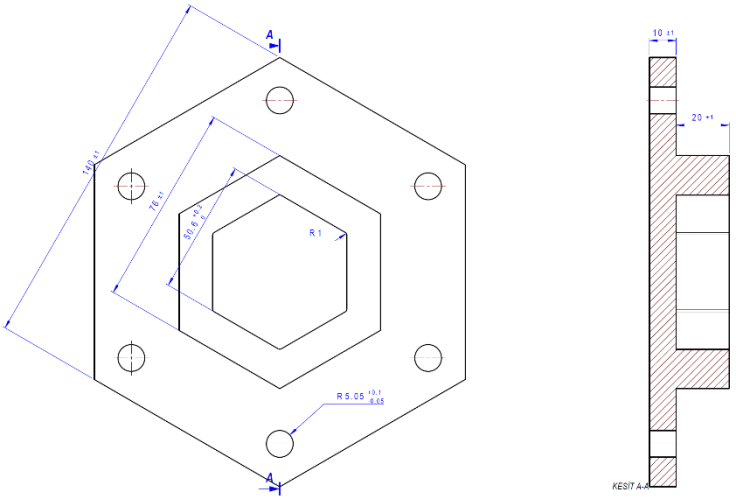

Figure A.2 Pedestal component's detailed engineering drawing

Component numbered two is named test tube (shown in Figure A.3) and manufactured from different commercial-grade materials like PTFE, aluminum 1050, aluminum 5083, stainless steel AISI 316L. The test tube is used to create the desired environment for storage experiments. Importantly, each test tube is intended to be used only once.

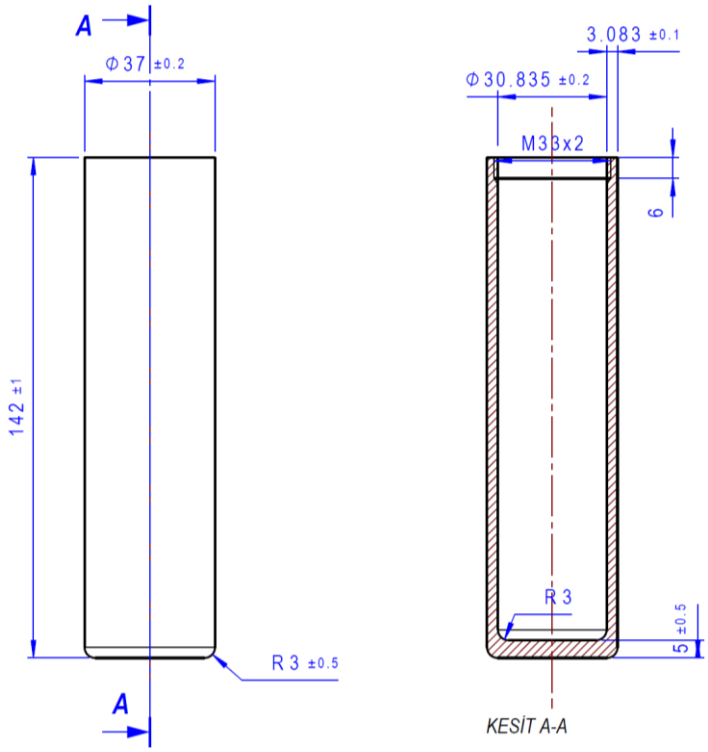

Figure A.3 Test tube component's detailed engineering drawing

Component numbered three is called pressure vessel body (shown in Figure A.4) and is manufactured from commercial-grade stainless steel AISI 304L. It could withstand pressures as high as 250 bar. As it provides a safe experiment environment, it also provides a relatively wide entrance hole, approximately 1.5 inches, which is required to put down the test tube inside the pressure vessel.

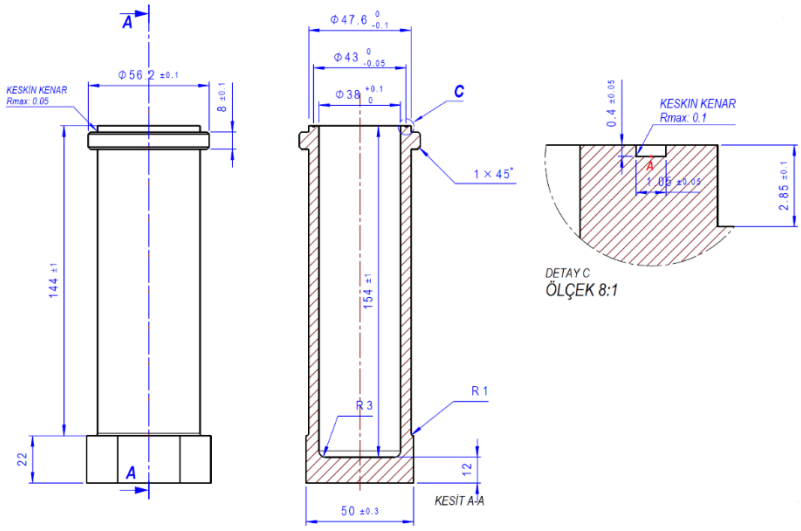

Figure A.4 Pressure vessel body component's detailed engineering drawing

Component numbered four is called test tube cap (shown in Figure A.5) and manufactured with PTFE teflon. This cap is required because liquid propellant gives a partially slow oxidation reaction with the vessel material and this phenomenon might affect the results. It is utilized to decrease the contacting surface area between the liquid chemical substance and stainless steel pressure vessel parts. The pressure homogeneity inside the system is satisfied by the small hole on top of the test tube cap. Importantly, each test tube cap is intended to be used only once.

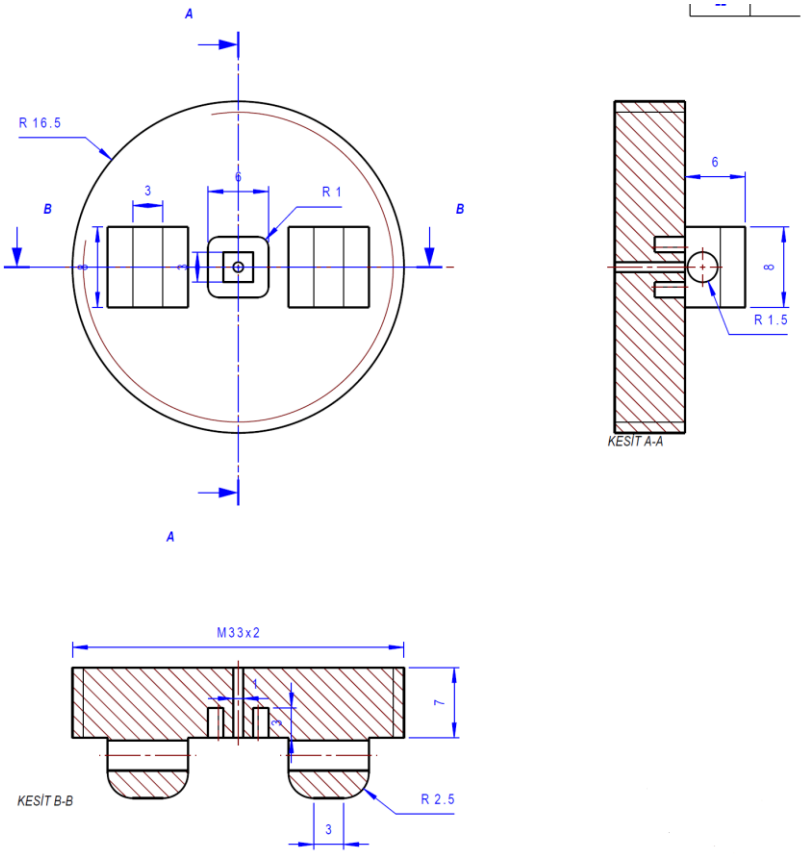

Figure A.5 Test tube cap component's detailed engineering drawing

Component numbered five is called the PTFE sealing gasket (shown in Figure A.6). Fundamentally, it is almost impossible to create a leak-free environment between in contact flat steel and steel surfaces without the use of an appropriate sealing gasket or o-ring. For this purpose, PTFE flat sealing gasket is utilized. This special type of sealing gaskets requires initial pressure loading to create and sustain a leak-free tight seal. Owing to the mechanical properties of PTFE, it could undergo plastic deformation in a way that improves the performance as it is used repetitively over time.

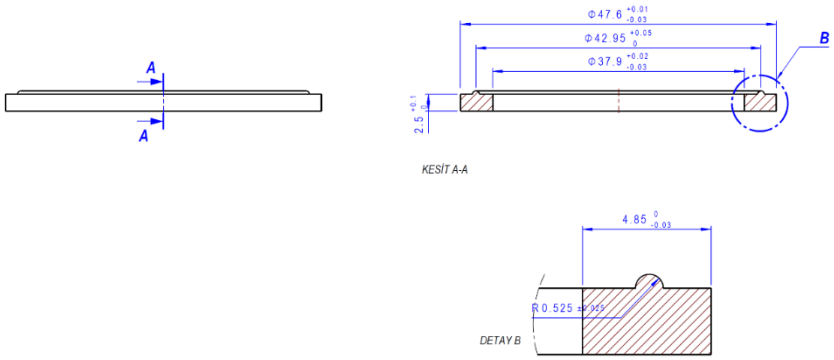

Figure A.6 Sealing gasket component's detailed engineering drawing

Component numbered six is named cover screw (shown in Figure A.7) and manufactured from commercial-grade stainless steel AISI 304L. It is used to fasten the cover part to the enclosing cap part. As a result, the enclosing cap pairs and the cover are entirely immobilized until the cover screw is removed.

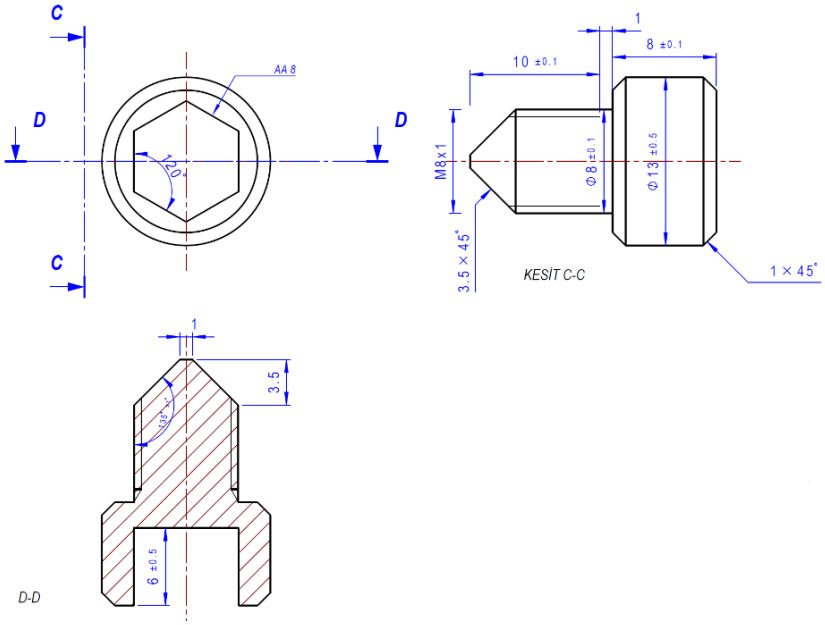

Figure A.7 Cover screw component's detailed engineering drawing

Component numbered seven is named cover (shown in Figure A.8) and manufactured from commercial-grade stainless steel AISI 304L. It helps to provide mechanical integrity to the top section of the vessel by constraining the movement of enclosing cap pairs.

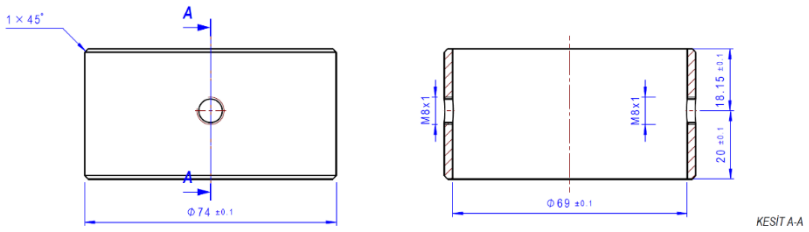

Figure A.8 Cover component's detailed engineering drawing

Component numbered eight is called the enclosing cap (shown in Figure A.9) and is manufactured from commercial grade stainless steel AISI 304L. It encloses the entire head of the vessel with two identical half circles. Furthermore, the enclosing cap provides the required screw holes for uniform pressure distribution and when it is combined with the cover apparatus, it helps to increase the pressure resistance of the top section of the vessel, which is relatively the weakest section of the vessel.

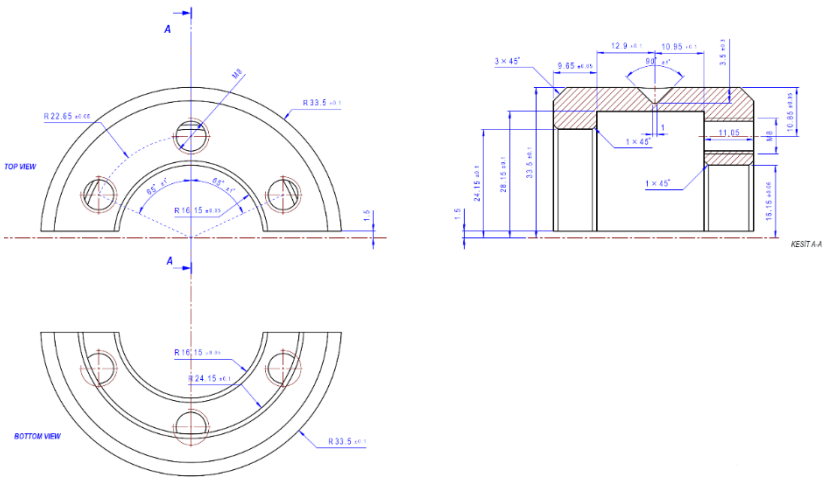

Figure A.9 Enclosing cap component's detailed engineering drawing

Component numbered nine is called sealing cap (shown in Figure A.10) and is manufactured from commercial grade stainless steel AISI 304L. It provides the secure transition of pressure forming inside the test tube to the vessel's upper section, which is the port multiplexer head. To provide satisfactory sealing between the sealing cap component and the pressure vessel body part, the best alternative is the utilization of a PTFE sealing gasket. For this purpose, a sealing cap with a gasket cavity is designed.

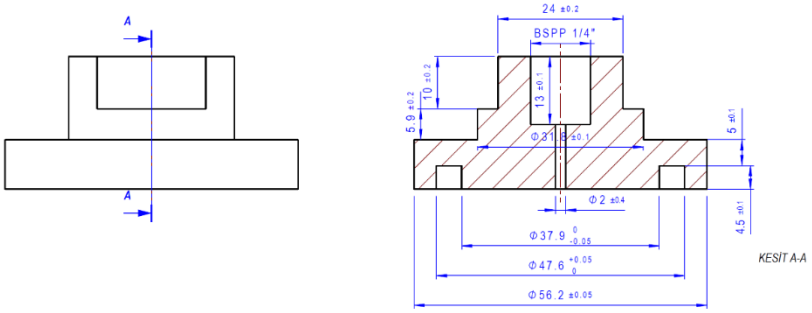

Figure A.10 Sealing cap component's detailed engineering drawing

Section numbered ten is named needle valve port. The storage condition tests require initial pressurization ranging from 2 bar to 5 bar. Moreover, according to the literature, during storage experiments, the pressure inside the vessel usually increases. Thus, a suitable type of valve is required both to pressurize the vessel and to release the accumulated vessel in the end. As a result, a needle valve is placed in that port.

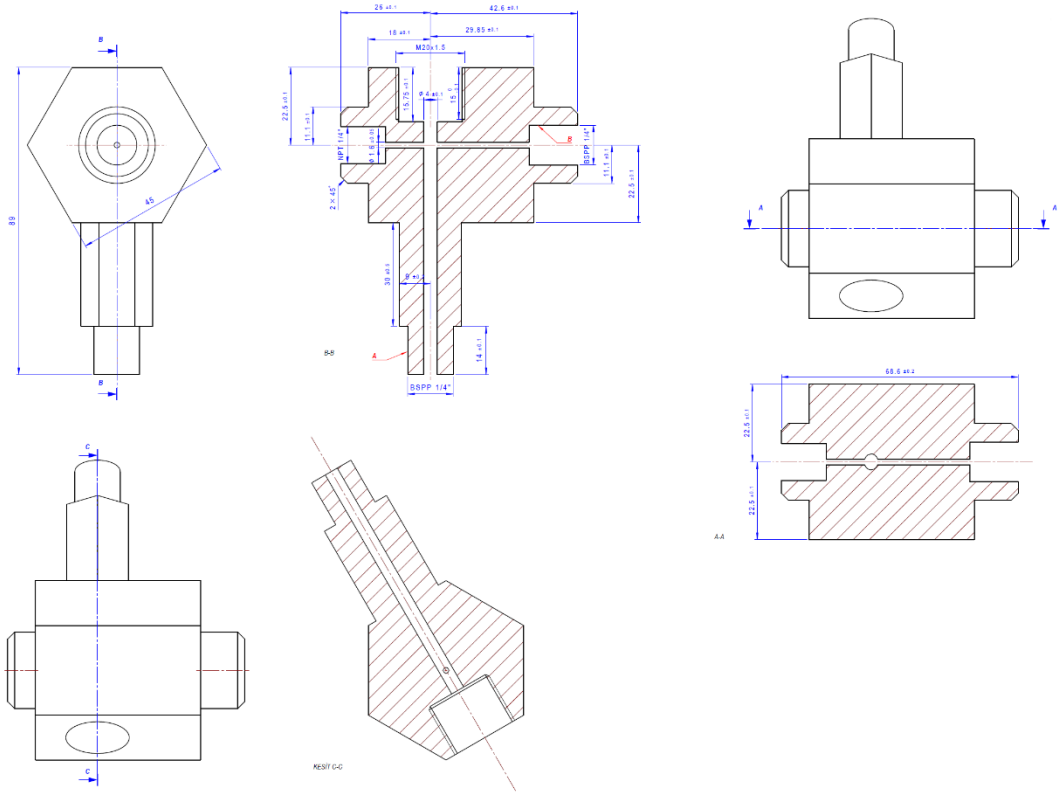

Figure A.11 Port multiplexer head component's detailed engineering drawing

Component numbered eleven is called port multiplexer head (shown in Figure A.11) and is manufactured from commercial grade stainless steel AISI 304L. The pressure vessel has only one external port via the top of the sealing cap part. To increase the number of utility ports for a better test experience a secondary part is required. For this purpose, a hexagonal-shaped block that could have an arbitrary number of ports depending on the need is designed. Currently, it has three female threaded ports.

Section numbered twelve is called the pressure instrument port. The storage condition tests are primarily based on the pressure build-up rate with respect to time inside the vessel. For this reason, obtaining the data regarding the change in pressure concerning time is extremely crucial for the success of the experiments.

Section numbered thirteen is named relief valve port. Due to the nature of the experiments, the closed system is expected to encounter pressures up to 100 bar. For this reason, the system is designed to withstand pressures up to 250 bar. However, as the system is being used, mechanical failure due to fatigue is a possibility. To overcome this phenomenon, a mechanical relief valve with a set value of 100 bar is stationed at the aforementioned port.

Section numbered fourteen is called the sealing screw hole. To maintain a leak-free system, pressure should be distributed as uniformly as possible around the PTFE sealing gasket. To achieve this, the sealing screw holes are drilled with 60 degrees equilateral angles around the center of the entire vessel.

Component numbered fifteen is named stainless steel gasket (shown in Figure A.12) and manufactured from commercial grade stainless steel AISI 304L. It provides uniform pressure distribution over the PTFE flat sealing gasket when sealing screw holes are utilized appropriately.

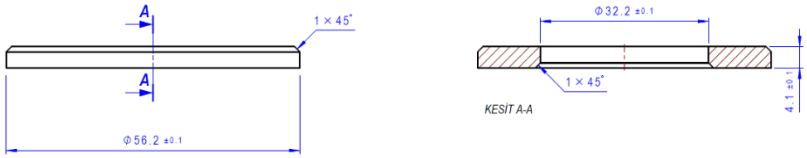

Figure A.12 Stainless steel gasket component’s detailed engineering drawing

Components used for places for ten, twelve, and thirteen are commercially available shelf products (shown in Table A.1) and their wetted parts are all made of commercial-grade stainless steel AISI 316L.

Table A.1 NSPV's commercial bill of materials (No's are according to Figure A.1)

No	Product Type	Catalog Number	Brand
10	Integral-Bonnet Needle Valve	H-300U-SS-L-V-1/4-RS	Ham-Let
12	Flush Membrane Transmitter	FPT.8235.83.23.91.35.19.33	Trafag
13	High Pressure Relief Valve	H-900-HP-SS-N-1/4-C	Ham-Let

Leak and pressure rating test of NSPV was performed according to the details given in section 3.1.2.1. In line with the test results (shown in Figure A.13), the NSPV system was proved to be leak proof and rated usable up to 200 bar at 25°C with a safety factor of 1.25.

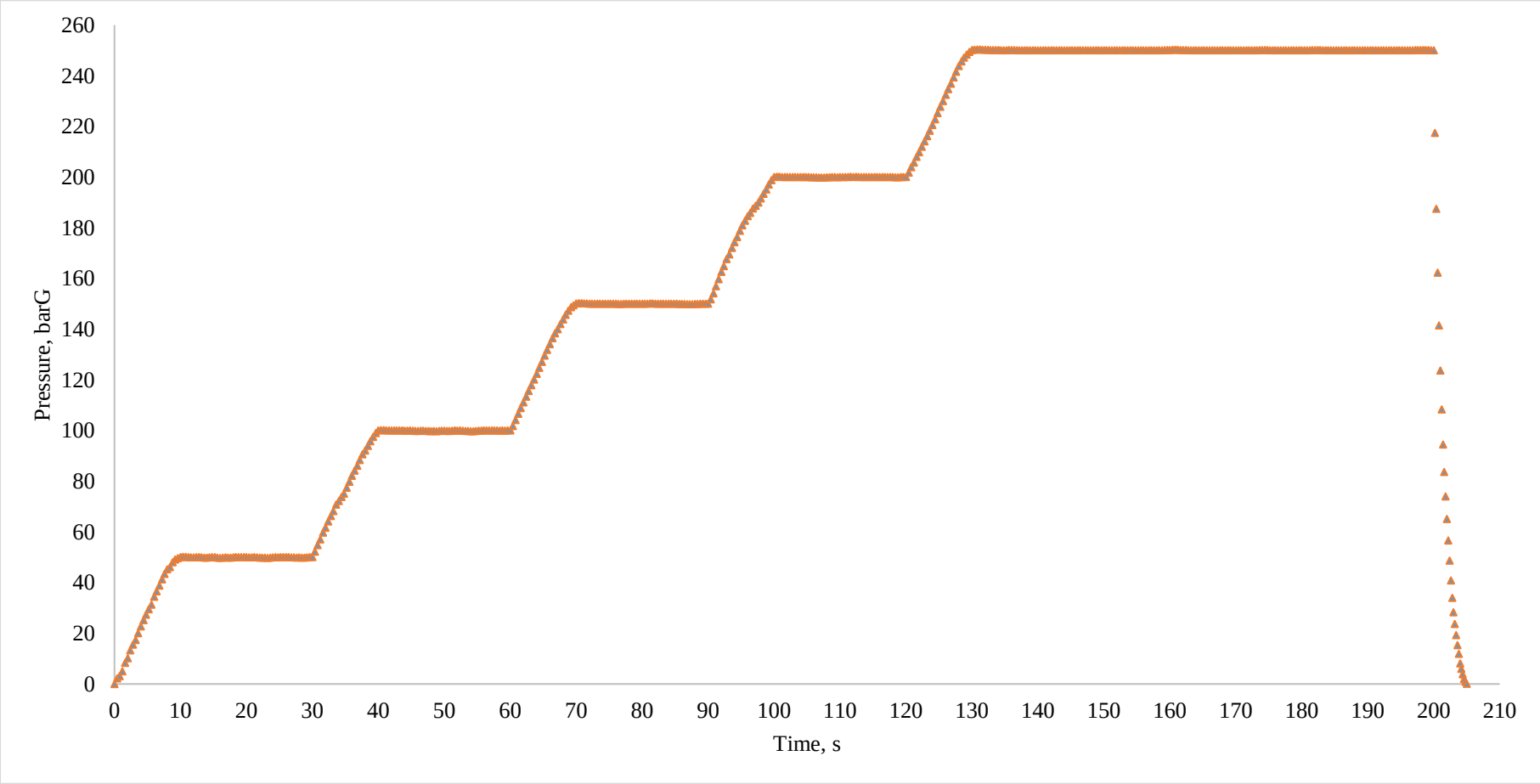

Figure A.13 Leak proofing and pressure rating test of NPSV

B MPV Design Details and Pressure Rating Test Results

Non-Stirred Pressure Vessel (NSPV) is highly superior equipment in terms of mechanical strength, reliability, and modifiable structure. However, there are some prominent drawbacks like tight manufacturing tolerances and excess production cost. For this reason, instead of manufacturing all the components specially, the second type of pressure vessel, named Mini Pressure Vessel (MPV) is designed and manufactured. MPV requires only three special components and the system is ready to use with a couple of additional purchased relatively cheap mechanical parts. In brief, the unit manufacturing cost was reduced by approximately sixty percent.

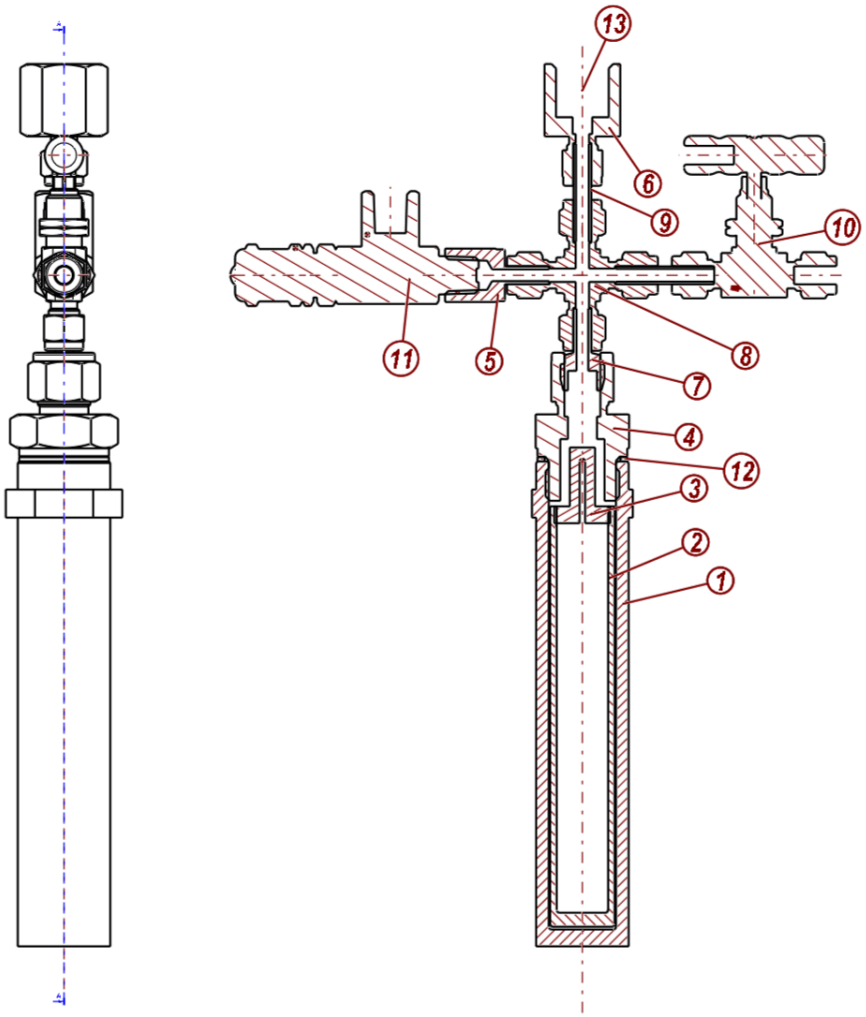

Figure B.1 Assembled and section view of MPV

Assembled and section view of MPV (shown in Figure B.1) is given together with each subcomponent's locations. Detailed technical properties and basic functions of each subcomponent are provided in this subtitle.

Component numbered one is named mini vessel body (shown in Figure B.2) and manufactured from commercial grade stainless steel AISI 316L. It could withstand pressures as high as 200 bar. Compared to NSPV, the entrance hole is only 0.75 inches wide in terms of diameter and this downside limits future utilization, however, it is sufficient for early stages of this study.

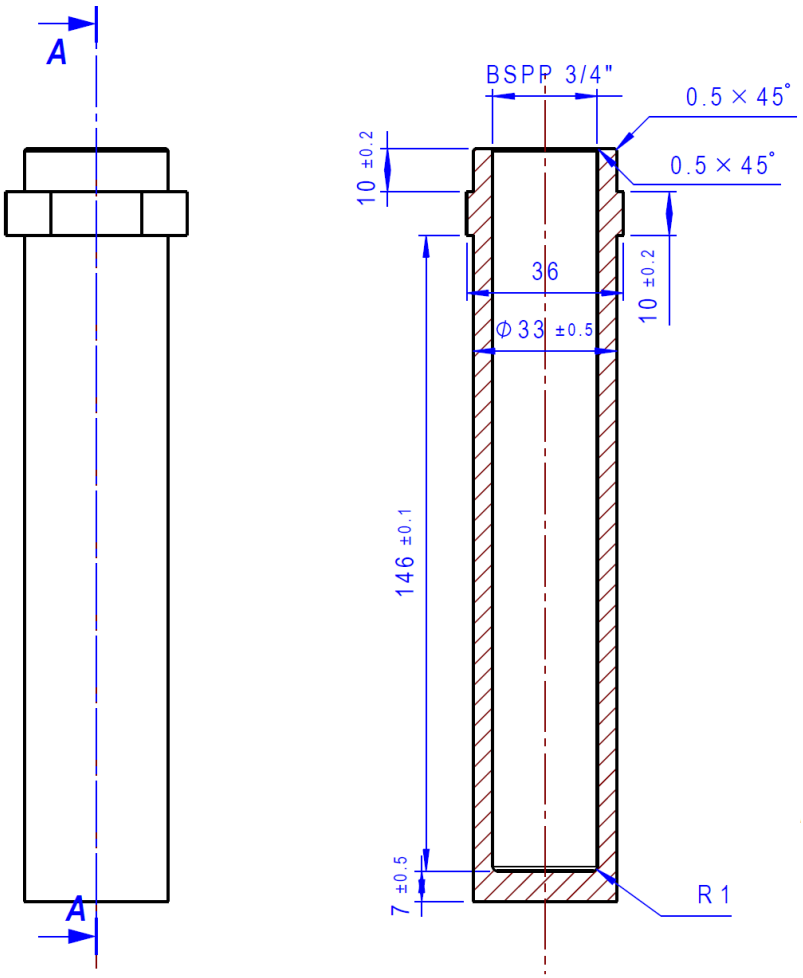

Figure B.2 Mini vessel body component's detailed engineering drawing

Component numbered two is named mini test tube (shown in Figure B.3) and manufactured from different commercial-grade materials like PTFE, aluminum

5083-H111, aluminum 6061-T6, stainless steel AISI 316L, and nickel alloy 904L. The test tube is used to create the desired material environment for storage experiments. Importantly, each test tube is intended to be used only once and discarded after the termination of the experiment.

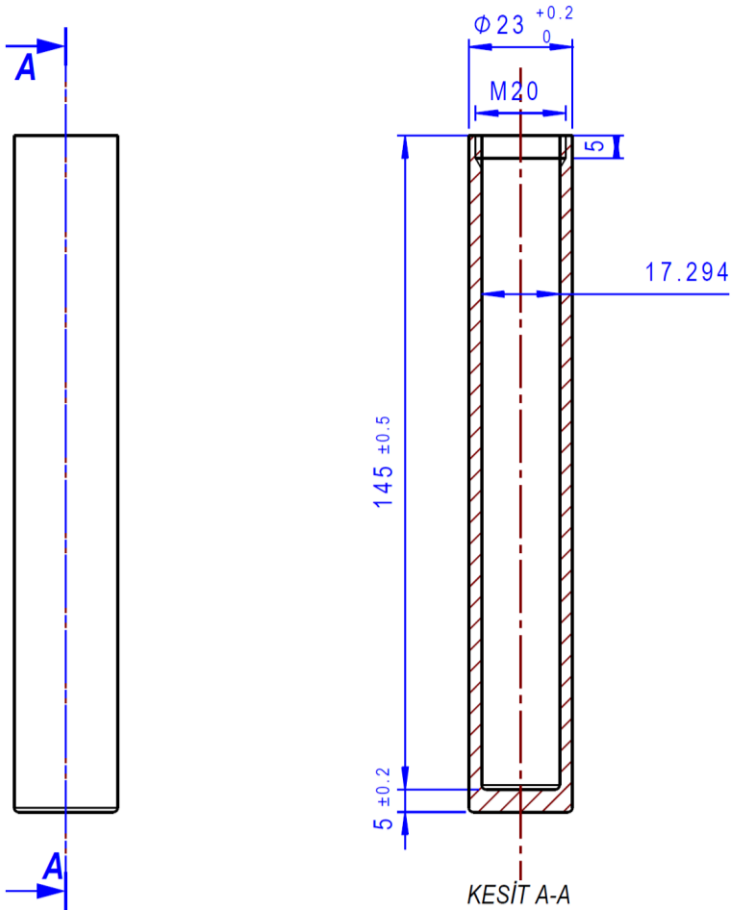

Figure B.3 Mini test tube component's detailed engineering drawing

Component numbered three is called mini test tube cap (shown in Figure B.4) and manufactured with PTFE teflon. This cap is required because liquid propellant gives a partially slow oxidation reaction with the vessel material and this phenomenon might affect the results. It is utilized to decrease the contacting surface area between the liquid chemical substance and stainless steel pressure vessel parts. Additionally, the pressure homogeneity inside the system is satisfied by a hole of two millimeters in diameter on top of the test tube cap.

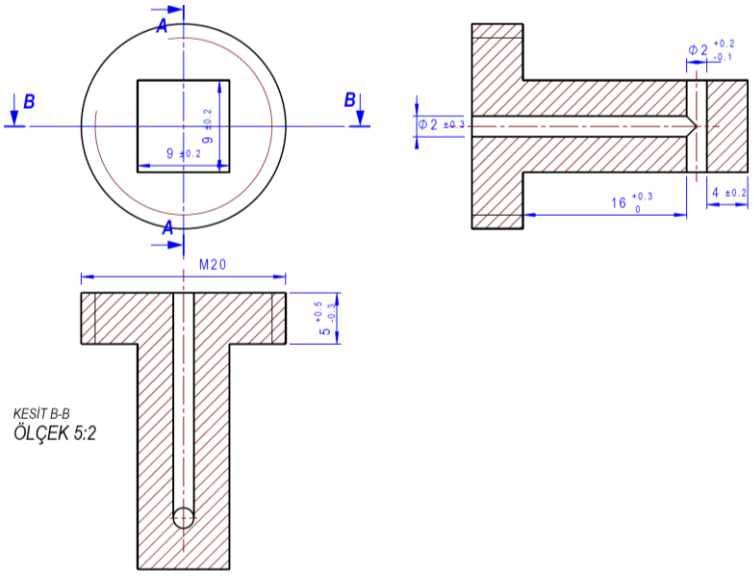

Figure B.4 Mini test tube cap component's detailed engineering drawing

Components numbered from four to eleven are commercially available shelf products (shown in Table B.1) and their wetted parts are made of commercial-grade AISI 316L stainless steel, polytetrafluorethylene (PTFE), and fluorocaoutchouc also known as VITON®.

Table B.1 MPV's commercial bill of materials (No's are according to Figure B.1)

No	Product Type	Catalog Number	Brand
4	Male Connector	768LG_1/2X3/4	Ham-Let
5	Female Adapter Tube to Pipe	739LF_1/4X1/4	Ham-Let
6	Female Connector	766LG_1/4X1/2	Ham-Let
7	Reducing Port Connector	767LM_1/2X1/4	Ham-Let
8	Union Cross	7102_1/4	Ham-Let
9	Stainless Steel Tube	22BWG 6.35X0.89 ASTM A 269 AISI 316L	Ham-Let
10	Integral-Bonnet Needle Valve	H-300U-SS-L-V-1/4-RS	Ham-Let
11	High Pressure Relief Valve	H-900-HP-SS-N-1/4-C	Ham-Let
12	Sealing Gasket	SS-GA-LG-3/4-FKM	Ham-Let
13	Flush Membrane Transmitter	FPT.8235.83.23.91.35.19.33	Trafag

Leak and pressure rating test of MPV was performed according to the details given in section 3.1.3.1. In terms of test results (shown in Figure B.5), the MPV structure was proved to be leak proof and rated usable up to 100 bar at 25°C with a safety factor of 1.5.

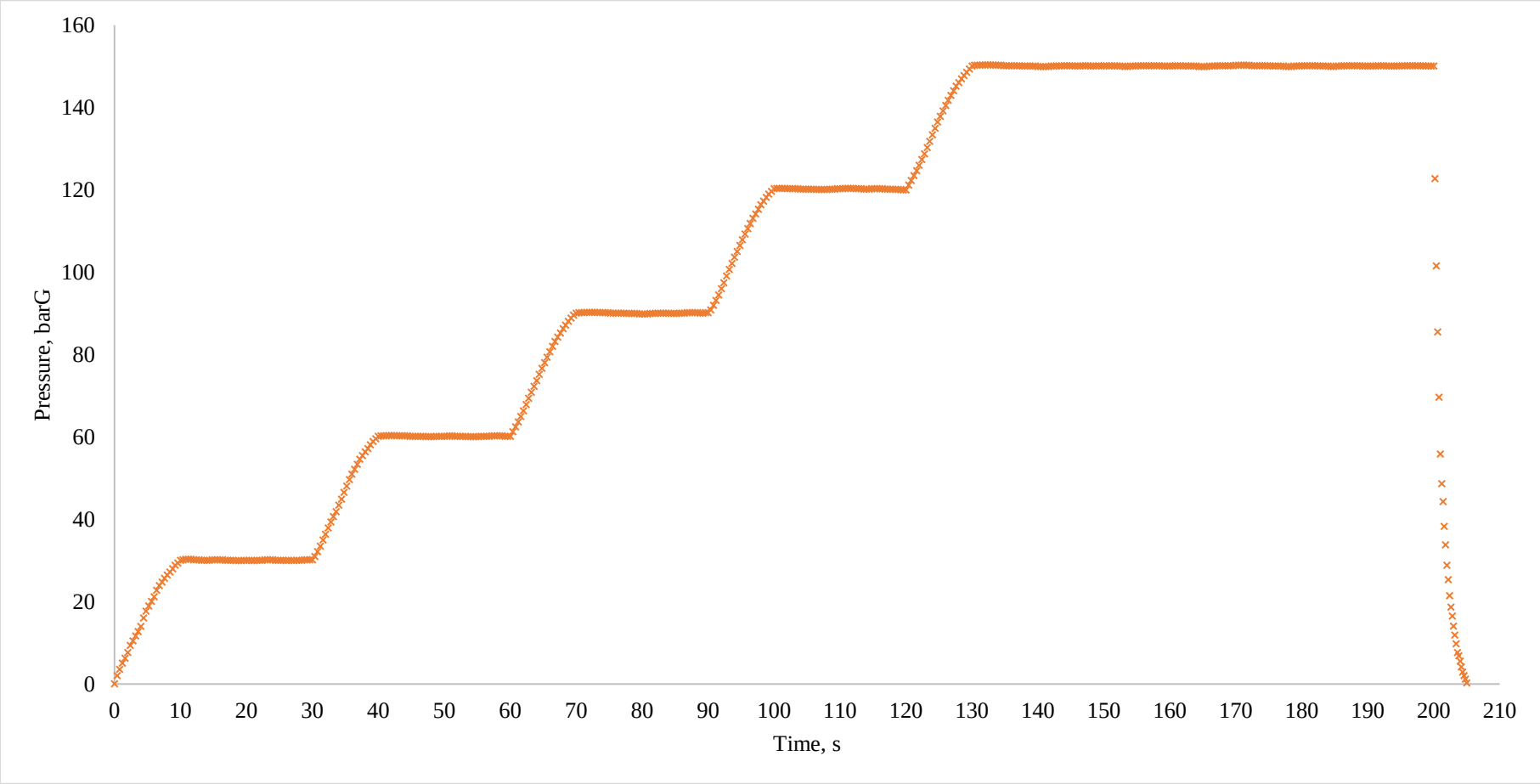

Figure B.5 Leak proofing and pressure rating test of MPV

C Detailed Experiment Initiation Steps

Table C.1 Experimental steps of storage tests

1. WFNA and MPV were kept at 20°C in a constant temperature water bath and temperature cabinet, respectively.
2. The pressure regulator was set to 2.5barG.
3. The test tube was filled with thermally conditioned WFNA to leave a certain ullage space.
4. The test tube cap was tightened to be hand tight.
5. The test tube was placed inside the pressure vessel body.
6. The mini pressure vessel (MPV) assembly was connected to the vacuum & pressurization system (VPS) (shown in Figure 3.6 and Figure 3.7).
7. When all the valves were closed, the vacuum pump was turned on then the vacuum valve and trap valve are turned on, respectively.
8. The vacuuming process was continued for no less than 10 minutes and the pressure value of 1.0 torr was stabilized.
9. The vacuum valve was turned off meanwhile the vessel valve was turned on slowly.
10. After about 2 minutes, the trap valve was turned off.
11. The tank valve and discharge valve were turned on, respectively.
12. The discharge valve was turned off after 15 seconds.
13. The pressure valve was turned on and kept open for 3 minutes.
14. Pressure stabilization was verified through pressure sensors after that the vessel valve was turned off.
15. Pressure vessel assembly was monitored for leaks with leak detection spray.
16. The tank valve was turned off.
17. The discharge valve was turned on and kept open until there was no pressure.
18. The connection between MPV and VPS was disconnected.
19. MPV was placed inside one of the slots on the reactor rack.
20. The reactor rack with the MPVs was put in the previously heated temperature cabinet.
21. The data acquisition program was initiated.

D Mechanical Testing of Tensile Specimens

Tensile test specimens were CNC machined according to the most recent ASTM E8/E8M – 16a standard and used to determine mechanical properties of materials utilized (shown in Figure D.1).

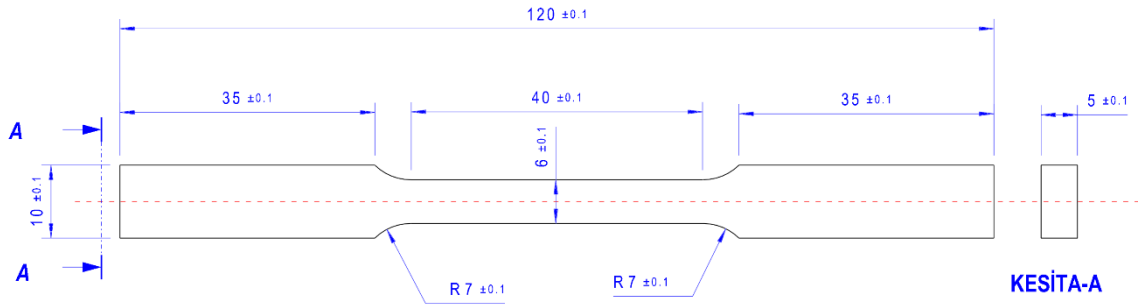

Figure D.1 Tensile test specimen according to ASTM designation E8/E8M – 16

Test specimens were separated into two different groups namely control and citric acid passivated, passivation procedures were performed according to section 3.2.4. Control samples were used to check and justify the material's mechanical properties in which test tubes were also produced. The latter group were used to determine the effect of passivation, if there was any, on the mechanical properties.

Accordingly, elongation at break (%), tensile yield strength (MPa), ultimate tensile strength (MPa), and Brinell hardness (HB) were obtained. These tensile tests were performed by an accredited laboratory at Roketsan, and the following results were given in Table D.1. As a result of the results obtained, it is safe to state that citric acid passivation does not affect the tensile test outputs.

Table D.1 Mechanical Properties of Tube and MPV Construction Materials

Specimen	Width (mm)	Thickness (mm)	HB	UTS (MPa)	TYS (MPa)	Elongation at Break (%)	Modules of Elasticity (GPa)
A-904L^{C}	6.08	5.03	195	632.74	398.89	44.17	190.9
B-904L^{P}	6.05	5.04	192	632.62	362.57	44.21	193.8
F-316L^{P}	6.03	5.00	178	610.47	427.53	38.43	191.4
G-316L^{C}	6.01	4.97	180	616.98	434.47	38.39	192.4
J-6061^{P}	5.98	5.15	90	303.36	265.17	18.26	68.7
K-6061^{C}	5.98	5.07	89	304.91	262.64	19.24	69.4
L-5083^{C}	6.00	5.07	74	323.83	161.88	17.26	69.6
M-5083^{P}	5.98	4.93	75	321.04	168.74	16.46	72.7

All the values are averages of three tensile specimens tested in the same manner.

E Compositional Analysis of Tube and MPV Construction Materials

Chemical composition of each metallic material were precisely determined by spectral analysis and optical emission spectroscopy[1], and it was found that presence of all the elements primary and trace elements lied well within the upper and lower acceptance bands (shown in Table E.1).

Table E.1 Spectral Analysis of Tube and MPV Construction Materials

Material	**Alloy 904L**		**AISI 316L**		**Al 5083-H111**		**Al 6061-T6**	
Element	**Measured**	**Limits**	**Measured**	**Limits**	**Measured**	**Limits**	**Measured**	**Limits**
Si	0.157	0.0 - 1.0	0.17	0.0 - 0.80	0.312	0.0 -0.40	0.541	0.40 - 0.80
Fe	Balance	Balance	Balance	Balance	0.337	0.0 - 0.40	0.189	0.0 - 0.70
Cu	1.452	1.20 - 2.00			0.067	0.0 - 0.40	0.182	0.15 - 0.40
Mn	0.895	0.0 - 2.0	1.17	0.0 - 2.0	0.496	0.40 - 1.00	0.024	0.0 - 0.15
Mg					4.812	4.00 - 4.90	0.869	0.80 - 1.20
Cr	20.14	19.00 - 21.00	17.71	16.0 - 18.0	0.125	0.05 - 0.25	0.087	0.04 - 0.35
Ni	25.15	24.00 - 26.00	12.95	11.0 - 14.0	0.039	0 0 – 0.05	0.034	0.0 – 0.05
Zn					0.002	0.0 - 0.25	0.013	0.0 - 0.25
Ti					0.018	0.0 - 0.15	0.011	0.0 - 0.15
C[1]	0.004	0.0 - 0.020	0.021	0.0 - 0.030				
S[1]	0.005	0.0 - 0.010	0.017	0.0 - 0.030				
Mo	4.48	4.00 - 5.00	2.34	2.0 - 2.5				
Al					93.642	92.4 - 95.6	98.039	95.9 - 98.6

Blanks in table E.1 were left intentionally.
All the values are averages of three test specimens taken from the same rod utilized.

F Visual State of WFNA before and after Long-Term Storage Tests

In consequence of storage tests, changes in visual appearance of WFNA such as blackening or staining were observed (shown in Figure F.1).

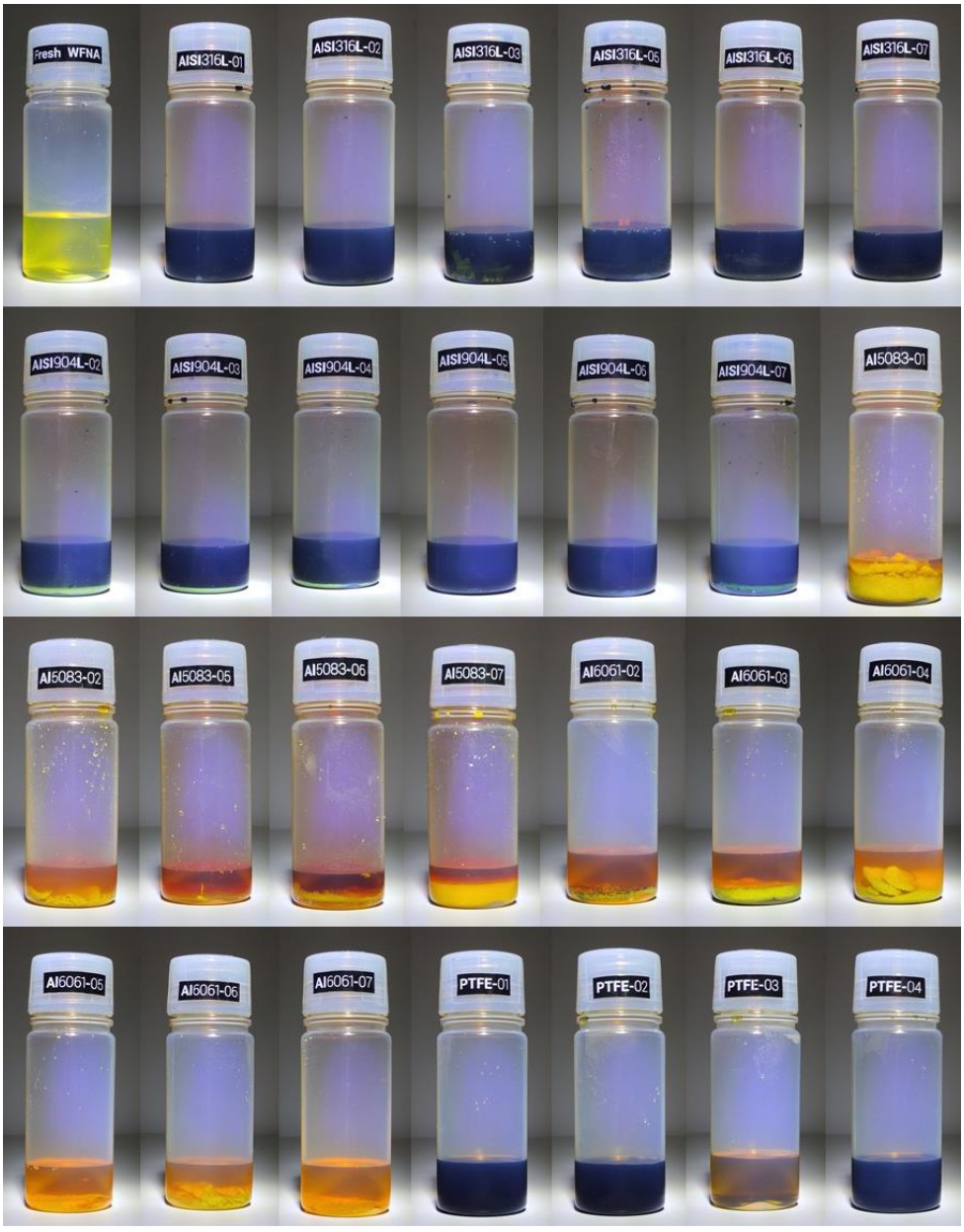

Figure F.1 Visual state of WFNA before and after long-term storage tests

G Corrosion Rate and Mass Loss of Tubes after Long-Term Storage Tests

The corrosive nature of WFNA led to variable mass losses in the metallic tubes.

Table G.1 Corrosion rate and mass loss of tubes after long-term storage tests

Tube Marking	Tube Mass @ ti (g)	Tube Mass @ tf (g)	Tube Mass Loss {ti (g) - tf (g)}	Actual Tube Mass Loss (%)	Corrosion Rate (mm/year)
AISI 316L-01	186.85	182.87	-3.98	2.13	0.97
AISI 316L-02^{P}	184.69	180.64	-4.05	2.19	0.99
AISI 316L-03	184.67	180.63	-4.04	2.19	0.98
AISI 316L-05	181.13	177.41	-3.72	2.05	0.77
AISI 316L-06^{P}	184.19	180.47	-3.72	2.02	0.77
AISI 316L-07	180.72	176.89	-3.83	2.12	0.79
Alloy 904L-02^{P}	191.15	188.74	-2.41	1.26	0.59
Alloy 904L-03	191.07	188.20	-2.87	1.50	0.70
Alloy 904L-04^{P}	192.84	190.59	-2.25	1.17	0.55
Alloy 904L-05	189.40	186.57	-2.83	1.49	0.58
Alloy 904L-06^{P}	193.48	190.62	-2.86	1.48	0.59
Alloy 904L-07	190.05	187.29	-2.76	1.45	0.57
Al 5083-01	61.82	60.00	-1.82	2.94	0.44
Al 5083-02^{P}	62.40	60.59	-1.81	2.90	0.44
Al 5083-05	62.72	60.55	-2.17	3.46	0.45
Al 5083-06^{P}	62.80	60.72	-2.08	3.31	0.43
Al 5083-07	62.84	60.58	-2.26	3.60	0.47
Al 6061-02^{P}	64.54	64.07	-0.47	0.73	0.11
Al 6061-03	64.12	63.62	-0.50	0.78	0.12
Al 6061-04^{P}	64.31	63.84	-0.47	0.73	0.11
Al 6061-05	64.59	64.06	-0.53	0.82	0.11
Al 6061-06^{P}	64.13	63.75	-0.38	0.59	0.08
Al 6061-07	64.46	63.99	-0.47	0.73	0.10

H Ignition Delay Tests via Fresh TMEDA

At the end of white fuming nitric acid storage experiments, fluid samples were taken from each tests that were completed successfully. Then, the ignition delay tests were performed by simple drop tests with equipment depicted in Figure 4.13.

Table H.1 Ignition delay times between WFNA and TMEDA

Tube Marking	Ignition Delay Times with Fresh TMEDA @ 20°C (ms)				
	Test #1	Test #2	Test #3	Test #4	Average
Fresh WFNA	27.1	27.1	25.0	25.0	26.0
AISI 316L-01	108.3	100.0	116.7	100.0	106.3
AISI 316L-02^{P}	104.2	112.5	100.0	100.0	104.2
AISI 316L-03	100.0	125.0	108.3	108.3	110.4
AISI 316L-05	133.3	104.2	112.5	120.8	117.7
AISI 316L-06^{P}	108.3	104.2	108.3	95.8	104.2
AISI 316L-07	108.3	112.5	108.3	95.8	106.3
Alloy 904L-02^{P}	29.2	31.3	29.2	33.3	30.7
Alloy 904L-03	29.2	25.0	29.2	29.2	28.1
Alloy 904L-04^{P}	29.2	29.2	29.2	25.0	28.1
Alloy 904L-05	41.7	37.5	37.5	33.3	37.5
Alloy 904L-06^{P}	33.3	33.3	29.2	29.2	31.3
Alloy 904L-07	29.2	33.3	33.3	25.0	30.2
Al 5083-01	16.7	10.4	12.5	8.3	12.0
Al 5083-02^{P}	8.3	8.3	6.3	8.3	7.8
Al 5083-05	NI[1]	250.0	NI	225.0	237.5
Al 5083-06^{P}	162.5	166.7	NI	162.5	163.9
Al 5083-07	83.3	54.2	70.8	41.7	62.5
Al 6061-02^{P}	8.3	8.3	8.3	8.3	8.3
Al 6061-03	12.5	8.3	8.3	8.3	9.4
Al 6061-04^{P}	8.3	12.5	12.5	8.3	10.4
Al 6061-05	8.3	8.3	8.3	8.3	8.3
Al 6061-06^{P}	8.3	10.4	10.4	8.3	9.4
Al 6061-07	8.3	4.2	4.2	6.3	5.7
PTFE-01	16.7	20.8	8.3	12.5	14.6
PTFE-02	12.5	12.5	16.7	8.3	12.5
PTFE-03	8.3	8.3	10.4	8.3	8.9
PTFE-04	20.8	22.9	16.7	18.8	19.8

[1] No ignition eventuated.

İ Elemental Analysis of Stored WFNA via ICP-OES

At the end of white fuming nitric acid storage experiments, fluid samples were taken from each tests that were completed successfully. Diluted solutions were prepared by mixing 1.0 ml of fluid sample with 99.0 ml of deionized water. Here, prepared solutions were stored inside 125ml bottles made of LDPE with polypropylene screw closure (shown in Figure İ.1).

Figure İ.1 Diluted test samples for elemental analysis via ICP-OES

Elemental analysis tests were performed by an accredited laboratory located at Roketsan with Varian model 720-ES ICP-OES instrument. The elemental analysis test results were given in Table İ.1.

Table İ.1 Elemental Analysis of Fresh and Stored WFNA via ICP-OES

Tube Marking	**ICP – OES Elemental Analysis (mg/L)**								
	Al	**Cr**	**Cu**	**Fe**	**Mg**	**Mn**	**Ni**	**Zn**	**Total**
Fresh WFNA	20	0	0	10	0	0	0	0	30
AISI 316L-01	50	14500	400	39500	0	1700	6100	40	62290
AISI 316L-02^{P}	50	13200	400	37400	0	1400	5900	50	58400
AISI 316L-03	50	14200	400	39100	0	1600	9900	70	65320
AISI 316L-05	50	14700	1000	39500	0	1700	10000	70	67020
AISI 316L-06^{P}	50	14000	400	38400	0	1500	9600	60	64010
AISI 316L-07	50	13700	1000	37300	0	1600	9500	60	63210
Alloy 904L-02^{P}	100	11600	900	24000	0	800	2000	10	39410
Alloy 904L-03	100	13000	1100	24800	0	900	2500	10	42410
Alloy 904L-04^{P}	100	11000	800	23100	0	700	2000	10	37710
Alloy 904L-05	100	12600	1000	25500	0	900	6700	40	46840
Alloy 904L-06^{P}	100	13000	1200	25000	0	1000	4500	30	44830
Alloy 904L-07	100	14000	1100	24900	0	920	5500	30	46550
Al 5083-01	18000	50	40	200	2500	400	200	60	21450
Al 5083-02^{P}	15500	40	30	200	2000	200	10	20	18000
Al 5083-05	32900	50	30	200	2000	400	10	60	35650
Al 5083-06^{P}	34300	100	50	600	2500	300	70	40	37960
Al 5083-07	26000	70	50	200	2400	300	5	40	29065
Al 6061-02^{P}	800	10	10	800	100	100	200	4	2024
Al 6061-03	900	4	30	900	140	50	230	2	2256
Al 6061-04^{P}	800	10	10	1000	100	100	140	3	2163
Al 6061-05	5600	3	3	40	100	60	0	3	5809
Al 6061-06^{P}	3300	100	20	400	100	5	60	0	3985
Al 6061-07	4800	10	3	100	100	60	10	3	5086
PTFE-01	20	2000	40	7400	0	200	1400	10	11070
PTFE-02	20	1000	10	3600	0	100	600	0	5330
PTFE-03	20	100	0	500	0	4	100	0	724
PTFE-04	20	2400	30	8500	0	200	1500	10	12660

J Chemical Composition Analysis of Stored WFNA

At the end of white fuming nitric acid storage experiments, fluid samples were taken from each tests that were completed successfully. Compositional tests were performed at Roketsan and the related results were given in Table J.1.

Table J.1 Chemical Analysis of Fresh and Stored WFNA

Tube Marking	Chemical Composition (wt. %)	
	H_2O	NO_2
Fresh WFNA	1.97	1.43
AISI 316L-01	7.36	15.94
AISI 316L-02^P	7.41	15.49
AISI 316L-03	8.04	17.09
AISI 316L-05	8.29	15.40
AISI 316L-06^P	7.98	17.73
AISI 316L-07	8.74	16.47
Alloy 904L-02^P	5.71	12.11
Alloy 904L-03	6.31	12.92
Alloy 904L-04^P	5.68	11.82
Alloy 904L-05	7.09	13.13
Alloy 904L-06^P	6.33	13.37
Alloy 904L-07	6.80	14.53
Al 5083-01	2.45	26.55
Al 5083-02^P	4.04	23.35
Al 5083-05	2.25	26.52
Al 5083-06^P	2.16	29.07
Al 5083-07	4.29	30.17
Al 6061-02^P	2.91	11.41
Al 6061-03	2.90	10.74
Al 6061-04^P	2.95	9.01
Al 6061-05	2.52	10.72
Al 6061-06^P	3.22	9.22
Al 6061-07	2.67	11.07
PTFE-01	5.00	9.13
PTFE-02	4.89	8.39
PTFE-03	3.95	7.76
PTFE-04	5.14	7.85